THE QUARTERLY JOURNAL OF
MECHANICS AND APPLIED MATHEMATICS

VOLUME XII PART 3
AUGUST 1959

OXFORD
AT THE CLARENDON PRESS
1959

Price 18*s. net*

PRINTED IN GREAT BRITAIN BY VIVIAN RIDLER AT THE UNIVERSITY PRESS, OXFORD

THE QUARTERLY JOURNAL OF MECHANICS AND APPLIED MATHEMATICS

THE QUARTERLY JOURNAL OF MECHANICS AND APPLIED MATHEMATICS is published at 18*s.* net for a single number with an annual subscription (for four numbers) of 60*s.* post free.

NOTICE TO CONTRIBUTORS

1. *Communication.* Papers should be communicated to Dr. D. M. A. Leggett, Department of Mathematics, King's College, Strand, London, W.C. 2.

If possible, to expedite publication, papers should be submitted in duplicate.

2. *Presentation.* Papers should be typewritten (double spacing) and should be preceded by a summary not exceding 300 words in length. References to literature should be given in standard order, *author, title of journal, volume number, date, page.* These should be placed at the end of the paper and arranged according to the order of reference in the paper.

3. *Diagrams.* The number of diagrams should be kept to the minimum consistent with clarity. The lines of the figures should be drawn in ink either on draughtsman's paper or on good quality white paper. Each individual line in the figure should bear reducing to one-half of the size of the original, and great care should be exercised to see that the lines are regular in thickness, especially where they meet. Lettering of the figure should be in pencil and should be sufficient to define clearly the lines and curves in it. The writing of formulae or of explanations on the diagram itself should be avoided. All explanations of symbols, etc., should be given in underline. Contributors should indicate on their manuscripts where figures should be inserted.

4. *Tables.* Tables should preferably be arranged so that they can be printed with the columns parallel to the longer edge of the page.

5. *Notation.* All single letters used to denote vectors in the manuscript should be marked by underlining with a wavy line. Scalar and vector products should be denoted by $\underset{\sim}{a} . \underset{\sim}{b}$ and $\underset{\sim}{a} \wedge \underset{\sim}{b}$ respectively. Real and imaginary parts of complex quantities should be denoted by re and im respectively.

6. *Offprints.* Authors of papers will be entitled to 25 free offprints. This number is available for sharing between authors of joint papers.

7. All correspondence other than that dealing with contributions should be addressed to the publishers:

OXFORD UNIVERSITY PRESS
AMEN HOUSE, LONDON, E.C. 4

A NOTE ON THE MOTION OF BUBBLES IN A HELE-SHAW CELL AND POROUS MEDIUM

By SIR GEOFFREY TAYLOR *and* P. G. SAFFMAN

(*Cavendish Laboratory, Cambridge*)

[Received 12 August 1958. Revise received 13 November 1958]

SUMMARY

Exact solutions are presented for the steady motion of a symmetrical bubble through a parallel-sided channel in a Hele–Shaw cell containing a viscous liquid. The solutions also describe two-dimensional motion in a porous medium, since the two cases are mathematically analogous. It is shown that the solutions are not mathematically unique and a purely analytical criterion for specifying a particular solution is given. When the bubble is large, these particular solutions are such that the maximum width of the bubble is almost half that of the channel. Solutions are also presented for the motion of large asymmetric bubbles through the channel. The three-dimensional motion of bubbles in a porous medium of infinite extent is also considered briefly.

1. Introduction

THE motion of the interface between two immiscible viscous fluids in a Hele–Shaw cell, that is, in the region between two parallel, closely spaced flat plates, was recently described in a paper by Saffman and Taylor (**1**). In particular, they studied the propagation of a long finger of fluid through a parallel-sided channel in a Hele–Shaw apparatus containing a more viscous liquid. The boundary conditions at the interface depend on the interfacial tension as well as on the viscosities of the two fluids, but the exact nature of this dependence is unknown. To calculate the flow in the Hele–Shaw apparatus, however, only the change in pressure on passing through the interface and the thickness of the two layers of the more viscous fluid which are left behind adhering to the flat plates after the interface has passed are required. In (**1**) it was shown that the simplifying assumption that both of these are constant leads to an exact solution in closed form for the propagation of a semi-infinite finger.

Actually, it was found that there exists a whole family of solutions corresponding to different values of the velocity of the finger and its asymptotic width. An experimental investigation showed that the width of fingers when the flow was not very slow was close to one-half that of the channel, and excellent agreement was found between the observed shape and the calculated one which was half the channel width. (At very

THE QUARTERLY JOURNAL OF MECHANICS AND APPLIED MATHEMATICS

THE QUARTERLY JOURNAL OF MECHANICS AND APPLIED MATHEMATICS is published at 18*s.* net for a single number with an annual subscription (for four numbers) of 60*s.* post free.

NOTICE TO CONTRIBUTORS

1. *Communication.* Papers should be communicated to Dr. D. M. A. Leggett, Department of Mathematics, King's College, Strand, London, W.C.2.

If possible, to expedite publication, papers should be submitted in duplicate.

2. *Presentation.* Papers should be typewritten (double spacing) and should be preceded by a summary not exceeding 300 words in length. References to literature should be given in standard order, *author, title of journal, volume number, date, page.* These should be placed at the end of the paper and arranged according to the order of reference in the paper.

3. *Diagrams.* The number of diagrams should be kept to the minimum consistent with clarity. The lines of the figures should be drawn in ink either on draughtsman's paper or on good quality white paper. Each individual line in the figure should bear reducing to one-half of the size of the original, and great care should be exercised to see that the lines are regular in thickness, especially where they meet. Lettering of the figure should be in pencil and should be sufficient to define clearly the lines and curves in it. The writing of formulae or of explanations on the diagram itself should be avoided. All explanations of symbols, etc., should be given in underline. Contributors should indicate on their manuscripts where figures should be inserted.

4. *Tables.* Tables should preferably be arranged so that they can be printed with the columns parallel to the longer edge of the page.

5. *Notation.* All single letters used to denote vectors in the manuscript should be marked by underlining with a wavy line. Scalar and vector products should be denoted by $\underset{\sim}{a} . \underset{\sim}{b}$ and $\underset{\sim}{a} \times \underset{\sim}{b}$ respectively. Real and imaginary parts of complex quantities should be denoted by re and im respectively.

6. *Offprints.* Authors of papers will be entitled to 25 free offprints. This number is available for sharing between authors of joint papers.

7. All correspondence other than that dealing with contributions should be addressed to the publishers:

OXFORD UNIVERSITY PRESS
AMEN HOUSE, LONDON, E.C.4

A NOTE ON THE MOTION OF BUBBLES IN A HELE-SHAW CELL AND POROUS MEDIUM

By SIR GEOFFREY TAYLOR *and* P. G. SAFFMAN

(*Cavendish Laboratory, Cambridge*)

[Received 12 August 1958. Revise received 13 November 1958]

SUMMARY

Exact solutions are presented for the steady motion of a symmetrical bubble through a parallel-sided channel in a Hele–Shaw cell containing a viscous liquid. The solutions also describe two-dimensional motion in a porous medium, since the two cases are mathematically analogous. It is shown that the solutions are not mathematically unique and a purely analytical criterion for specifying a particular solution is given. When the bubble is large, these particular solutions are such that the maximum width of the bubble is almost half that of the channel. Solutions are also presented for the motion of large asymmetric bubbles through the channel. The three-dimensional motion of bubbles in a porous medium of infinite extent is also considered briefly.

1. Introduction

THE motion of the interface between two immiscible viscous fluids in a Hele–Shaw cell, that is, in the region between two parallel, closely spaced flat plates, was recently described in a paper by Saffman and Taylor (1). In particular, they studied the propagation of a long finger of fluid through a parallel-sided channel in a Hele–Shaw apparatus containing a more viscous liquid. The boundary conditions at the interface depend on the interfacial tension as well as on the viscosities of the two fluids, but the exact nature of this dependence is unknown. To calculate the flow in the Hele–Shaw apparatus, however, only the change in pressure on passing through the interface and the thickness of the two layers of the more viscous fluid which are left behind adhering to the flat plates after the interface has passed are required. In (1) it was shown that the simplifying assumption that both of these are constant leads to an exact solution in closed form for the propagation of a semi-infinite finger.

Actually, it was found that there exists a whole family of solutions corresponding to different values of the velocity of the finger and its asymptotic width. An experimental investigation showed that the width of fingers when the flow was not very slow was close to one-half that of the channel, and excellent agreement was found between the observed shape and the calculated one which was half the channel width. (At very

low flow rates, the observed shapes had a width greater than one-half that of the channel and did not conform with the calculated shapes having the same width. In this case it appears that the assumption that the pressure change across the interface is constant is not valid.)

The primary purpose of the present note is to give the mathematical solution of the problem in which a bubble of finite size, i.e. a bubble bounded by a closed contour as opposed to the infinite ones considered in (**1**), moves steadily through a parallel-sided channel in a Hele–Shaw cell containing another viscous fluid, under the same simplifying assumptions about the boundary conditions at the interface. Such bubbles sometimes occurred in the experiments described in (**1**), although it was usually desirable to remove them, and the solution may not be without practical interest. However, it appears that the range of circumstances for which the solution is a reasonably close description of the actual motion is somewhat more restricted than for the long fingers. This is because, for reasons not yet fully understood, the physical conditions at the rear of the bubble, where the interface is retreating, may be different from those at the front where the interface is advancing, except in the case of very slow motion where very little fluid is left behind after the passage of the interface; but then the assumption of a constant pressure drop across the interface becomes less accurate.

The analysis, therefore, is probably mainly of academic interest, but nevertheless may give a fair approximation to the shape of the front of the bubble where the assumptions are likely to be reasonable; this approximation will be better the larger the bubble, and a long finger can indeed be regarded as the front of a very large bubble. Also, for the case of very slow motion and a bubble whose dimensions are small compared with the width of the channel, the pressure change across the interface due to surface tension and the interfacial curvature in the plane of the flat sides of the cell can be taken into account and the analysis should not be without physical significance.

It is found that for bubbles of given area and for given conditions at infinity the solution is not unique, and that there exists a whole family of possible solutions. It is worth noting, however, that for the case in which the viscosity of the fluid inside the bubble and hydrostatic pressure gradients are negligible, a particular solution can be singled out by imposing arbitrarily the condition that the product of the velocity and maximum width of the bubble is a minimum. For very large bubbles, whose front portion resembles a long finger, the width given in this way is half that of the channel, in agreement with the experiments, but a satisfactory physical explanation of this result has not been found. For

very small bubbles, the solution selected in this way is that bounded by a circular contour.

The analysis of bubbles of finite size is restricted, for the sake of simplicity, to bubbles which are symmetrical about the centre line of the channel. Solutions will be presented, however, for the steady motion of very large asymmetric bubbles, that is, of long fingers similar to those considered in (**1**). The general asymmetric case seems to be capable of solution, but it did not appear to be of sufficient interest to justify the labour involved.

The motion in a Hele–Shaw cell is mathematically analogous to two-dimensional flow in a porous medium in which the motion is governed by Darcy's law. Simple closed solutions exist for the three-dimensional motion of bubbles in a porous medium of infinite extent, according to which the bubbles are ellipsoids of revolution. It is noted in section 7 that the particular solution for which the bubble is a sphere is singled out by a minimum condition similar to that just mentioned above.

2. Motion of a bubble in a Hele-Shaw cell

In this section the analysis of the steady motion of a bubble in a parallel-sided channel in a Hele–Shaw cell is presented for the case in which the bubble is symmetrical about the centre line of the channel. We suppose first that the viscosity of the fluid inside the bubble is negligible and that pressure gradients due to gravity may be ignored (this will be so if the cell is horizontal). The mean velocity across the stratum of the viscous fluid through which the bubble is moving is given by

$$u = -\frac{b^2}{12\mu}\frac{\partial p}{\partial x} = \frac{\partial \phi}{\partial x} = \frac{\partial \psi}{\partial y}, \qquad v = -\frac{b^2}{12\mu}\frac{\partial p}{\partial y} = \frac{\partial \phi}{\partial y} = -\frac{\partial \psi}{\partial x} \tag{1}$$

(see, for example, Lamb (**2**) section 330), where x and y are coordinates in the plane of the plates bounding the cell, u and v are the components of mean velocity parallel to these axes, p is the pressure, μ the viscosity, $\phi = -(b^2/12\mu)p$ is a velocity potential, ψ is the stream function (which exists by virtue of the equation of continuity), and the gap between the plates b is assumed sufficiently small for (1) to hold. (Equations (1) are satisfied by the two-dimensional flow in a porous medium of permeability $b^2/12$.)

Taking the walls of the channel as $y = \pm 1$ and supposing the viscous fluid has unit velocity at infinity in front of and behind the bubble, ϕ and ψ satisfy the conditions

$$\psi = \pm 1 \quad \text{on} \quad y = \pm 1, \qquad \phi \to x \quad \text{as} \quad x \to \pm\infty \tag{2}$$

(edge effects which invalidate (1) within a distance of order b from the channel walls are neglected).

To obtain boundary conditions satisfied by ϕ and ψ on the interface, we first assume that the pressure drop across the interface is constant. When the fluid inside is of negligible viscosity, the pressure inside is constant and hence

$$\phi = \text{const.} = 0, \quad \text{say,} \tag{3}$$

on the interface. The other assumption is that there is no film of viscous fluid left behind between the bubble and the plates bounding the cell, i.e. the advancing interface expels all the viscous fluid in front of it, from which it follows that the velocity of the interface normal to itself is equal to the component of the mean velocity in the same direction. Expressed analytically, this is

$$\frac{\partial \phi}{\partial n} = \frac{\partial \psi}{\partial s} = U \frac{\partial y}{\partial s}, \tag{4}$$

where n, s denote differentiation in the normal and tangential directions, respectively, and U is the velocity of the bubble. Integrating (4) and noting that the arbitrary constant of integration is zero because the bubble is supposed to be symmetrical about $y = 0$ gives, finally,

$$\psi = Uy \quad \text{on} \quad \phi = 0. \tag{5}$$

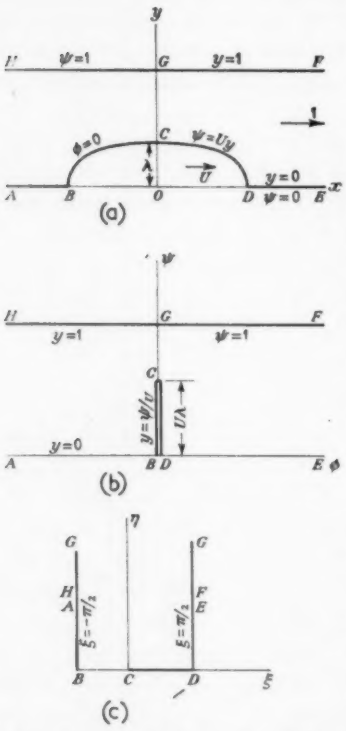

FIG. 1. The motion of a bubble through a channel: (*a*) physical plane, (*b*) potential plane, (*c*) transformed potential plane.

A discussion of these assumptions is given in (**1**). It is also shown there how, by a simple transformation, the solution for the case in which there is a film of *constant* thickness between the bubble and the plates may be obtained from that in which the films are of zero thickness.

Now it follows from (1) that $w = \phi + i\psi$ is an analytic function of $z = x + iy$, and the solution of the problem is therefore effected by constructing an analytic function of z which satisfies the boundary conditions expressed in (2) and (5). In Fig. 1 (*a*) is shown the upper half of the physical plane; the maximum half-width of the bubble is denoted by λ.

The potential plane, the boundaries of which are given by (2) and (5), is shown in Fig. 1 (*b*), corresponding points being marked with the same letter. Note that we must have $U\lambda < 1$ in order that the potential and physical planes should be simple images of one another. The transformation

$$i\cos\zeta = \tanh(\tfrac{1}{2}\pi w)\cot(\tfrac{1}{2}\pi U\lambda),$$

where $\zeta = \xi + i\eta$, transforms the potential plane into the semi-infinite strip $\eta > 0$, $-\frac{1}{2}\pi < \xi < \frac{1}{2}\pi$, shown in Fig. 1 (*c*), corresponding points again being marked with the same letter. At the bubble interface, where $\phi = 0$ and $\eta = 0$, this transformation may be written as

$$\psi = \frac{2}{\pi}\tan^{-1}(\cos\xi\tan\tfrac{1}{2}\pi U\lambda).$$

Writing $z = w + z_1$, $z_1(\zeta) = x_1(\xi,\eta) + iy_1(\xi,\eta)$, we find that the boundary conditions (2) and (5) become in the ζ-plane,

$$y_1 = 0 \quad \text{on} \quad \xi = \pm\tfrac{1}{2}\pi, \tag{6}$$

and

$$y_1 = \psi\left(\frac{1}{U} - 1\right) = -\frac{4}{\pi}\frac{U-1}{U}\operatorname{im}\tanh^{-1}(ie^{i\xi}\tan\tfrac{1}{4}\pi U\lambda). \tag{7}$$

Here we have used the general formula

$$\tanh^{-1}(a+ib) = \tfrac{1}{2}\tanh^{-1}\left(\frac{2a}{1+a^2+b^2}\right) + \tfrac{1}{2}i\tan^{-1}\left(\frac{2b}{1-a^2-b^2}\right).$$

It may now be verified directly that

$$z_1 = -\frac{4}{\pi}\frac{U-1}{U}\tanh^{-1}(ie^{i\zeta}\tan\tfrac{1}{4}\pi U\lambda) \tag{8}$$

is regular in the strip and satisfies (6) and (7). The velocity potential and stream function are therefore given implicitly in terms of x and y by (expressing ζ in terms of w)

$$z = w + \frac{4}{\pi}\frac{U-1}{U}\tanh^{-1}\left[\frac{\tan(\frac{1}{4}\pi U\lambda)}{\tan(\frac{1}{2}\pi U\lambda)}\{(\tanh^2\tfrac{1}{2}\pi w + \tan^2\tfrac{1}{2}\pi U\lambda)^{\frac{1}{2}} - \tanh\tfrac{1}{2}\pi w\}\right]. \tag{9}$$

Since the fluid inside the bubble is of negligible viscosity, the bubble will move faster than the fluid at infinity, i.e. $U > 1$. Mathematically, this result arises as the condition that the transformation (9) be one-one (as may be seen without difficulty by considering the relation between x and ϕ on the axis $\psi = 0$).

The interface is the image in the physical plane of $\phi = 0$, $-U\lambda < \psi < U\lambda$,

and has the equation (remembering that $\psi = Uy$ and making use of the expression for the real part of $\tanh^{-1}(a+ib)$)

$$x = \frac{2}{\pi}\frac{U-1}{U}\tanh^{-1}\{\sin^2(\tfrac{1}{2}\pi U\lambda) - \cos^2(\tfrac{1}{2}\pi U\lambda)\tan^2(\tfrac{1}{2}\pi Uy)\}^{\frac{1}{2}}. \tag{10}$$

The length BOD of the bubble is

$$\frac{4}{\pi}\frac{U-1}{U}\tanh^{-1}\{\sin(\tfrac{1}{2}\pi U\lambda)\} = L, \text{ say},$$

and the area bounded by the interface, i.e. by the closed contour given by (10), can be shown to be (see the Appendix)

$$\frac{16}{\pi}\frac{U-1}{U^2}\tanh^{-1}\{\tan^2(\tfrac{1}{4}\pi U\lambda)\} = S, \text{ say}. \tag{11}$$

The analytical solution (9) contains two parameters, U (the velocity of the bubble) and λ (its maximum half-width), and it is clear that specifying the area S of the bubble provides only one relation between them. That is, if the area of the bubble and the velocity at infinity are specified, then there exists a whole family of solutions and possible bubble shapes corresponding to the various combinations of U and λ which satisfy (11). The extreme shapes are $\lambda = 0$, for which $U = \infty$, $L = \infty$, and the bubble has zero thickness; and $\lambda = 1$, for which $U = 1$ (since $U\lambda \not> 1$) and the velocity everywhere is equal to the velocity at infinity. In the latter case, the bubble is bounded by the channel walls and the lines $x = \pm\frac{1}{2}L = \pm\frac{1}{4}S$. The shapes intermediate between these are ovals of length L and width 2λ, moving with velocities between $U = 1$ and $U = \infty$.

If $U\lambda \to 1$, keeping U fixed, the area of the bubble becomes very large and it is easily seen, changing the origin to the vertex of the bubble, that we recover the solution obtained in (1) for the motion of a long finger whose asymptotic width is λ times that of the channel, namely,

$$z = w + \frac{2}{\pi}(1-\lambda)\log\tfrac{1}{2}\{1+\exp(-\pi w)\}. \tag{12}$$

3. The hypothesis of minimum $U\lambda$

Although the motion of a bubble in a channel does not possess, when formulated as above, a mathematically unique solution, we should expect it to be physically unique and that there is some mechanism, not accounted for in the analysis, to single out one particular solution. The search for some such effect has so far been unsuccessful, but several features of the analysis which distinguish a particular solution have been noticed. One of these is as follows.

Writing (11) in the form

$$S = \frac{16}{\pi}\frac{\lambda(U\lambda-\lambda)}{U^2\lambda^2}\tanh^{-1}\{\tan^2(\tfrac{1}{4}\pi U\lambda)\},$$

it follows that S is a maximum for given $U\lambda$ and varying λ when $\lambda = \frac{1}{2}U\lambda$, i.e. when $U = 2$. Alternatively, $U\lambda$ is a minimum for given S and varying U when $U = 2$. Thus, if we make the hypothesis that the motion is such that $U\lambda$ is a minimum, then the bubble whose velocity is twice that at infinity is selected, and the corresponding value of λ is given by (11) with $U = 2$.

The product $U\lambda$ of the velocity of the bubble and half its maximum width does not have a clear physical significance, although it may be identified intuitively with the rate at which fluid is pushed aside by the bubble. We have in fact been unable to place the hypothesis on a sound physical basis (attempts to relate it to a minimum rate of energy dissipation fail), but it has the interesting feature that when the bubble is large and $U\lambda$ is close to 1, it gives a value for λ close to $\frac{1}{2}$, and this is the value observed experimentally with long fingers.

It is perhaps worth mentioning, as a curiosity, that the shape for $U = 2$ arises as the unique solution of a problem in the steady two-dimensional flow of an electric current in a uniform conducting medium. Suppose [see Fig. 1 (*a*)] that HF and AOE are two parallel electrodes at unit potential difference, separated by a medium of uniform conductivity, and that a perfect conductor of given area is laid on AE, the boundary of this conductor being $BCDOB$ in the figure. If we now determine the shape of this conductor so that the amount of current entering it, i.e. flowing across the curvilinear boundary BCD, is a minimum, then it turns out (the details of the analysis are omitted for brevity) that the conductor has the same shape as the bubble of the same area for which $U = 2$.

Another unique feature of the solution for a semi-infinite finger which is half the channel width may perhaps also be mentioned here. As has been pointed out by Zhuralev (**3**), the velocity potential due to the superposition of a uniform stream of inviscid fluid in a channel bounded by parallel walls $y = \pm 1$ and a two-dimensional source of strength m placed midway between the walls at the origin of coordinates is

$$w = qz + \frac{m}{2\pi}\log(2\sinh\tfrac{1}{2}\pi z), \tag{13}$$

where q is the velocity of the stream (a different coordinate system is used in (**3**) and the expression given there is accordingly different).

It will be noticed that (12) and (13) would be closely similar if z and w

were interchanged in one of them. Now (12) may be written

$$e^{-\pi w} - 2e^{-\pi w/2(1-\lambda)} e^{\pi z/2(1-\lambda)} + 1 = 0$$

which can be solved explicitly for w when $\lambda = \frac{1}{2}$, giving

$$w = \tfrac{1}{2}z' + \frac{1}{\pi}\log(2\sinh \tfrac{1}{2}\pi z'),$$

where $z' = z - (\log 2)/\pi$. This last expression is identical with (13) when $m = 4q$, except for a change of origin and a multiplicative constant. That is, the potential for a finger which is half the channel width is identical with that arising from the superposition of a uniform stream and source of appropriate strengths; and only the finger with $\lambda = \frac{1}{2}$ can be obtained in this simple way.† (It can be shown that the potential for a finger for which $\lambda \neq \frac{1}{2}$ arises from a rather complicated system of sources, sinks, and dipoles superposed on a uniform stream.)

Further, the dividing streamline of the flow due to a source in a uniform stream can be shown to have the equation

$$x = \frac{1}{\pi}\log\left(\frac{\sin \pi y/\lambda}{\sin(1-\lambda)\pi y/\lambda}\right),$$

where $2\lambda = 4m/(4q+m)$ is its asymptotic width; equation (13) can be interpreted as giving the flow past a fixed obstacle of this shape in the channel. Similarly, by taking axes fixed relative to the finger, we can deduce from (12) the flow past a fixed obstacle having the same shape as the finger, this shape having the equation (see **1**)

$$x = \frac{1-\lambda}{\pi}\log \tfrac{1}{2}\left(1+\cos\frac{\pi y}{\lambda}\right) = \frac{2(1-\lambda)}{\pi}\log\left(\cos\frac{\pi y}{2\lambda}\right).$$

When $\lambda = \frac{1}{2}$, the shapes of these obstacles are identical.

4. The motion of small bubbles

When λ is small compared with 1 and U is finite, the dimensions of the bubble are small compared with the width of the channel, and (10) reduces to

$$\frac{x^2}{(U-1)^2} + y^2 = \lambda^2. \tag{14}$$

That is, small bubbles are ellipses with axis ratio $U-1$. The solution for a small bubble is obtained, in effect, by letting the width of the channel tend to infinity, so that (14) gives the shape of a bubble in an unbounded

† This result for the potential of the motion outside the finger remains true if the fluid inside the finger is not of negligible viscosity, the effect of gravity is taken into account and it is supposed that layers of fluid of constant thickness are left behind after the passage of the interface. However, the values of q and m will depend upon the particular circumstances.

Hele–Shaw cell. The corresponding complex potential is

$$z = \frac{U-1}{U}(w^2+U^2\lambda^2)^{\frac{1}{2}}+\frac{w}{U}.$$

The bubble of given size with a minimum value of $U\lambda$ is a circle of radius λ moving with twice the velocity at infinity. Now the analysis has been based on the assumption that the pressure drop across the interface is constant. This pressure drop consists of a term T/R, where T is the interfacial tension and R is the radius of curvature of the projection of the interface onto the plates bounding the cell, plus a term due to the curvature of the meniscus in a plane perpendicular to the bounding plates. A necessary condition for this assumption to be valid is that variations in T/R should be small compared with changes in the pressure of the fluid surrounding the bubble, that is, small compared with $12\mu UR/b^2$ (this condition may not be sufficient). When the bubble is small, this condition may not be satisfied, but it is interesting that the circular bubble remains an exact solution when the T/R term is taken into account, since R is then constant.

This effect of surface tension tends to make the perimeter of the bubble as short as possible, and therefore to make the bubble circular. It is noteworthy that in this case this effect of surface tension and the condition of minimum $U\lambda$ give the same result.

Visual observations of small bubbles which occurred during the experiments reported in (**1**) indicated that they were circular when sufficiently small. When larger, they were often pear-shaped with a rounded front and pointed back; some on the other hand seemed to be ovoid with the sharper end pointed in the direction of motion. These phenomena are probably due to the physical conditions at the retreating interface over the back of the bubble being different from those at the front; there is, however, no clear evidence on this matter.

5. Bubbles of fluid with non-zero viscosity

The previous analysis has been concerned entirely with the case in which the viscosity of the fluid inside the bubble is negligible and gravity forces are ignored. We shall now suppose that the fluid inside the bubble has a non-zero viscosity, that the x-axis is vertically upwards parallel to the channel walls, and that gravity forces are acting. The mean velocity across the stratum between the plates is now derived from a velocity potential

$$\phi = -\frac{b^2}{12\mu}(p+\rho gx),$$

where ρ is the density of the fluid and g is the acceleration of gravity.

We shall denote quantities inside the bubble by the suffix 2 and quantities outside by the suffix 1. The boundary conditions (2), (3), and (5) now become (still making the same simplifying assumptions about the physical conditions at the interface)

$$\psi_1 = \pm V \quad \text{on} \quad y = \pm 1, \qquad \phi_1 \to Vx \quad \text{as} \quad x \to \pm\infty, \tag{2}'$$

where the velocity at infinity is now denoted by V; also

$$\mu_1\phi_1 + \frac{b^2\rho_1 gx}{12\mu} = \mu_2\phi_2 + \frac{b^2\rho_2 gx}{12\mu}, \tag{3}'$$

$$\psi_1 = \psi_2 = Uy, \tag{5}'$$

on the interface.

It follows from (5)′ that the motion inside the bubble is given by

$$\phi_2 = Ux, \quad \psi_2 = Uy. \tag{15}$$

After some algebra we find that Φ and Ψ defined by

$$W = \Phi + i\Psi = \frac{\phi_1 + i\psi_1 - U^*z}{V - U^*}, \tag{16}$$

where

$$U^* = \frac{\mu_2 U}{\mu_1} - \frac{b^2 g}{12\mu_1}(\rho_1 - \rho_2), \tag{17}$$

satisfy (2), (3), and (5) with U replaced by

$$\frac{U - U^*}{V - U^*} = U', \quad \text{say.}$$

The expressions (9) and (10) with U replaced by U' therefore give the relation between z and W and also the equation of the interface. In particular, it is to be noted that the family of possible shapes is independent of the physical properties of the fluid.

The particular solution with $U' = 2$ (and λ close to $\frac{1}{2}$ for large bubbles) is now obtained by minimizing $U'\lambda$ for given bubble size. U^* is the velocity with which the fluid outside the bubble would move under the action of the actual pressure gradient inside the bubble, and the hypothesis of minimum $U\lambda$ has to be replaced by an hypothesis in which velocities are measured relative to U^*. The physical significance of this result is not clear.

6. Penetration of an asymmetrical finger into a channel

In this section we shall give solutions of the equations of motion which describe the steady motion of bubbles not symmetrical about the centre line of the channel for the case in which the bubble is very large and may be regarded as a semi-infinite finger. The motion of symmetrical fingers was considered in (1), and it was stated that there exists a singly infinite family of solutions for the problem of the penetration of a finger into a

channel filled with a more viscous fluid. This statement is in fact erroneous, and was made because it was not realized that further asymmetrical solutions existed. Actually, there exists a doubly infinite family of steady solutions, of which the symmetrical ones form a singly infinite sub-set, and it was thought worthwhile describing these here.

It has already been noted that the question as to why long fingers formed experimentally are half the channel width, when their velocity is not too slow, remains unanswered, although several criteria of a purely mathematical nature have been discovered; the further question now arises as to why these fingers are apparently symmetrical, and a satisfactory answer has yet to be found.

It will be supposed in the analysis that the viscosity of the fluid inside the finger is negligible and that gravity may be neglected. The solutions for the more general case may be obtained immediately by methods identical with those employed in section 5 above. (It is also assumed that no fluid is left behind adhering to the flat plates bounding the Hele–Shaw apparatus after the interface has passed by. Solutions for the case in which films of constant thickness are left behind may be derived in the manner described in (**1**).) We employ the same notation here as in section 2, except that the origin of coordinates will no longer be the centre of the bubble.

The velocity potential satisfies

$$\phi = 0 \tag{3}$$

on the interface, by virtue of the assumption that the pressure drop across it is constant. For the stream function, the boundary condition (4) now integrates to

$$\psi = U(y-y_0) \tag{18}$$

where U is the velocity of propagation of the finger and y_0 is a constant whose value is as yet unspecified. (y_0 may be taken positive without loss of generality, solutions with y_0 negative being mirror images in $y = 0$ of those with y_0 positive.) Taking unit velocity at infinity ahead of the finger, we have the further conditions $\phi \sim x$, $\psi \sim y$ as $x \to +\infty$.

The symmetrical solutions are obtained by putting $y_0 = 0$. It was shown in (**1**) that the complex potential for the steady motion of a symmetric semi-infinite finger is given by equation (12), where λ is the ratio of the asymptotic width of the finger to that of the channel and the velocity of propagation $U = 1/\lambda$. The equation of the interface (i.e. the image of $\phi = 0$) may be written in the form

$$x = \frac{2(1-U^{-1})}{\pi} \log(\cos \tfrac{1}{2}\pi U y), \tag{19}$$

the origin of coordinates being taken at the nose of the finger. The potential plane (see Fig. 6 of (1)) is the semi-infinite strip $\phi > 0$, $-1 < \psi < 1$; the line $\phi = 0$, $-1 < \psi < 1$ is the image of the interface, and the lines $\phi > 0$, $\psi = \pm 1$ of the channel walls.

The method by which the symmetrical solutions are obtained may be extended with little difficulty to deal with the asymmetrical case in which the boundary condition (18) applies. We have that x and y are conjugate harmonic functions of ϕ and ψ such that $y = \pm 1$ on $\psi = \pm 1$, $\phi > 0$; $y \sim \psi$ as $\phi \to +\infty$; and $y = U^{-1}\psi + y_0$ on $\phi = 0$, $-1 < \psi < 1$. Take therefore

$$y = \psi + \sum_{n=1}^{\infty} A_n e^{-n\pi\phi} \sin n\pi\psi + \sum_{n=1}^{\infty} B_n e^{-\frac{1}{2}n\pi(\psi+1)} \sin \tfrac{1}{2}n\pi(\psi+1),$$

thereby satisfying the boundary conditions on $\psi = \pm 1$ and at $\phi = \infty$. The boundary condition on $\phi = 0$ is satisfied if

$$U^{-1}\psi + y_0 = \psi + \sum_{1}^{\infty} A_n \sin n\pi\psi + \sum_{1}^{\infty} B_n \sin \tfrac{1}{2}n\pi(\psi+1) \quad (-1 < \psi < 1).$$

Calculating A_n and B_n by the usual method of Fourier series, we find that

$$A_n = -\frac{2}{n\pi}(1 - U^{-1}), \qquad B_n = \frac{2y_0}{n\pi}\{1 - (-1)^n\}.$$

The series for $z = x + iy$ may be summed, giving finally

$$z = w + \frac{2}{\pi}(1 - U^{-1}) \log \tfrac{1}{2}(1 + e^{-\pi w}) + \frac{2y_0}{\pi} \log\left(\frac{1 + ie^{-\frac{1}{2}\pi w}}{1 - ie^{-\frac{1}{2}\pi w}}\right). \tag{20}$$

The interface is the image of $\phi = 0$ and has the equation (remembering that $\psi = U(y - y_0)$)

$$x = \frac{2}{\pi}(1 - U^{-1}) \log \cos \tfrac{1}{2}\pi U(y - y_0) + \frac{2y_0}{\pi} \log \tan\{\tfrac{1}{4}\pi + \tfrac{1}{4}\pi U(y - y_0)\}. \tag{21}$$

Now it may be verified that the transformation (20) is one-one and free from singularities if $U > 1$ and $y_0 + U^{-1} < 1$. The former of these conditions is clear physically because the fluid in the finger is less viscous than that in the channel. The latter condition arises from the fact that all the streamlines must originate on the interface (simply by continuity, because the velocity of the fluid at $x = -\infty$ is zero since conditions must be uniform along the straight sides of the finger; hence $\phi = 0$ for all y at $x = -\infty$). Hence, the value of y at the point where the streamline $\psi = 1$ meets the interface must be less than one, and by (18) this value is $y_0 + U^{-1}$. y_0 is in fact the value of y at the point where the streamline $\psi = 0$ meets the interface.

As regards the shape of the interface given by (21), we note that as $y \to y_0 + U^{-1}$, $x \sim (1 - U^{-1} - y_0) \log(y_0 + U^{-1} - y) \to -\infty$; and as $y \to y_0 - U^{-1}$,

$x \sim (1-U^{-1}+y_0)\log(y-U^{-1}+y_0) \to -\infty$. The interface therefore has the two asymptotes $y = y_0+U^{-1}$, $y = y_0-U^{-1}$, and lies between them, being nearer the wall $y = 1$ than the wall $y = -1$. The asymptotic width of the finger is $2U^{-1} = 2\lambda$, say. The interface for the values $U = 2$, $y_0 = \frac{1}{4}$ is sketched in Fig. 2.

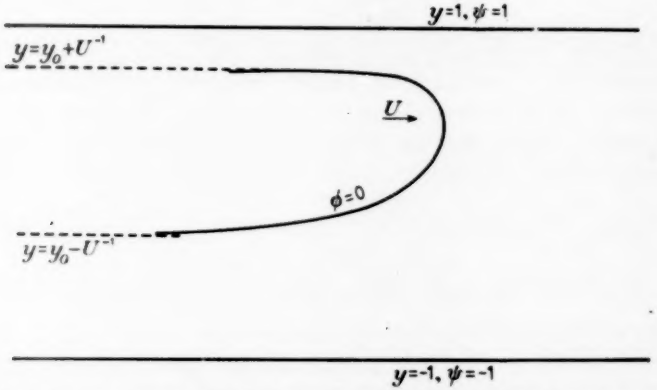

FIG. 2. An asymmetric finger penetrating a channel. The interface is calculated from (21) with $U = 2$, $y_0 = \frac{1}{4}$.

If $y_0+U^{-1} = 1$, the interface intersects the wall $y = 1$ at right angles. In this case, the interface is half of a symmetrical finger between the walls $y = -1$ and $y = 3$, as is clear from the fact that (21) may then be written in the form

$$\tfrac{1}{2}x = \frac{2}{\pi}(1-U^{-1})\log\cos\tfrac{1}{4}\pi U(y-1).$$

There is no feature of the analysis which specifies the values of λ (or U) and y_0, and therefore there is a doubly infinite family of mathematical solutions for the penetration of a finger into a channel containing a more viscous fluid. It remains to explain why the fingers obtained in the experiments described in (1) appear to conform with the shape calculated from $\lambda = \frac{1}{2}$, $y_0 = 0$.

7. Bubbles in three dimensions

Provided that the same simplifying assumptions are made about the physical conditions at the interface, the motion in three dimensions of a bubble in a uniform unbounded porous medium, filled with viscous fluid moving uniformly at infinity, and in which the motion is governed by Darcy's law, possesses simple solutions in which the interface is an ellipsoid of revolution. These solutions are briefly referred to in an article by Polubarinova-Kochina and Falkovich (4), but since they are apparently

not well-known, it was thought worthwhile to present the results in a more general form than hitherto, and to point out the lack of uniqueness.

If $\mathbf{V}$ denotes the velocity at infinity, $\mathbf{U}$ the velocity of the bubble, $\mathbf{g}$ the acceleration due to gravity, and

$$\mathbf{U}^* = \frac{k}{\mu_1}\left\{(\rho_2-\rho_1)\mathbf{g}-\frac{\mu_2}{k}\mathbf{U}\right\},$$

where k is the permeability of the medium and the suffixes 1 and 2 refer to the fluid outside and inside the bubble, respectively, then the boundary conditions that the pressure and normal velocity are continuous across the interface can be satisfied by taking the bubble as any ellipsoid of revolution with axis parallel to $\mathbf{U}-\mathbf{U}^*$. The relation between $\mathbf{U}$ and $\mathbf{V}$ is

$$\left(\tfrac{1}{2}\log\frac{1+e}{1-e}-e\right)(\mathbf{U}-\mathbf{U}^*) = \frac{e^3}{1-e^2}(\mathbf{V}-\mathbf{U}^*) \quad \text{(prolate ellipsoid)},$$

$$(e-(1-e^2)^{\frac{1}{2}}\sin^{-1}e)(\mathbf{U}-\mathbf{U}^*) = e^3(\mathbf{V}-\mathbf{U}^*) \quad \text{(oblate ellipsoid)},$$

where e is the eccentricity of a meridian section.

The solution for a bubble of given volume is again mathematically not unique, but a particular solution is singled out by the hypothesis that the product of the equatorial area A and the velocity measured relative to $\mathbf{U}^*$ should be a minimum for a bubble of given size and for a given velocity at infinity relative to $\mathbf{U}^*$, i.e. that

$$A\,|\mathbf{U}-\mathbf{U}^*|\,/\,|\mathbf{V}-\mathbf{U}^*|$$

is a minimum. The bubble shape is then spherical and $\mathbf{U}-\mathbf{U}^* = 3(\mathbf{V}-\mathbf{U}^*)$; this solution remains exact if interfacial stress effects are present whose effect is to produce a pressure drop proportional to the interfacial curvature. There does not appear to be at present any experimental evidence on the motion of bubbles in porous media.

APPENDIX

To calculate the area bounded by the contour given by equation (10), we note that on the interface (where $\phi = 0$ and $\psi = Uy$),

$$x_1 = x-\phi = x \quad \text{and} \quad y_1 = y-\psi = -y(U-1).$$

Hence, we have from (8)

$$x-(U-1)y = -\frac{4}{\pi}\frac{U-1}{U}\tanh^{-1}\{ie^{i\xi}\tan(\tfrac{1}{4}\pi U\lambda)\}$$

$$= -\frac{4}{\pi}\frac{U-1}{U}\sum_{n=0}^{\infty}\frac{i(-1)^n e^{i(2n+1)\xi}\tan^{2n+1}(\frac{1}{4}\pi U\lambda)}{2n+1}$$

on the interface (remembering that $\eta = 0$ there). The equation of the interface may

therefore be expressed parametically by

$$x = \frac{4}{\pi}\frac{U-1}{U}\sum_{0}^{\infty}(-1)^n \frac{\sin(2n+1)\xi \tan^{2n+1}(\frac{1}{4}\pi U\lambda)}{2n+1},$$

$$y = \frac{4}{\pi U}\sum_{0}^{\infty}(-1)^n \frac{\cos(2n+1)\xi \tan^{2n+1}(\frac{1}{4}\pi U\lambda)}{2n+1},$$

and the complete contour corresponds with $-\pi < \xi < \pi$. These series are uniformly convergent if $\tan(\frac{1}{4}\pi U\lambda) < 1$, which is the case if the bubble dimensions are finite. We have now

$$S = \int_{-\pi}^{\pi} y\frac{dx}{d\xi}\,d\xi = \frac{16}{\pi}\frac{U-1}{U^2}\sum_{0}^{\infty}\frac{\tan^{4n+2}(\frac{1}{4}\pi U\lambda)}{2n+1} = \frac{16}{\pi}\frac{U-1}{U^2}\tanh^{-1}(\tan\tfrac{1}{4}\pi U\lambda)^2,$$

by virtue of the relations

$$\int_{-\pi}^{\pi}\cos m\xi\cos n\xi\,d\xi = 0 \quad \text{if } m \neq n$$
$$= \pi \quad \text{if } m = n.$$

REFERENCES

1. P. G. Saffman and Sir Geoffrey Taylor, *Proc. Roy. Soc.* A, **245** (1958) 312.
2. H. Lamb, *Hydrodynamics*, 6th ed. (Cambridge, 1932).
3. P. A. Zhuralev, *Zap. Leningr. Gorn. In-ta.* **33** (1956) 54.
4. P. Ya. Polubarinova-Kochina and S. B. Falkovich, *Advances in Appl. Mech.* **2** (1951) 153.

MOTIONS WITH INITIAL GRADIENT

By ST. I. GHEORGHITZA (*University of Bucharest*)

[Received 22 May 1958]

SUMMARY

This paper is concerned with the motion of incompressible fluids in a porous medium taking place only when the modulus of the gradient of the dynamic pressure surpasses a given value. The equation (12) which is satisfied by the function ϕ defined by (1) and (3) is deduced.

A general approximate method of solution is described, and some particular exact solutions are obtained.

1. Introduction

A DETAILED study of the motions in porous media shows that Darcy's law, or the linear law, expressed by the relation

$$\mathbf{v} = -k\,\mathrm{grad}\left(\frac{p}{\rho g}+z\right) \equiv -k\,\mathrm{grad}\,H, \text{ say,} \tag{1}$$

in the case of isotropic media, is valid only over a limited range of velocities. In particular for very small velocities the fluid is moving more slowly than is required by (1). Consequently, a limiting velocity may exist under which (1) ceases to be valid. We must mention that, at the same time as Darcy, Schmidt (see **1**), by studying the motion through animal membranes, found that fluids can pass through the membranes only after the pressure gradient exceeds a certain value; until this value is reached the membranes are practically impervious; but an animal membrane is a particular porous medium. Recently, Swedish and other scientists found the existence of a limit gradient at which fluid motion in the ground stops (**2**). This limit gradient will be named initial gradient; motion occurs only when this initial gradient is exceeded.

These remarks show that it is not without interest—theoretical and practical—to study the motions in porous media with initial gradient, as defined above. The existence of the initial gradient shows that in certain conditions account must also be taken of the rheological aspect of the motion.

In this work we shall derive the equations which describe the motion in porous media, illustrated by some simple examples, and shall apply a classical approximate method. A result worthy of mention is that, in the plane case at least, the discharge below a dam on a homogeneous unlimited porous medium is no longer infinite.

2. The equations of motion

Mathematically, the motions with initial gradient can be expressed as follows:

$$\left.\begin{aligned} &\mathbf{v} = 0 \quad \text{for } |\operatorname{grad} H| \leqslant K^* \\ &\mathbf{v} = -k\left(\operatorname{grad} H - \frac{K^* \operatorname{grad} H}{|\operatorname{grad} H|}\right) \quad \text{for } |\operatorname{grad} H| > K^* \end{aligned}\right\}, \tag{2}$$

where the critical value of $|\operatorname{grad} H|$ is denoted by K^*, that is, the magnitude of the initial gradient. These equations show that in the domain filled by the fluid there may exist regions in which there is motion, and regions in which there is no motion. We shall confine ourselves to the case of homogeneous and isotropic media and to incompressible fluids. Introducing the velocity 'potential' ϕ and the constant K, defined by the relations

$$\phi = -kH, \qquad K = kK^*, \tag{3}$$

(2) may be written

$$\mathbf{v} = 0 \quad \text{for } |\operatorname{grad}\phi| \leqslant K, \tag{4}$$

$$\mathbf{v} = \left(1 - \frac{K}{|\operatorname{grad}\phi|}\right)\operatorname{grad}\phi \quad \text{for } |\operatorname{grad}\phi| > K; \tag{5}$$

when $|\operatorname{grad}\phi|$ is sufficiently large, (5) tends to (1). The relations (4) and (5) will be the basis of our study. The relation (5) is valid for steady motion, but it can be generalized for unsteady motion to the form

$$\frac{k}{mg}\frac{\partial \mathbf{v}}{\partial t} = \left(1 - \frac{K}{|\operatorname{grad}\phi|}\right)\operatorname{grad}\phi - \mathbf{v}; \tag{6}$$

for $K = 0$ we obtain again the general vectorial equation of the motion in porous media (see for example **3**), while for $K \neq 0$ and steady motion we obtain the equation (5).

Taking, as in the classical case,

$$\mathbf{V} = \mathbf{v} + \frac{k}{mg}\frac{\partial \mathbf{v}}{\partial t}, \tag{7}$$

the equation (6) becomes

$$\mathbf{V} = \left(1 - \frac{K}{|\operatorname{grad}\phi|}\right)\operatorname{grad}\phi. \tag{8}$$

There is no reason for introducing the vector **V** defined by (7) in the regions where $|\operatorname{grad}\phi| \leqslant K$; in these regions **V** and **v** must be zero. But in the regions where $|\operatorname{grad}\phi| > K$, we shall have from (7) and (8), and assuming that ϕ has been determined,

$$\mathbf{v} = \mathbf{v}_0 e^{-mgt/k} + \frac{mg}{k} e^{-mgt/k} \int_0^t e^{mgt/k}\left(1 - \frac{K}{|\operatorname{grad}\phi|}\right)\operatorname{grad}\phi \, dt. \tag{9}$$

3. The equation for ϕ

It is known that in the case of Darcy motions ϕ is a harmonic function in the domain occupied by the fluid. By using (5) or (8) and the continuity equation, we can derive an equation for ϕ in the regions where the motion takes place; further the equation

$$\operatorname{div} \mathbf{v} = 0 \tag{10}$$

implies that $\operatorname{div} \mathbf{V} = 0$. From (5) and (10) we obtain for ϕ the equation

$$\left(1-\frac{K}{|\operatorname{grad}\phi|}\right)\nabla^2\phi+\operatorname{grad}\phi.\operatorname{grad}\left(1-\frac{K}{|\operatorname{grad}\phi|}\right)=0 \tag{11}$$

or

$$\nabla^2\phi = \frac{K}{|\operatorname{grad}\phi|}\left(\nabla^2\phi-\frac{\operatorname{grad}\phi.\operatorname{grad}|\operatorname{grad}\phi|^2}{2|\operatorname{grad}\phi|^2}\right). \tag{12}$$

Putting $K = 0$ we obtain $\nabla^2\phi = 0$.

We need now an equation which gives us ϕ for $|\operatorname{grad}\phi| < K$. The most natural hypothesis would be one of the following: in the regions in which $|\operatorname{grad}\phi| < K$, either ϕ satisfies the equation (11), or it is a harmonic function, as in the case of Darcy motions. Here we shall use the first hypothesis, because the use of the second one presents very great difficulties. In particular, we would have to impose some boundary conditions connecting the functions $\phi^{(1)}$ and $\phi^{(2)}$ of the two subdomains: D_1, the domain in which there is motion, and the domain D_2 in which there is no motion. First, we would impose the continuity of the pressure, which is expressed by

$$\phi^{(1)} = \phi^{(2)} \quad \text{on } S, \tag{13}$$

S being the common frontier of the two domains. Secondly on the boundary separating the two domains we must have the limiting value of $|\operatorname{grad}\phi^{(1)}|$, i.e.

$$|\operatorname{grad}\phi^{(1)}| = K \quad \text{on } S. \tag{14}$$

The boundary of the domain in which the velocity vanishes would then behave for the fluid in motion like the surface of an impervious body for a viscous fluid.

However, with the first hypothesis mentioned above, (13) is satisfied automatically, and (14) is the only condition requiring to be satisfied on the boundary of the domain in which there is motion.

There are also conditions to be satisfied on the boundary of the domain filled by the fluid in the porous medium. But these are the ordinary boundary conditions relative to the function ϕ, which are found in any special treatise on underground hydrodynamics.

In this way the problem is reduced to the integration of equation (12) with certain boundary conditions, the boundary of the domain where we

have motion being determined by the condition (14), and the velocity being given by (5) once ϕ is known.

4. An approximate method

To solve particular problems a classical approximate method is sometimes useful. Put

$$\phi = \phi_0 + K\phi_1 + K^2\phi_2 + \dots, \tag{15}$$

where K is a small parameter having the dimensions of a velocity. Now introduce a dimensionless parameter K_0 defined by the relation

$$K_0 = KV_0^{-1}, \tag{16}$$

V_0 being the modulus of a characteristic velocity which is actually realized in the domain D_1. We shall always have $K_0 < 1$, and we may write

$$\phi = \phi_{0,0} + K_0\phi_{0,1} + K_0^2\phi_{0,2} + \dots; \tag{17}$$

$\phi_{0,j}$ $(j = 0, 1, 2, \dots)$ denote the functions corresponding to the expansion in terms of K_0. It is evident that

$$\phi_j = V_0^{-j}\phi_{0,j} \quad (j = 0, 1, 2, \dots). \tag{18}$$

The equations which determine ϕ_0, ϕ_1, ϕ_2,... are immediately deduced by the substitution of the expansion (15) in the equations (12). We find

$$\nabla^2\phi_0 = 0, \tag{19}$$

$$\nabla^2\phi_1 = -\frac{\operatorname{grad}\phi_0 . \operatorname{grad}|\operatorname{grad}\phi_0|^2}{2|\operatorname{grad}\phi_0|^3}, \tag{20}$$

$$\begin{aligned}\nabla^2\phi_2 = -\frac{1}{2|\operatorname{grad}\phi_0|^3}\big[&|\operatorname{grad}\phi_0|^{-1}\operatorname{grad}\phi_0 . \operatorname{grad}|\operatorname{grad}\phi_0|^2 + \\ &+\operatorname{grad}\phi_1 . \operatorname{grad}|\operatorname{grad}\phi_0|^2 + 2\operatorname{grad}\phi_0 . \operatorname{grad}(\operatorname{grad}\phi_0 . \operatorname{grad}\phi_1) - \\ &-2|\operatorname{grad}\phi_0|^{-1}(\operatorname{grad}\phi_0 . \operatorname{grad}\phi_1)(\operatorname{grad}\phi_0 . \operatorname{grad}|\operatorname{grad}\phi_0|^2)\big]\end{aligned} \tag{21}$$

and so on. After solving these equations, subject to their boundary conditions, the boundary of D_1 is found from the relation

$$|\operatorname{grad}\phi| = K, \tag{14'}$$

that is

$$\begin{aligned}|\operatorname{grad}\phi_0| + K|\operatorname{grad}\phi_0|^{-1}\operatorname{grad}\phi_0 . \operatorname{grad}\phi_1 + \tfrac{1}{2}K^2(|\operatorname{grad}\phi_1|^2|\operatorname{grad}\phi_0|^{-1} + \\ +2|\operatorname{grad}\phi_0|^{-1}\operatorname{grad}\phi_0 . \operatorname{grad}\phi_2 - (\operatorname{grad}\phi_0 . \operatorname{grad}\phi_1)^2|\operatorname{grad}\phi_0|^{-3} + \\ + \dots = K.\end{aligned} \tag{14''}$$

Then, from (5), the velocity is

$$\begin{aligned}\mathbf{v} = \operatorname{grad}\phi_0 + K\left(\operatorname{grad}\phi_1 - \frac{\operatorname{grad}\phi_0}{|\operatorname{grad}\phi_0|}\right) + \\ + K^2\left(\operatorname{grad}\phi_2 + \frac{\operatorname{grad}\phi_0 . \operatorname{grad}\phi_1}{|\operatorname{grad}\phi_0|^3}\operatorname{grad}\phi_0\right) + \dots .\end{aligned} \tag{22}$$

The first boundary-value problem determines a harmonic function and the others determine functions which satisfy the Poisson type equation.

5. Examples

We shall now consider some important examples of motions for which exact solutions are obtainable.

(*a*) One-dimensional motion in the x-direction, of a layer stretching from $x = 0$ to $x = l$, with p_{I} and p_{II} denoting the pressures at the extremities. We obtain for the velocity u

$$u = k(p_{\mathrm{I}} - p_{\mathrm{II}})(\rho g l)^{-1} - K. \tag{23}$$

(*b*) A plane motion with spherical symmetry, denoting by p_{I} and p_{II} the pressures for $r = r_{\mathrm{I}}$ and $r = r_{\mathrm{II}}$ (taking $r_{\mathrm{II}} > r_{\mathrm{I}}$, $p_{\mathrm{I}} > p_{\mathrm{II}}$, to fix our ideas) and by q the fluid discharge for unit thickness of layer; from the equation

$$\frac{q}{2\pi r} = \frac{d\phi}{dr} - K,$$

we obtain at once

$$q = 2\pi[k(p_{\mathrm{I}} - p_{\mathrm{II}})(\rho g)^{-1} - K(r_{\mathrm{II}} - r_{\mathrm{I}})]\left(\ln\frac{r_{\mathrm{II}}}{r_{\mathrm{I}}}\right)^{-1}. \tag{24}$$

(*c*) For three-dimensional motion with spherical symmetry, and using similar definitions to those in example (*b*) we have

$$Q = 4\pi[k(p_{\mathrm{I}} - p_{\mathrm{II}})(\rho g)^{-1} - K(r_{\mathrm{II}} - r_{\mathrm{I}})](r_{\mathrm{I}}^{-1} - r_{\mathrm{II}}^{-1})^{-1}; \tag{25}$$

here Q represents the total fluid discharge.

From the formulae (23)–(25) it follows that the discharge diminishes for the motions with initial gradient, as was to be expected.

(*d*) Let us take now a porous medium with the following boundary: $x < -R$, $y = 0$; $x > R$, $y = 0$; $-R < x < R$, $y = \sqrt{(R^2 - x^2)}$, the y-axis being directed vertically downwards and in the medium $y > 0$. We consider the rectilinear parts of the boundary as supply surfaces and the curvilinear one as an impervious surface, so that

$$\phi = \begin{cases} 0 & \text{for } y = 0,\ x > R \\ -kH & \text{for } y = 0,\ x < -R \end{cases}$$

$$\frac{\partial\phi}{\partial n} = 0 \quad \text{on } y = \sqrt{(R^2 - x^2)} \quad (-R < x < R). \tag{26}$$

It is easily seen that the exact solution of the problem is given by the harmonic function

$$\phi = -\frac{kH\theta}{\pi}, \tag{27}$$

where θ is the angle made by the x-axis with the radius vector to a given point. The velocity will then have the expression

$$\mathbf{v} = -\left(\frac{kH}{\pi r} - K\right)\boldsymbol{\epsilon}, \tag{28}$$

where $\boldsymbol{\epsilon}$ is a unit vector normal to the radius vector. We find that the boundary of the domain in which there is no motion is a semicircle with centre the origin, and of radius

$$R^* = \frac{kH}{\pi K}, \tag{29}$$

that is, $\mathbf{v} = 0$ for $r > R^*$.

On calculating the discharge of fluid from upstream to downstream, we find

$$Q = \frac{kH}{\pi}\ln\left(\frac{R^*}{R}\right) - K(R^* - R),$$

or

$$Q = \frac{kH}{\pi}\left\{\ln\left(\frac{kH}{\pi RK}\right) - 1\right\} + KR, \tag{30}$$

so that we obtain a finite discharge; if $K \to 0$, then $Q \to \infty$, as for Darcy motions.

(*e*) Finally, let us consider the following unsteady one-dimensional motion:

$$\left.\begin{aligned} &t \leqslant 0, \quad p(0) = p_{\mathrm{I}}^*, \quad p(L) = p_{\mathrm{II}}, \quad p_{\mathrm{I}}^* > p_{\mathrm{II}} \\ &t > 0, \quad p(0) = p_{\mathrm{I}}, \quad p(L) = p_{\mathrm{II}}, \quad p_{\mathrm{I}} > p_{\mathrm{II}}, \quad p_{\mathrm{I}} \neq p_{\mathrm{I}}^* \end{aligned}\right\}. \tag{31}$$

As $p = ax + b$ (a, b are constants), it follows that we have for p

$$t \leqslant 0, \quad p = p_{\mathrm{I}}^* + (p_{\mathrm{II}} - p_{\mathrm{I}}^*)xL^{-1};$$

$$t > 0, \quad p = p_{\mathrm{I}} + (p_{\mathrm{II}} - p_{\mathrm{I}})xL^{-1}.$$

The equation of motion will then be

$$\frac{dv}{dt} + \frac{mg}{k}v + \frac{m}{\rho}\frac{p_{\mathrm{II}} - p_{\mathrm{I}}}{L}\left(1 - \frac{\rho gKL}{k(p_{\mathrm{I}} - p_{\mathrm{II}})}\right) = 0, \tag{32}$$

of which the solution is

$$v = v_0 e^{-mgt/k} + \frac{p_{\mathrm{I}} - p_{\mathrm{II}}}{L}\frac{k}{\rho g}\left(1 - \frac{\rho gKL}{k(p_{\mathrm{I}} - p_{\mathrm{II}})}\right)(1 - e^{-mgt/k}), \tag{33}$$

where v_0 is

$$v_0 = \frac{k(p_{\mathrm{I}}^* - p_{\mathrm{II}})}{\rho gL}\left(1 - \frac{\rho gKL}{k(p_{\mathrm{I}}^* - p_{\mathrm{II}})}\right). \tag{34}$$

For $t \to \infty$, we have

$$\lim v = \frac{k}{\rho g}\frac{p_{\mathrm{I}} - p_{\mathrm{II}}}{L}\left(1 - \frac{\rho gKL}{k(p_{\mathrm{I}} - p_{\mathrm{II}})}\right),$$

as should be the case.

REFERENCES

1. E. Duclaux, 'Recherches sur les lois des mouvements des liquides dans les espaces capillaires', *Ann. chim. phys.* (4) **25** (1872) 442.
2. —— *La Houille Blanche*, p. 468 (1952).
3. P. Ya. Polubarinova-Kochina and S. B. Falkovich, 'Theory of filtration of liquids in porous media', *Advances in Appl. Mech.* **2** (1951) 210.

THE BEHAVIOUR OF AN AXIALLY SYMMETRIC SONIC JET NEAR TO THE SONIC PLANE

By M. G. SMITH†

(*Armament Research and Development Establishment, Fort Halstead, Sevenoaks, Kent*)

[Received 15 May 1958]

SUMMARY

The behaviour near the sonic plane of an axially symmetric sonic jet of gas, emerging into a region of lower pressure, is studied. The form of the singularity at the sonic plane is found, and the lowest terms of the series expansions of the variables of state near to the plane are obtained. In particular the corresponding solutions for this case and for the two-dimensional problem are compared, and it is shown that there are important differences between them.

1. Introduction

If a gas emerges as a jet from a plane circular orifice into a region of lower pressure, in such a way that the velocity in the plane of the orifice is uniform and supersonic, and so that the streamlines are everywhere normal to this plane, then the jet will expand, and the velocity will increase. The behaviour of the jet near the orifice has been studied by Johannesen and Meyer (1). An expansion wave arises from the edge of the orifice which interacts with itself, and is reflected from the jet boundary, giving rise to a series of interactions and reflections (see Fig. 1).

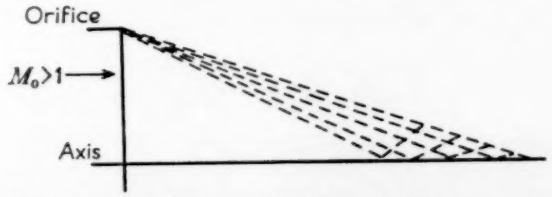

Fig. 1. Initial characteristics for flow from a slightly supersonic orifice.

If the velocity at the orifice is sonic the situation is more complex. The characteristics which form the upstream limit of the expansion fan at each point of the edge, all lie in the plane of the orifice. Thus instead of a point intersection, they intersect at each point, and the region of interaction begins at the orifice instead of downstream, as in the former case (Fig. 2). It is clear, therefore, that in this case a singularity must

† Now at Sir John Cass College, Jewry St., London E.C.

occur in the plane of the orifice; the study of this singularity forms the content of this paper.

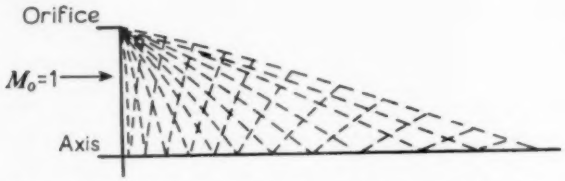

FIG. 2. Initial characteristics for flow from a sonic orifice.

The singularity is not of course peculiar to the axially symmetric problem. The equivalent two-dimensional problem was studied in (**2**). The singularity in this case was representable in terms of the Weierstrassian elliptic function. It is of interest to compare the two solutions, and this has been done in this paper.

The equations for the subsequent terms in the expansion will be non-homogeneous ordinary linear differential equations of the second order. Thus in principle a numerical solution to any order of accuracy can be obtained from this solution.

2. The equations of motion

The equations of motion of a homentropic perfect gas in axially symmetric steady flow can be expressed in the form

$$\frac{\partial u}{\partial r}-\frac{\partial v}{\partial z}=0, \tag{2.1}$$

$$u\frac{\partial}{\partial z}\{\log(\rho/\rho_*)\}+v\frac{\partial}{\partial r}\{\log(\rho/\rho_*)\}+\frac{\partial u}{\partial z}+\frac{\partial v}{\partial r}+\frac{v}{r}=0, \tag{2.2}$$

$$u^2+v^2+\frac{2}{\gamma-1}a^2=\frac{\gamma+1}{\gamma-1}a_*^2, \tag{2.3}$$

$$(a/a_*)^2=(\rho/\rho_*)^{\gamma-1}, \tag{2.4}$$

where conventional notation has been used, and where the starred values are those reached on the sonic line.

Consider the flow in a meridian plane. It is convenient to transform to coordinates with origin at the upper lip of the orifice. If the radius of the orifice is r_0 let

$$r_0^2\xi^2=z^2+(r_0-r)^2, \tag{2.5}$$

and

$$\{r_0-r\}\tan\phi=z, \tag{2.6}$$

as shown in Fig. 3. Let Ua_* be the component of velocity in the direction of increasing ξ, and Va_* be the component in the direction of increasing ϕ.

Let $A = a/a_*$ and $\eta = \log\{\rho/\rho_*\}$. In terms of the new variables equations (2.1) to (2.4) become

$$\xi\frac{\partial V}{\partial \xi}+V-\frac{\partial U}{\partial \phi}=0, \tag{2.7}$$

$$\xi U\frac{\partial \eta}{\partial \xi}+V\frac{\partial \eta}{\partial \phi}+\xi\frac{\partial U}{\partial \xi}+\frac{\partial V}{\partial \phi}+U+\frac{\xi}{1-\xi\cos\phi}\{V\sin\phi-U\cos\phi\}=0, \tag{2.8}$$

$$U^2+V^2+\frac{2}{\gamma-1}A^2=\frac{\gamma+1}{\gamma-1}, \tag{2.9}$$

$$\log A=\frac{\gamma-1}{2}\eta. \tag{2.10}$$

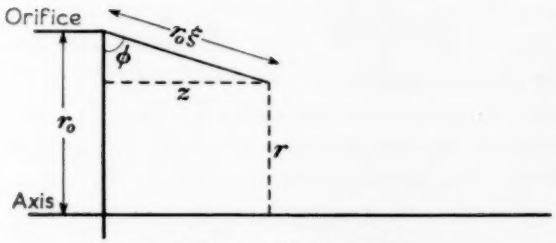

FIG. 3. The coordinate systems.

The interesting region is that for which ϕ is small. The obvious approach, therefore, is to expand the dependent variables in powers of ϕ. The symmetries of the problem show that the appropriate expansions are:

$$\begin{aligned}
A &= 1+A_2(\xi)\phi^2+A_4(\xi)\phi^4+O(\phi^6),\\
V &= 1+V_2(\xi)\phi^2+V_4(\xi)\phi^4+O(\phi^6),\\
U &= \phi+U_2(\xi)\phi^3+U_4(\xi)\phi^5+O(\phi^7),\\
\eta &= \eta_2(\xi)\phi^2+\eta_4(\xi)\phi^4+O(\phi^6).
\end{aligned}$$

The boundary conditions are that at the edge of the orifice the flow must be locally a Prandtl–Meyer expansion, and, since the coordinate system is biased by being rooted on one lip of the orifice, that the solution must be invariant to a change to a coordinate system based on the other lip.

The first condition is most conveniently expressed by

$$A = V \quad \text{at} \quad \xi = 0, \quad \text{for all } \phi. \tag{2.11}$$

The second condition consists of four equations of the form

$$\eta(\xi_1;\phi_1)=\eta(\xi_2;\phi_2), \tag{2.12}$$

where the suffixes refer to opposite edges of the orifice. Only one of these

equations is actually required as a boundary condition, the others, with the equations of motion, being satisfied identically. These two coordinate systems are related by the equations

$$\xi_2^2 = 4+\xi_1^2-4\xi_1\cos\phi_1,$$

and

$$\tan\phi_2 = \frac{\xi_1\sin\phi_1}{2-\xi_1\cos\phi_1}.$$

Expanding these in series for small ϕ_1, they become

$$\xi_2 = X[1+\xi_1\{\phi_1/X\}^2]+O(\phi_1^4),$$

and

$$\phi_2 = \xi_1\{\phi_1/X\}[1-\tfrac{1}{6}\{X^2+3\xi_1 X+2\xi_1^2\}\{\phi_1/X\}^2]+O(\phi_1^4),$$

where $X = 2-\xi_1$. Substitution into (2.12) gives

$$X^2\eta_2(\xi_1)\phi_1^2 = \xi_1^2\eta_2(X)\phi_1^2+O(\phi_1^4). \tag{2.13}$$

3. The first approximation

If the series expansions are substituted into equations (2.7) to (2.10), and the coefficients of the lowest powers of ϕ are equated to zero, only two independent equations are derived, namely

$$2(\eta_2+V_2)+1 = 0, \tag{3.1}$$

and

$$A_2 = \frac{\gamma-1}{2}\eta_2. \tag{3.2}$$

It will easily be seen that, in general, from the set of four equations obtained from the coefficients of successive powers of ϕ, the functions with highest suffix can be eliminated to give a non-linear relation between the functions with lower suffixes.

Thus the next powers of ϕ give

$$3U_2 = \xi\frac{dV_2}{d\xi}+V_2, \tag{3.3}$$

$$\xi\frac{d\eta_2}{d\xi}+2\eta_2V_2+4\eta_4+\xi\frac{dU_2}{d\xi}+4V_4+U_2+\frac{\xi}{1-\xi}(V_2-U_2+\tfrac{1}{3}) = 0, \tag{3.4}$$

$$2U_2+2V_4+V_2^2+\frac{4}{\gamma-1}A_4+\frac{2}{\gamma-1}A_2^2 = 0, \tag{3.5}$$

and

$$A_4-\tfrac{1}{2}A_2^2 = \frac{\gamma-1}{2}\eta_4. \tag{3.6}$$

Eliminating η_4, V_4, and A_4 from (3.4), (3.5), and (3.6) we find

$$\xi\frac{d\eta_2}{d\xi}+2\eta_2V_2+\xi\frac{dU_2}{d\xi}-3U_2-2V_2^2-\frac{8}{\gamma-1}A_2^2+\frac{\xi}{1-\xi}(V_2-U_2+\tfrac{1}{3}) = 0. \tag{3.7}$$

If this is combined with (3.1), (3.2), and (3.3) an equation for η_2 is derived, namely,

$$\xi^2\frac{d^2\eta_2}{d\xi^2}-\left(4+\frac{\xi}{1-\xi}\right)\xi\frac{d\eta_2}{d\xi}+\left(6+\frac{2\xi}{1-\xi}\right)\eta_2+6(\gamma+1)\eta_2^2=0, \tag{3.8}$$

and this can be simplified by the substitution

$$(\gamma+1)\eta_2=-\xi^2F(\xi),$$

to the form

$$(1-\xi)F''-F'=6(1-\xi)F^2. \tag{3.9}$$

Using (2.11) and (2.13), the boundary conditions become

$$\xi\to+0, \qquad \xi^2F(\xi)\to 1, \tag{3.10}$$

and

$$F(\xi)=F(2-\xi). \tag{3.11}$$

As pointed out in the introduction, a problem equivalent to the two-dimensional problem was solved in (**2**). The analysis is very similar to the above, but instead of equation (3.9) the resulting equation is

$$F''=6F^2, \tag{3.12}$$

though the boundary conditions are identical. Thus in the usual notation for the Weierstrassian elliptic function the solution is

$$F(\xi)=\alpha^2\wp(\alpha\xi), \tag{3.13}$$

where α is chosen to give the function a period of 2.

4. Solution of the fundamental equation

It is easily established that equation (3.9) has no solution in known functions. Near $\xi=1$, almost all solutions of (3.9) behave like

$$F(\xi)=k(1-\xi)^{-2}+O(1),$$

and so $F(\xi)$ has a double pole at this point. In this problem, however, the only possible singularities which could arise physically are at $\xi=0$ and $\xi=2$. Thus since $F(\xi)$ has no singularity at $\xi=1$, $k=0$, and since further $F(\xi)$ is an even function of $(1-\xi)$, the boundary condition (3.11) can be written

$$F'=0 \quad \text{at} \quad \xi=1. \tag{4.1}$$

If in (3.9) we write

$$1-\alpha x=\xi, \quad \text{and} \quad \beta f(x)=F(\xi)$$

and choose α and β to satisfy

$$\alpha^2\beta=1,$$

then the equation becomes

$$\frac{d}{dx}\{xf'(x)\}=6xf^2. \tag{4.2}$$

If further $\psi=\log x$, $y=x^2f(x)$, and $\lambda=\dfrac{dy}{d\psi}$,

then (4.2) reduces to the first order equation

$$\lambda\frac{d\lambda}{dy}-4\lambda+4y-6y^2=0. \tag{4.3}$$

The boundary conditions are that

$$\lambda=0 \quad \text{when} \quad y=0,$$

and is a regular function of y near the origin, and secondly that

$$(\psi_0-\psi)^2y\to 1 \quad \text{as} \quad \psi\to\psi_0=\tfrac{1}{2}\log\beta.$$

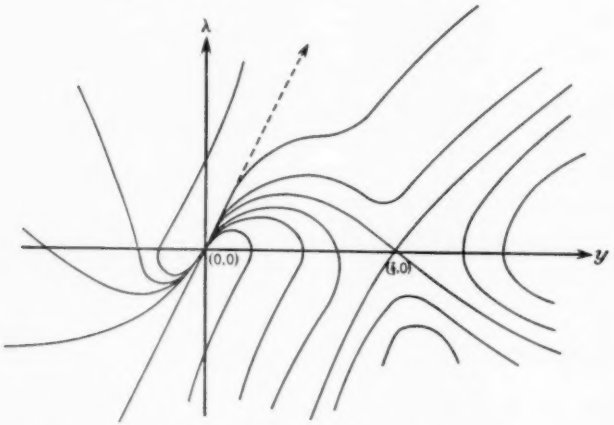

FIG. 4. Integral trajectories for small y.

As this implies that

$$(\psi_0-\psi)^3\lambda\to 2 \quad \text{as} \quad \psi\to\psi_0,$$

an equivalent condition is that

$$\lambda=2y^{\frac{1}{2}}+o(y^{\frac{1}{2}}) \quad \text{as} \quad y\to\infty.$$

The finite singular points of equation (4.3) are at the points

$$y=0, \qquad \lambda=0,$$

and at

$$y=\tfrac{2}{3}, \qquad \lambda=0.$$

It is easy to see (Fig. 4) that the first point is an unstable node, while the second is a saddle point. Only one of the integral curves through $(0,0)$ is regular in the region around the singular point. This is the one which behaves like

$$\lambda=2y$$

in the neighbourhood of the origin. Since, physically, our solution must be regular at this point, this is the required solution.

In the neighbourhood of $y = 0$ therefore a series expansion of the form

$$\lambda = 2y\left\{1+\sum_{r=1}^{\infty} a_r y^r\right\} \tag{4.4}$$

is valid.

Substituting into the equation, and equating to zero separately the coefficients of the various powers of y, the following recurrence relations are obtained:

$$2a_1 = 3 \tag{4.5}$$

and if $r \geqslant 2$

$$2a_r = -\frac{r+2}{r}\sum_{s=1}^{r-1} a_s a_{r-s}, \tag{4.6}$$

so that the coefficients alternate in sign. Now if $r \geqslant 2$,

$$2r \geqslant r+2 \geqslant r,$$

and so

$$\tfrac{1}{2}\sum_{s=1}^{r-1}|a_s||a_{r-s}| \leqslant |a_r| \leqslant \sum_{s=1}^{r-1}|a_s||a_{r-s}|.$$

Consider the series

$$L_*(y) = 1+\sum_{r=1}^{\infty} A_{*r} y^r,$$

and

$$L^*(y) = 1+\sum_{r=1}^{\infty} A_r^* y^r,$$

where

$$A_{*1} = A_1^* = a_1,$$

and for $r \geqslant 2$

$$A_{*r} = \tfrac{1}{2}\sum_{s=1}^{r-1} A_{*s} A_{*r-s}, \qquad A_r^* = \sum_{s=1}^{r-1} A_s^* A_{r-s}^*.$$

Then for all r

$$A_{*r} \leqslant |a_r| \leqslant A_r^*.$$

If R_* is the radius of convergence of L_*, R^* that of L^*; and if R is the radius of convergence of the series contained in (4.4), then

$$R^* \leqslant R \leqslant R_*.$$

But

$$L_*^2(y) = 1+\sum_{r=1}^{\infty}\left\{2A_{*r}+\sum_{s=1}^{r-1} A_{*s}A_{*r-s}\right\}y^r$$

$$= 1+2A_{*1}y+4\sum_{r=2}^{\infty} A_{*r}y^r = 4L_*(y)-2a_1 y-3.$$

Thus

$$L_*(y) = 2-\{1-2a_1 y\}^{\frac{1}{2}},$$

and

$$R_* = \frac{1}{2a_1}$$

It can therefore be established that

$$\tfrac{1}{2} \geqslant Ra_1 \geqslant \tfrac{1}{4},$$

and so the series contained in (4.4) converges uniformly within a circle whose radius is at least $\frac{1}{6}$.

To study the other end of the range it is convenient to put

$$\lambda = 2y^{\frac{1}{2}}\Gamma \quad \text{and} \quad y\zeta^2 = 1.$$

Then (4.3) gives $$\zeta\Gamma\frac{d\Gamma}{d\zeta}+4\zeta\Gamma-3\Gamma^2-2\zeta^2+3 = 0. \tag{4.7}$$

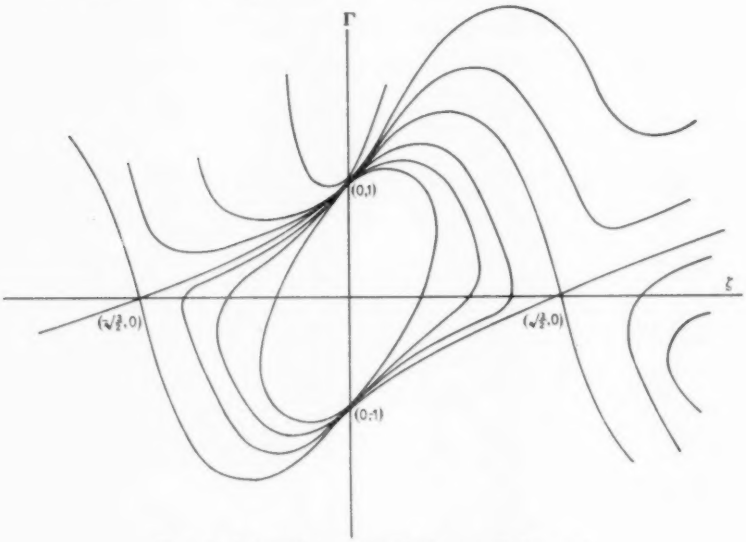

FIG. 5. Integral trajectories for small $\zeta = y^{-\frac{1}{2}}$.

The singularities of equation (4.7) are at the points

$$\zeta = 0, \qquad \Gamma = \pm 1,$$

and $$\zeta = \pm\sqrt{\tfrac{3}{2}}, \qquad \Gamma = 0.$$

The first two singularities are unstable nodes, and the latter are saddle points. Fig. 5 shows the form of the integral curves. Near $\zeta = 0$, the solution will behave like the solution of

$$\zeta\frac{d\Gamma}{d\zeta}-6(\Gamma-1)+4\zeta = 0, \tag{4.8}$$

and it is at once obvious that the integer coefficient of the second term will be troublesome. Put

$$\Gamma(\zeta) = 1+{}_0b_1\zeta+{}_0b_2\zeta^2+{}_0b_3\zeta^3+{}_0b_4\zeta^4+{}_0b_5\zeta^5+\gamma(\zeta),$$

and choose the coefficients ${}_0b_1$, ${}_0b_2$,..., ${}_0b_5$ so that when this expression is substituted into (4.7), the resulting terms in the first five powers of ζ vanish. Then

$$\zeta\frac{d\gamma}{d\zeta}-6\gamma+4\,{}_0b_5\zeta^6+o(\zeta^6) = 0, \tag{4.9}$$

and so
$$\gamma = -4\,{}_0b_5\zeta^6\log\zeta + {}_0b_6\zeta^6 + o(\zeta^6). \tag{4.10}$$

Thus the solution of (4.7), valid for small ζ, is

$$\Gamma(\zeta) = \sum_{r=0}^{\infty}\sum_{s=0}^{\infty} {}_sb_r\,\zeta^{6s+r}\{\log\zeta\}^s. \tag{4.11}$$

If in this expansion we have

$${}_0b_0 = 1,$$

and
$${}_1b_0 + 4\,{}_0b_5 = 0,$$

then all the other coefficients are determined by the recurrence relations obtained by substituting (4.11) into (4.7), with the exception of ${}_0b_6$, and there is no recurrence relation which determines this. Thus ${}_0b_6$ appears as an arbitrary constant, and the later coefficients are functions of it. In fact it may easily be shown that the coefficient ${}_sb_r$ is a polynomial in ${}_0b_6$ of order $[r/6]$, where $[x]$ means the integral part of x.

5. The integration and the results

Since it has been shown that the series (4.4) is uniformly convergent within a finite region of the origin, within this region (4.4) may be used to give numerical values not only for λ, but also for its derivatives of all orders.

The trajectory chosen avoids the other singularities in the finite part of the plane, and so equation (4.3) may be integrated numerically to as large a value of y as is required.

Unfortunately it does not seem possible, by elementary processes, to establish the convergence of the series (4.11). An intuitive argument for its validity can however be found. If the numerical solution of (4.3) for large enough y is equated with the solution (4.11) of equation (4.7) for the corresponding value of ζ, the unknown ${}_0b_6$ can be found. If then, as does in fact happen, different values of y give the same value of ${}_0b_6$ the process is justified.

Thus by the above process the function $\eta_2(\xi)$ was calculated, and is plotted in Fig. 6. Also in this figure for comparison is plotted the corresponding two-dimensional solution. It will be seen at once that there is a fundamental difference between the two curves, as the two-dimensional solution not only passes through the origin but does so with zero slope, while the axially symmetric solution has a finite slope at the origin. Also the value of $\eta_2(1)$ is greater than 2, whereas the corresponding value of the two-dimensional solution is less than 1·5.

After the non-linear equation for the function $\eta_2(\xi)$, the equation for $\eta_4(\xi)$ and the higher functions will be non-homogeneous linear equations.

The equation, however, and its boundary conditions are rather tedious to set out, and so are omitted.

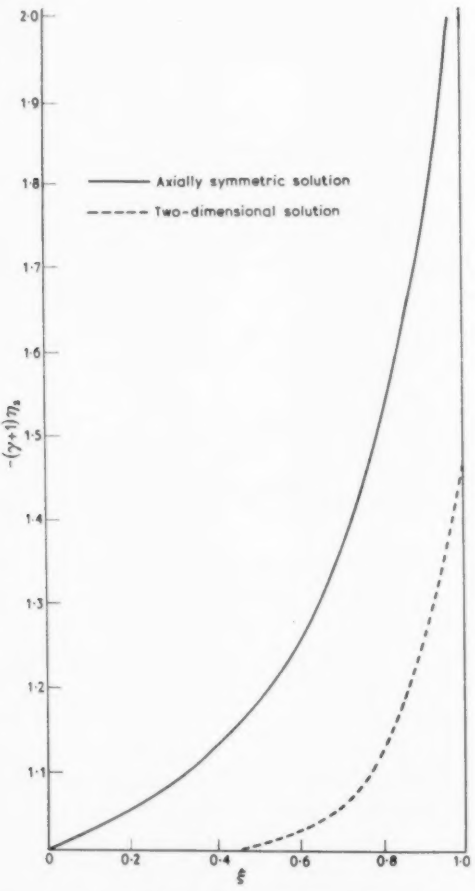

FIG. 6. A comparison of the variation of $-(\gamma+1)\log(\rho/\rho_*)$ with ξ, in the two-dimensional and axially symmetric flows.

6. Conclusions

An approximate solution has been computed for the flow in an axially symmetric sonic jet near its sonic plane. In particular the singularity in the sonic plane has been examined. The solution obtained here could be used as the starting conditions for a characteristic net, which would determine the flow through the sonic jet.

In conclusion the author wishes to thank Mr. H. J. Gawlik, formerly of the Ministry of Supply, who did the major work of computation, and his wife, for helping prepare this paper in its present form.

REFERENCES

1. N. H. Johannesen and R. E. Meyer, 'Axially symmetric supersonic flow near the centre of an expansion', *Aero. Quart.* **2** (1950) 127–42.
2. R. Hill and D. C. Pack, 'An investigation, by the method of characteristics, of the lateral expansion of the gases behind a detonating slab of explosive', *Proc. Roy. Soc.* A, **191** (1947) 524–41.
3. M. G. Smith, Unpublished Ministry of Supply Report.

THE FLOW PAST A CLOSED BODY IN A HIGH SUBSONIC STREAM

By J. B. HELLIWELL

(*The Royal College of Science and Technology, Glasgow*)

and A. G. MACKIE

(*St. Salvator's College, University of St. Andrews*)

[Received 15 May 1958]

SUMMARY

A solution of Tricomi's equation is obtained for the flow past a thin, doubly symmetric body placed at zero incidence in a high subsonic stream in which sonic velocity is attained along a segment of the body. This flow is the compressible analogue of the Riabouchinsky model for incompressible fluids. The singularity in the hodograph plane corresponding to the point at infinity in the physical plane is essentially different from that which occurs in other similar problems. The boundary value problem is of mixed type and this is shown to lead to a pair of dual integral equations for which the solution is obtained. Numerical results are given which specify the dimensions of the body corresponding to a range of incident Mach numbers. By symmetry the total drag on the body is zero.

1. Introduction

THE study of problems in transonic flow in two dimensions is frequently based on solutions of Tricomi's equation

$$\frac{\partial^2 y}{\partial u^2} + u\frac{\partial^2 y}{\partial v^2} = 0, \tag{1}$$

where u and v are related to the velocity components and y is the coordinate measured at right angles to the main stream. This equation is an approximation to the full hodograph equation of a perfect gas and is valid for small perturbations about a uniform flow at a Mach number of unity. In recent years a number of solutions have been found to represent the flow past a symmetric body whose axis of symmetry is parallel to the direction of the main stream when the flow at infinity is sonic or slightly subsonic. These bodies usually have straight sides but they may also consist of portions on which the magnitude of the velocity instead of its direction is constant. Such problems may be formulated precisely in the hodograph plane and the corresponding solutions obtained. For wedge-shaped bodies the sonic point is taken at the shoulder of the wedge. However, the continuation of the flow beyond this point presents difficulties. In a classical paper, Guderley and Yoshihara (1) have obtained

the solution for a wedge in a sonic stream up to the limiting characteristic emanating from the shoulder. Further continuation of the solution can then be undertaken by the method of characteristics. The given solution up to the limiting characteristic is complicated and some approximation is unavoidable in the analysis. Cole (**2**) has used a model in which the sonic line is straight and at right angles to the direction of the main stream. But there is no way of continuing this solution into the supersonic region beyond the shoulder of the wedge. It is usually argued in this case that the upstream influence of the flow in this region is bound to be small and that the flow upstream from the shoulder may be well represented by a solution which ignores the influence of the region downstream. More recently Helliwell and Mackie (**3**) discussed a solution based on the modification of the usual Helmholtz flow which was first suggested by Roshko (**4**) for some problems in incompressible flow. In this model a free streamline at sonic velocity leaves the shoulder of the wedge and after a finite distance becomes parallel to the direction of the main stream. The velocity on this streamline then decreases to the velocity at infinity. This solution possesses the advantage of mapping the entire physical plane (outside the wake) onto the hodograph plane but it cannot be said to give an altogether physically satisfactory description of the downstream flow. The object of the present paper is to formulate and solve a problem in which the flow closes up completely behind a symmetric body placed in a uniform stream with a high subsonic velocity at infinity. The body is to be symmetric about both axes and the Mach number is everywhere less than unity except on a part of the body where it attains this value. To enable us to formulate the problem in the hodograph plane we shall choose a body such that in the given flow the magnitude or the direction of the velocity is constant along its profile. We must bear in mind that the most obvious shape to choose, the double wedge or rhombus, cannot be considered because the sharp corners give rise to supersonic regions and these lead to shock waves. (An approximate treatment of flow past this body is given by Trilling (**5**).) Consequently we are led to consider the profile shown in Fig. 1 in which BC and EF are straight and the curvature of CDE is adjusted so that the velocity will be exactly sonic along it. The precise shape of CDE will be determined *a posteriori* from the solution. This model is suggested by the work of Riabouchinsky (**6**) on cavities in incompressible flow.

The first step in finding the solution is the identification of the singularity in the hodograph plane. It is shown in the next section that the character of the singularity is essentially different from that in the solution discussed by Cole (**2**) and in the earlier paper of Helliwell and Mackie (**3**).

It is pointed out that the particular singular solution obtained is itself a formal solution of the whole problem for the fictitious gas discussed by Germain and Liger (7). However, in order to complete the solution in terms of the 'Tricomi gas' it is necessary to satisfy an additional boundary condition on the line $v = v_0$, the mapping of the wedge face in the hodograph plane. In the problems mentioned at the beginning of this paragraph this is achieved without difficulty by superposing an infinite system of images. This method does not succeed in the present case because of the mixed type boundary conditions on the axis $v = 0$. The addition of an

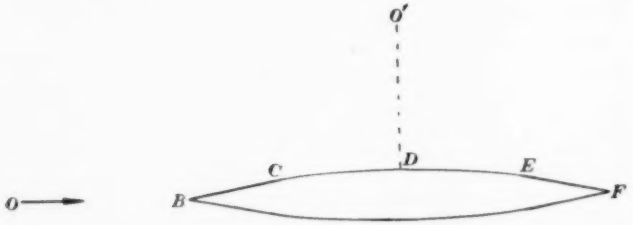

FIG. 1. Physical plane.

image system, however, does lead to a solution which satisfies the boundary conditions on $v = v_0$ and on part of the axis. The difference between this and the exact solution of the boundary value problem is examined in detail in section 3 where a complete solution is obtained as a series in powers of the transonic similarity parameter. It appears that the error involved when this difference is neglected is very small and that in most cases it lies well within the error inherent in the use of the transonic approximation. Finally, in section 4, some qualitative and also some numerical results are given to show the type of profile for which a flow pattern of this nature exists.

2. The boundary value problem

We return now to equation (1) where u and v are dimensionless expressions for the velocity perturbations on a uniform flow with sonic velocity a^*. Specifically

$$u = \frac{(\gamma+1)(a^*-U)}{a^*}, \qquad v = \frac{(\gamma+1)V}{a^*},$$

where U, V are the components of the actual velocity, y is the position coordinate measured at right angles to the uniform stream and within the limits of the transonic approximation is proportional to the stream

function ψ, and γ is the ratio of specific heats of the gas. The position coordinates x and y are related through the differential equations

$$\frac{\partial x}{\partial v} = -\frac{\partial y}{\partial u}, \quad \frac{\partial x}{\partial u} = u\frac{\partial y}{\partial v}. \tag{2}$$

It is convenient at this stage to introduce a new variable r defined by $r = \frac{2}{3}u^{\frac{3}{2}}$. The solution of equation (1) obtained by the separation of variables is then

$$y = r^{\frac{1}{2}}e^{\pm\lambda r}\mathscr{C}_{\pm\frac{1}{3}}(\lambda r),$$

where $\mathscr{C}_{\pm\frac{1}{3}}(z)$ is any linear combination of Bessel functions of order $\pm\frac{1}{3}$.

The boundary value problem appropriate to Fig. 1 can now be formulated. It is clear from symmetry that only one-quarter of the physical

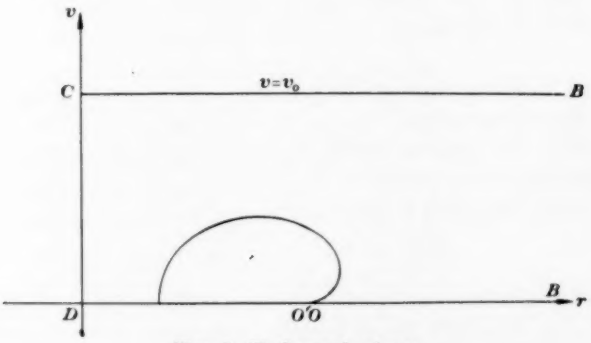

FIG. 2. Hodograph plane.

plane need be considered. Thus the upper left section of Fig. 1 is mapped into the semi-infinite rectangle $r \geqslant 0$, $0 \leqslant v \leqslant v_0$ in the hodograph plane which is shown in Fig. 2. Here $v_0 = (\gamma+1)\delta$ and this is the value of v on the straight part of the profile if δ is the semi-angle at the nose. The following boundary conditions in the hodograph plane have to be satisfied:

(i) y must have a certain singularity at $O'O$, the point in the hodograph plane which corresponds to the point at infinity in the physical plane. This point has coordinates $(r_1, 0)$ where r_1 is the value of r corresponding to the (subsonic) flow at infinity.

(ii) $y = 0$ on OB.

(iii) $y = 0$ on BC.

(iv) $y = 0$ on CD.

(v) $x =$ constant on DO'.

We have used $r \to \infty$ to represent the stagnation condition at the front

of the body in accordance with the usual approximating procedure. Conditions (ii), (iii), and (iv) have to be satisfied since the line $OBCD$ in Fig. 1 is part of the dividing streamline. (v) is essentially the condition which has to be satisfied if the flow is to be symmetric about a line drawn through the centre of the body parallel to the y-axis. It could be written alternatively as $\partial y/\partial v = 0$ but it will be seen later that the present form is preferable because it avoids certain difficulties of convergence.

A typical streamline is sketched in Fig. 2 and it is observed to meet the r-axis at right angles. If the streamline were extended across the r-axis it would be 'heart-shaped' as distinct from the double oval shape which is the characteristic type encountered in the singularities obtained by Cole, and by Helliwell and Mackie, in the problems mentioned in the previous section. This distinction is important. It leads to the usual mathematical difficulties which result from boundary conditions of mixed type.

We shall now examine the singularity at $O'O$ in more detail. It is apparent that y varies from 0 to ∞ as r varies from 0 to r_1 on $v = 0$, that is along DO'. To examine the strength of the singularity we consider a typical incompressible problem. In this case the leading terms in the velocity for the flow past a body with no circulation are given by

$$U - iV = U_1 + \frac{C}{(x+iy)^2},$$

where U_1 is the velocity at infinity and C is a constant. Thus on $x = 0$,

$$y \sim \frac{C}{(U-U_1)^{\frac{1}{2}}} \quad \text{as } U \to U_1.$$

For the high-speed case we may assume that far away from the body the effects of compressibility will be negligible and we therefore look for a singularity of the same strength.

In order to obtain a representation of the singularity we try a solution of the type

$$y_s = r^{\frac{1}{2}} \int_0^\infty f(\lambda) e^{-\lambda v} J_{\frac{1}{2}}(\lambda r)\, d\lambda.$$

The choice of $J_{\frac{1}{2}}(\lambda r)$ is made in order to satisfy the condition (iv) which requires y to vanish on $r = 0$. The corresponding value of x_s is found from equations (2) to be

$$x_s = (\tfrac{3}{2})^{\frac{1}{2}} r^{\frac{3}{2}} \int_0^\infty f(\lambda) e^{-\lambda v} J_{-\frac{1}{2}}(\lambda r)\, d\lambda.$$

For conditions (ii) and (v) to be satisfied it is necessary that

$$\int_0^\infty f(\lambda) J_{\frac{1}{2}}(\lambda r)\, d\lambda = 0 \quad (r > r_1), \tag{3}$$

$$r^{\frac{1}{2}} \int_0^\infty f(\lambda) J_{-\frac{1}{2}}(\lambda r)\, d\lambda = \text{constant} \quad (0 < r < r_1). \tag{4}$$

Finally, $\int_0^\infty f(\lambda) J_{\frac{1}{2}}(\lambda r)\, d\lambda$ must become infinite like $(r_1 - r)^{-\frac{1}{2}}$ as $r \to r_1 - 0$. It is easily verified from a suitable table of Hankel transforms (e.g. Erdélyi (8)), that if

$$f(\lambda) = \lambda^{\frac{1}{2}} J_{\frac{1}{2}}(\lambda r_1),$$

then the resulting integrals satisfy the conditions (3) and (4). Accordingly

$$y_s = r^{\frac{1}{2}} \int_0^\infty \lambda^{\frac{1}{2}} e^{-\lambda v} J_{\frac{1}{2}}(\lambda r_1) J_{\frac{1}{2}}(\lambda r)\, d\lambda,$$

$$x_s = (\tfrac{3}{2})^{\frac{1}{2}} r^{\frac{1}{2}} \int_0^\infty \lambda^{\frac{1}{2}} e^{-\lambda v} J_{\frac{1}{2}}(\lambda r_1) J_{-\frac{1}{2}}(\lambda r)\, d\lambda,$$

and on $v = 0$

$$y_s = \frac{2^{\frac{1}{2}} r^{\frac{1}{2}}}{\pi^{\frac{1}{2}} r_1^{\frac{1}{2}}} (r_1^2 - r^2)^{-\frac{1}{2}} \quad (0 < r < r_1),$$

$$= 0 \quad (r > r_1),$$

while

$$x_s = \frac{3^{\frac{1}{2}} 2^{\frac{1}{3}} \Gamma(\frac{5}{6})}{r_1^{\frac{1}{3}} \{\Gamma(\frac{1}{3})\}^2} \quad (0 < r < r_1).$$

In addition it may be shown that $x_s \to 0$ as $r \to \infty$ which fixes the origin of coordinates at the stagnation point at the leading edge of the body.

Every condition except (iii), the condition on BC, has now been satisfied. It is therefore necessary to add non-singular solutions to y_s to satisfy the condition on BC but without upsetting any of the other conditions which have already been satisfied. It is this problem that is particularly difficult because of the mixed boundary conditions on the r-axis. If the boundary condition on $v = 0$ were $y = 0$, it would be possible to satisfy the conditions on $v = 0$ and $v = v_0$ simultaneously by adding image singularities at the points $r = r_1$, $v = 2kv_0$, where $k = \pm 1, \pm 2, \ldots$, the singularities being of the same strength as the original and having the same sign as k. When added together these would give

$$y = r^{\frac{1}{2}} \int_0^\infty \lambda^{\frac{1}{2}} \frac{\sinh \lambda(v_0 - v)}{\sinh \lambda v_0} J_{\frac{1}{2}}(\lambda r_1) J_{\frac{1}{2}}(\lambda r)\, d\lambda. \tag{5}$$

For the present problem, however, this solution would fail to satisfy the condition on DO'. Alternatively we might attempt to add images at the same points but with negative signs for odd values of k and positive

signs for even values of k. These would give a solution

$$y = r^{\frac{1}{2}} \int_0^\infty \lambda^{\frac{1}{2}} \frac{\sinh \lambda(v_0 - v)}{\cosh \lambda v_0} J_{\frac{1}{2}}(\lambda r_1) J_{\frac{1}{2}}(\lambda r)\, d\lambda.$$

Now the boundary condition on DO' is satisfied but not that on OB. Nevertheless, it is reasonable to suppose that the discrepancy in either case will be small and will decrease as v_0 increases compared with r_1 (that is as the transonic similarity parameter becomes small). For then the image singularities are further away from the r-axis and the influence they have in upsetting the boundary conditions on this axis is correspondingly reduced. In the following section we examine the correction terms which have to be added to complete the solution.

Before proceeding to this, however, we point out that in one sense y_s is itself a solution of the problem. This is when it is considered in conjunction with the transformation described briefly by Germain and Liger (**7**) and in detail by Liger (**9**). By means of this transformation, the hodograph equation for a fictitious gas whose behaviour is very similar to that of a polytropic gas is transformed into Tricomi's equation. At the same time the strip in which the solution of a problem of the type considered is to be found is mapped into an entire quarter-plane in the variables of this equation. It follows that if we have to solve a problem in a strip for the new gas, we have to solve the equivalent problem in the quarter-plane for Tricomi's equation, effectively ignoring the boundary condition on $v = v_0$. Thus y_s is the solution, for this new gas, of the original problem. By the suitable choice of parameters arising in the transformation we may interpret this as a flow past a thin body or alternatively we may take $\delta = \frac{1}{2}\pi$ and consider the flow past a flat-nosed obstacle. However, the mathematical details of the transformation are somewhat intricate and will not be pursued further here.

3. Investigation of the correction terms

The solution of the boundary value problem formulated in the previous section will now be completed by the addition of terms to the expression (5) which will correct the boundary condition on $v = 0$ without disturbing those already satisfied on the other sides of the rectangle $BCDB$ in the hodograph plane in Fig. 2. Accordingly the complete solution will be written

$$y = r^{\frac{1}{2}} \int_0^\infty \{A(\lambda r_1)^{\frac{1}{2}} J_{\frac{1}{2}}(\lambda r_1) + F(\lambda)\} \frac{\sinh \lambda(v_0 - v)}{\sinh \lambda v_0} J_{\frac{1}{2}}(\lambda r)\, d\lambda,$$

$$x = (\tfrac{2}{3})^{\frac{1}{2}} r^{\frac{1}{2}} \int_0^\infty \{A(\lambda r_1)^{\frac{1}{2}} J_{\frac{1}{2}}(\lambda r_1) + F(\lambda)\} \frac{\cosh \lambda(v_0 - v)}{\sinh \lambda v_0} J_{-\frac{1}{2}}(\lambda r)\, d\lambda, \qquad (6)$$

where A is a constant which has been introduced as a scale factor in order to make the length of the straight part of the profile unity. A factor $r_1^{\frac{1}{2}}$ has also been introduced for convenience later. Clearly $y = 0$, as required on $r = 0$ and $v = v_0$, and in addition the singularity at $r = r_1$, $v = 0$ is of the correct strength, provided the contribution from the integral involving $F(\lambda)$ is non-singular at the point. This will be verified from the subsequent solution.

If the conditions on $v = 0$ are to be satisfied,

$$(\tfrac{2}{\pi})^{\frac{1}{2}} r^{\frac{1}{2}} \int_0^\infty \{A(\lambda r_1)^{\frac{1}{2}} J_{\frac{1}{2}}(\lambda r_1) + F(\lambda)\} \coth \lambda v_0 J_{-\frac{1}{2}}(\lambda r)\, d\lambda = \text{constant} \quad (0 < r < r_1), \tag{7}$$

$$r^{\frac{1}{2}} \int_0^\infty \{A(\lambda r_1)^{\frac{1}{2}} J_{\frac{1}{2}}(\lambda r_1) + F(\lambda)\} J_{\frac{1}{2}}(\lambda r)\, d\lambda = 0 \quad (r > r_1). \tag{8}$$

We recall now the relations satisfied by x_s and y_s on $v = 0$, namely,

$$(\tfrac{2}{\pi})^{\frac{1}{2}} r^{\frac{1}{2}} \int_0^\infty A(\lambda r_1)^{\frac{1}{2}} J_{\frac{1}{2}}(\lambda r_1) J_{-\frac{1}{2}}(\lambda r)\, d\lambda = \text{constant} \quad (0 < r < r_1), \tag{9}$$

$$r^{\frac{1}{2}} \int_0^\infty A(\lambda r_1)^{\frac{1}{2}} J_{\frac{1}{2}}(\lambda r_1) J_{\frac{1}{2}}(\lambda r)\, d\lambda = 0 \quad (r > r_1). \tag{10}$$

If (9), (10) are now subtracted from (7), (8) respectively, a pair of dual integral equations is obtained for the unknown function $F(\lambda)$. In order to bring these to a form in which they can be solved, the first one is differentiated with respect to r. The following pair of equations is then obtained for $F(\lambda)$:

$$\int_0^\infty \lambda F(\lambda) \coth \lambda v_0 J_{\frac{1}{2}}(\lambda r)\, d\lambda = -A r_1^{\frac{1}{2}} \int_0^\infty \lambda^{\frac{1}{2}} (\coth \lambda v_0 - 1) J_{\frac{1}{2}}(\lambda r_1) J_{\frac{1}{2}}(\lambda r)\, d\lambda \quad (0 < r < r_1), \tag{11}$$

$$\int_0^\infty F(\lambda) J_{\frac{1}{2}}(\lambda r)\, d\lambda = 0 \quad (r > r_1). \tag{12}$$

The above manipulations have been necessary in order to avoid the occurrence of divergent integrals. It is possible to obtain the complete solution by working from the beginning with a pair of dual integral equations derived from the boundary conditions on $v = 0$. The procedure is to regard the flow first of all as contained in a channel of width $2k$ and then to let k tend to infinity at a suitable stage in the subsequent analysis. The expression (5) which incorporates the correct singularity at $O'O$ then appears as the first approxir ion in an iterative solution of the integral equations obtained in this wa y. However, this approach involves a certain amount of formal manipulation with divergent integrals. The reason for

this is that integrals representing $\partial y/\partial v$ are divergent when v is put equal to zero although their limits as $v \to 0$ exist. It follows that if the problem is reduced at the very beginning to that of solving a pair of dual integral equations obtained by specifying the boundary conditions on $v = 0$, the interpretation of certain integrals as limits when $v \to 0$ is no longer possible. The method which led to the equations (11) and (12) was therefore adopted in order to set up the problem in a formally correct manner.

If the substitutions $r = \rho r_1$, $t = \lambda r_1$, and $\phi(t) = F(\lambda)$ are made, equations (11) and (12) become

$$\int_0^\infty t\phi(t)\coth\left(\frac{v_0 t}{r_1}\right)J_{\frac{1}{2}}(\rho t)\,dt = -A\int_0^\infty t^{\frac{1}{2}}\left\{\coth\left(\frac{v_0 t}{r_1}\right)-1\right\}J_{\frac{1}{2}}(t)J_{\frac{1}{2}}(\rho t)\,dt \qquad (0<\rho<1),$$

$$\int_0^\infty \phi(t)J_{\frac{1}{2}}(\rho t)\,dt = 0 \qquad (\rho > 1).$$

Integral equations of this and of a more general type have been investigated by B. Noble to whom the authors are indebted for supplying them with the results of work as yet unpublished. By means of these results it may be shown that the above system can be reduced to

$$\int_0^\infty t^{\frac{1}{2}}\phi(t)J_{\frac{1}{2}}(\alpha t)\,dt = H(\alpha) \quad (0<\alpha<1), \tag{13}$$

$$= 0 \qquad (\alpha > 1), \tag{14}$$

where

$$H(\alpha) + \int_0^1 \lambda H(\lambda)K(\lambda,\alpha)\,d\lambda = G(\alpha),$$

$$K(\lambda,\alpha) = \int_0^\infty \frac{t\exp(-tv_0/r_1)}{\sinh(tv_0/r_1)}J_{\frac{1}{2}}(\alpha t)J_{\frac{1}{2}}(\lambda t)\,dt, \tag{15}$$

and $$G(\alpha) = -\frac{A2^{\frac{1}{2}}}{\pi^{\frac{1}{2}}}\alpha^{-\frac{1}{2}}\int_0^\alpha \rho^{\frac{1}{2}}(\alpha^2-\rho^2)^{-\frac{1}{2}}\int_0^\infty t^{\frac{1}{2}}J_{\frac{1}{2}}(t)J_{\frac{1}{2}}(\rho t)\frac{\exp(-tv_0/r_1)}{\sinh(tv_0/r_1)}\,dt d\rho.$$

If the orders of integration in the expression for $G(\alpha)$ are inverted we find first that the integration with respect to ρ gives essentially Sonine's first integral and, finally, that

$$G(\alpha) = -AK(1,\alpha).$$

$\phi(t)$ is now found by an application of the Hankel inversion theorem to (13) and (14) and, if we replace the original variables, we obtain

$$F(\lambda) = (\lambda r_1)^{\frac{1}{2}}\int_0^1 \alpha H(\alpha)J_{\frac{1}{2}}(\lambda r_1\alpha)\,d\alpha, \tag{16}$$

where $H(\alpha)$ is the solution of the integral equation

$$H(\alpha)+\int_0^1 \lambda H(\lambda)K(\lambda,\alpha)\,d\lambda = -AK(1,\alpha), \tag{17}$$

and the kernel $K(\lambda,\alpha)$ is given by (15).

It is now necessary to rewrite the expression for $K(\lambda,\alpha)$ as an expansion in a power series. It will be recalled that the extra correction terms are expected to be small when r_1 is small compared with v_0. Accordingly we expand the term $\operatorname{cosech}(tv_0/r_1)$ which appears in the integrand in powers of $\exp(-tv_0/r_1)$. If the orders of summation and integration are exchanged it follows that

$$K(\lambda,\alpha) = 2\sum_{n=1}^{\infty}\int_0^{\infty} t\exp(-2tv_0 n/r_1)J_{\frac{1}{3}}(\alpha t)J_{\frac{1}{3}}(\lambda t)\,dt.$$

Each term in this series may be written as an infinite sum of hypergeometric functions (Erdélyi (8)) to give, after a certain amount of algebra,

$$K(\lambda,\alpha) = (\lambda\alpha)^{\frac{1}{3}}\sum_{m=0}^{\infty} a_m(r_1/v_0)^{11/3+2m}\lambda^{2m}{}_2F_1(-m,-\tfrac{5}{6}-m;\tfrac{11}{6};\alpha^2/\lambda^2), \tag{18}$$

where

$$a_m = \frac{(-1)^m\Gamma(\frac{7}{3}+m)\zeta(\frac{11}{3}+2m)}{2^{2m+\frac{1}{3}}\pi^{\frac{1}{3}}\Gamma(\frac{11}{6})m!}$$

and $\zeta(z)$ is the Riemann zeta function. The values of a_m for $m = 0, 1,..., 8$ are shown in Table 1 and the rapid decrease in their magnitude is apparent.

TABLE 1

m	0	1	2	3	4	5	6	7	8
a_m	0·2497	−0·1341	0·05495	−0·01977	0·006583	−0·002085	0·0006371	−0·0001896	0·00005530

The hypergeometric functions occurring in (18) reduce to polynomials of degree m. If $K(\lambda,\alpha)$ is expanded in powers of α we obtain

$$K(\lambda,\alpha) = (r_1/v_0)^{11/3}(\lambda\alpha)^{\frac{1}{3}}\sum_{m=0}^{\infty} b_m(\alpha/\lambda)^{2m},$$

where the b_m are certain functions of $\lambda r_1/v_0$ consisting of series of even powers starting with the term $(\lambda r_1/v_0)^{2m}$.

It is now possible to obtain an iterative solution of the integral equation (17). A sequence $H_n(\alpha)$ is determined by means of the relation

$$H_n(\alpha) = -AK(1,\alpha)-\int_0^1 \lambda H_{n-1}(\lambda)K(\lambda,\alpha)\,d\lambda.$$

$H_0(\alpha)$ is taken to be 0. Then

$$H_1(\alpha) = -AK(1,\alpha)$$
$$= -A(r_1/v_0)^{11/3}\alpha^{\frac{1}{3}}(\bar{b}_0+\bar{b}_1\alpha^2+\ldots),$$

where $\bar{b}_m$ is the value of b_m when $\lambda = 1$. The next approximation is

$$H_2(\alpha) = -AK(1,\alpha)+A\int_0^1 \lambda K(1,\lambda)K(\lambda,\alpha)\,d\lambda.$$

$K(1,\lambda)$ and $K(\lambda,\alpha)$ are now expanded as power series and the resulting integration performed with respect to λ. It is found that

$$H_2(\alpha) = -A\alpha^{\frac{1}{3}}(c_0+c_1\alpha^2+c_2\alpha^4+\ldots),$$

where the c_m are certain functions of r_1/v_0. It is not necessary to proceed with further iteration as the convergence is extremely rapid and the above solution for $H_2(\alpha)$ gives $H(\alpha)$ up to terms of order $(r_1/v_0)^{10}$. Hence we may write

$$H(\alpha) = -A\sum_{m=0}^{\infty} c_m\,\alpha^{\frac{1}{3}+2m}. \tag{19}$$

Finally, we return to the original function $F(\lambda)$ which is given by (16). If the series for $H(\alpha)$ given by (19) is substituted in this integral it is found that expressions of the form $\int_0^{\lambda r_1} t^{11/6+2m}J_{\frac{1}{3}}(t)\,dt$ have to be evaluated. On integration by parts this becomes

$$(\lambda r_1)^{11/6+2m}J_{11/6}(\lambda r_1)-2m(\lambda r_1)^{\frac{1}{3}+2m}J_{17/6}(\lambda r_1)+$$
$$+2m(2m-2)(\lambda r_1)^{-\frac{1}{3}+2m}J_{23/6}(\lambda r_1)+\ldots.$$

Hence combining all the terms we find

$$F(\lambda) = A\sum_{m=1}^{\infty}(-1)^m e_m\frac{J_{\frac{1}{3}+m}(\lambda r_1)}{(\lambda r_1)^{m-\frac{1}{3}}},$$

where the e_m are functions of r_1/v_0. It is convenient to define $e_0 = 1$ so that equation (6) can now be written

$$y = A\sum_{m=0}^{\infty}(-1)^m e_m\int_0^{\infty}\frac{r_1^{\frac{1}{3}}}{(\lambda r_1)^{m-\frac{1}{3}}}\frac{\sinh\lambda(v_0-v)}{\sinh\lambda v_0}J_{\frac{1}{3}}(\lambda r)J_{\frac{1}{3}+m}(\lambda r_1)\,d\lambda. \tag{20}$$

This expression is the complete solution of the boundary value problem. Table 2 gives the values of e_m corresponding to a range of values of r_1/v_0, correct to three decimal places.

4. Analysis of the solution

The expression (20) represents the solution for y in terms of the velocity variables of the flow past a thin doubly symmetric body. The velocity is nowhere supersonic in the flow field but sonic velocity is attained along

a segment of the boundary. An important physical property apparent from symmetry is that the total drag on the body is zero. It is now necessary to investigate (20) and allied equations in detail in order to find the geometrical ratios which determine the shape of the profiles which are obtained.

First we note that for $v = 0$, (20) gives for y the series

$$y = A \sum_{m=0}^{\infty} (-1)^m e_m \int_0^{\infty} r^{\frac{1}{2}} (\lambda r_1)^{\frac{1}{2}-m} J_{\frac{1}{2}}(\lambda r) J_{\frac{1}{2}+m}(\lambda r_1)\, d\lambda,$$

and the evaluation of the integrals gives

$$\begin{aligned} y &= A \sum_{m=0}^{\infty} (-1)^m e_m \frac{2^{\frac{1}{2}-m} r^{\frac{1}{2}}}{\Gamma(m+\frac{1}{2}) r_1^{2m+\frac{1}{2}}} (r_1^2 - r^2)^{m-\frac{1}{2}} \quad (0 < r < r_1), \\ &= 0 \qquad\qquad (r > r_1). \end{aligned}$$

TABLE 2

r_1/v_0	0	0·1	0·2	0·3	0·4	0·5	0·6
e_0	1	1	1	1	1	1	1
e_1	0	0	0·001	0·003	0·007	0·015	0·027
e_2	0	0	0	0	−0·001	−0·003	−0·007
e_3	0	0	0	0	0	0·001	0·003
e_4	0	0	0	0	0	0	−0·002

This shows that the singularity at $r = r_1$, $v = 0$ is still of the correct strength and that the asymptotic behaviour of y near it is not affected by the addition of the extra terms to the original solution (that is, the terms for which $m > 0$).

By means of equations (2) the value of x for the complete solution can be obtained. It is

$$x = A(\tfrac{3}{2})^{\frac{1}{2}} \sum_{m=0}^{\infty} (-1)^m e_m \int_0^{\infty} r^{\frac{1}{2}} (\lambda r_1)^{\frac{1}{2}-m} \frac{\cosh \lambda(v_0 - v)}{\sinh \lambda v_0} J_{\frac{1}{2}+m}(\lambda r_1) J_{-\frac{1}{2}}(\lambda r)\, d\lambda. \quad (21)$$

A is now determined from the condition that the straight segment (BC in Fig. 1) is of unit length. We therefore let $x = 1$ when $r = 0$, $v = v_0$. If $r \to 0$ in (21) when $v = v_0$ we obtain

$$1 = A(\tfrac{3}{2})^{\frac{1}{2}} \sum_{m=0}^{\infty} (-1)^m e_m \frac{2^{\frac{1}{2}}}{\Gamma(\frac{1}{3})} r_1^{\frac{1}{2}-m} \int_0^{\infty} \frac{\operatorname{cosech} \lambda v_0}{\lambda^{m+\frac{1}{2}}} J_{\frac{1}{2}+m}(\lambda r_1)\, d\lambda.$$

If the substitution $t = \lambda v_0$ is made, the Bessel function expanded as a series and the orders of integration and summation of this series are interchanged, the above expression becomes

$$1 = \frac{A 6^{\frac{1}{2}}}{v_0^{\frac{1}{2}} \Gamma(\frac{1}{3})} \sum_{m=0}^{\infty} \frac{(-1)^m e_m}{2^m} \sum_{n=0}^{\infty} \frac{(-1)^n (r_1/v_0)^{2n+\frac{1}{2}}}{2^{2n+\frac{1}{2}} n!\, \Gamma(m+n+\frac{11}{6})} \int_0^{\infty} \frac{t^{2n+\frac{1}{2}}}{\sinh t}\, dt.$$

The integrals in this equation can be written in terms of the Riemann zeta function and a form suitable for computation is finally given by

$$\frac{v_0^{\frac{4}{3}}}{r_1^{\frac{4}{3}}A} = \frac{3^{\frac{1}{3}}2^{\frac{1}{3}}}{\Gamma(\frac{1}{3})}\sum_{m=0}^{\infty}\frac{(-1)^m e_m}{2^m}\sum_{n=0}^{\infty}\frac{(-1)^n\Gamma(2n+\frac{5}{3})(1-2^{-2n-\frac{5}{3}})\zeta(2n+\frac{5}{3})}{2^{2n}n!\,\Gamma(m+n+\frac{11}{6})}\left(\frac{r_1}{v_0}\right)^{2n}.$$

In Table 3 the value of $Ar_1^{\frac{4}{3}}/v_0^{\frac{4}{3}}$ is given for a range of values of r_1/v_0. It is worth pointing out that the values obtained by using only the term e_0 in the summation with respect to m contribute 99 per cent or more of the total. This lends considerable support to the argument put forward in section 2 that the correction terms would probably be of very small magnitude.

TABLE 3

r_1/v_0	0	0·1	0·2	0·3	0·4	0·5	0·6
$Ar_1^{\frac{4}{3}}/v_0^{\frac{4}{3}}$	0·9385	0·9426	0·9542	0·9740	1·001	1·036	1·077

Series expansions can be found for x on the dividing streamline for all values of $r > r_1$. When $v = 0$ in (21)

$$x = A(\tfrac{3}{2})^{\frac{1}{3}}\sum_{m=0}^{\infty}(-1)^m e_m\int_0^{\infty} r^{\frac{1}{3}}(\lambda r_1)^{\frac{1}{3}-m}\coth\lambda v_0\, J_{-\frac{1}{3}}(\lambda r)J_{\frac{1}{3}+m}(\lambda r_1)\,d\lambda. \quad (22)$$

If the partial fraction expansion

$$\coth\lambda v_0 = \frac{1}{\lambda v_0}+2\sum_{n=1}^{\infty}\frac{\lambda v_0}{(\lambda v_0)^2+(n\pi)^2}$$

is substituted in (22), the resulting integrals can be evaluated and we obtain

$$x = -A2^{\frac{2}{3}}3^{\frac{1}{3}}v_0^{-1}r^{\frac{1}{3}}\sum_{m=0}^{\infty}(-1)^m e_m\sum_{n=1}^{\infty}\left(\frac{n\pi r_1}{v_0}\right)^{\frac{1}{3}-m}I_{\frac{1}{3}+m}\left(\frac{n\pi r_1}{v_0}\right)K_{\frac{1}{3}}\left(\frac{n\pi r}{v_0}\right)$$
$$(r > r_1). \quad (23)$$

This gives x on the axis of symmetry as a function of r. When $v = v_0$, $\coth\lambda v_0$ is replaced by $\operatorname{cosech}\lambda v_0$ in (22) and this has the effect of introducing a term $(-1)^n$ in the inner series. In this way a series for x is found on the straight part of the profile up to the value $r = r_1$. Bearing in mind the extremely rapid convergence of the summation with respect to m it is seen that the series provides the best way of computing the velocity on the dividing streamline, provided $r > r_1$ and is not too close to r_1. This in turn leads to a knowledge of the pressure distribution on part of the profile. These series also serve to confirm at once the location of the origin of coordinates at the stagnation point for it is clear that $x \to 0$ in (23) as $r \to \infty$.

After the evaluation of the constant A, two other quantities have to be

found before the shape of the profile can be determined quantitatively. These are $2h$, the total length of the body, and $2d$, its width at the mid-point. This is the maximum width of the body since the free streamline is known to be convex to the flow. In theory a series of points should be plotted along the free streamline to determine its shape accurately, but in practice the body is thin enough for an excellent estimate to be obtained from a knowledge of d and h. The value of h is given by the value of x when $v = 0$ and is independent of r for $r < r_1$. However, for facility in calculation, the value $r = 0$ is naturally selected. This will give the x coordinate of the point D in Fig. 1. When $v = 0$ and r is allowed to tend to zero in (21) we obtain

$$h = A\frac{6^{\frac{1}{3}}}{\Gamma(\frac{1}{3})}\sum_{m=0}^{\infty}(-1)^m e_m r_1^{\frac{1}{3}-m}\int_0^{\infty}\lambda^{-m-\frac{1}{3}}\coth\lambda v_0 J_{\frac{1}{3}+m}(\lambda r_1)\,d\lambda.$$

In order to express this in a form in which h can be determined numerically $\coth\lambda v_0$ is written as the series

$$\coth\lambda v_0 = 1+2\sum_{k=1}^{\infty}\exp(-2k\lambda v_0).$$

The resulting integrals are evaluated term by term, each term containing

TABLE 4

r_1/v_0	0	0·1	0·2	0·3	0·4	0·5	0·6
h	∞	30·4	9·99	5·37	3·62	2·72	2·21

a hypergeometric function which must itself be expanded. Further rearrangement of terms and summation leads eventually to the form

$$h = \frac{Ar_1^{\frac{1}{3}}(\frac{3}{2})^{\frac{1}{3}}}{v_0^{\frac{5}{3}}\Gamma(\frac{1}{3})}\sum_{m=0}^{\infty}(-1)^m e_m\left\{\frac{\Gamma(\frac{5}{6})(r_1/v_0)^{-\frac{1}{3}}}{2^{m-\frac{1}{3}}m!}+\sum_{n=0}^{\infty}\frac{(-1)^n\Gamma(\frac{5}{3}+2n)\zeta(\frac{5}{3}+2n)}{2^{\frac{1}{3}+m+4n}\Gamma(m+n+\frac{11}{6})n!}\left(\frac{r_1}{v_0}\right)^{2n}\right\}.$$

Despite the complicated appearance of the above series, convergence is fairly rapid and in Table 4 the value of h is given for a range of values of r_1/v_0.

There remains the problem of finding d. This cannot be found directly from the coordinates because the procedure of the transonic approximation has identified the body contour with the line $y = 0$. However, it is not difficult to see from Fig. 1 that d is given by

$$d = \delta+\int_C^D \theta\,ds,$$

where θ is the angle which the velocity vector makes with the x-axis and the integration is carried out along the body. An equivalent form is

$$d = \delta + \int_C^D \frac{v\,dx}{\gamma+1} = \delta + \left[\frac{vx}{\gamma+1}\right]_C^D - \int_{v_0}^0 \frac{x\,dv}{\gamma+1},$$

on integrating by parts, so that finally

$$d = \frac{1}{\gamma+1}\int_0^{v_0} x\,dv.$$

In this integral x is given as a function of v by letting $r \to 0$ in (21). Hence, after performing the integration with respect to v,

$$d = \frac{A6^{\frac{1}{3}}}{(\gamma+1)\Gamma(\frac{1}{3})}\sum_{m=0}^{\infty}(-1)^m e_m r_1^{\frac{1}{3}-m}\int_0^{\infty}\lambda^{-\frac{1}{3}-m}J_{\frac{1}{3}+m}(\lambda r_1)\,d\lambda.$$

These integrals can be evaluated without difficulty and the final form is

$$\frac{d}{\delta} = \frac{Ar_1^{\frac{1}{3}}3^{\frac{1}{2}}2^{\frac{1}{3}}}{v_0^{\frac{1}{3}}\pi^{\frac{1}{2}}}\left(\frac{r_1}{v_0}\right)^{-\frac{2}{3}}\sum_{m=0}^{\infty}\frac{(-1)^m e_m}{1.3.5\ldots(2m+1)}.$$

Table 5 gives values of d/δ for the range of values of r_1/v_0 considered.

TABLE 5

r_1/v_0	0	0·1	0·2	0·3	0·4	0·5	0·6
d/δ	∞	4·84	3·08	2·40	2·03	1·81	1·66

TABLE 6

r_1/v_0	0	0·1	0·2	0·3	0·4	0·5	0·6
Width ratio	0	0·207	0·325	0·417	0·493	0·552	0·602
Length ratio	0	0·0329	0·100	0·186	0·276	0·368	0·452
$(1-M_1^2)/\{(\gamma+1)\delta\}^{\frac{2}{3}}$	0	0·282	0·448	0·587	0·711	0·825	0·932

It is now possible to present the essential results collectively. A given value of r_1/v_0 determines δ/d, which is the ratio of the width of the body at the end of the straight section to the maximum width of the body. We shall call this the *width ratio*. It also determines h, the ratio of the semi-length of the body to the length of a straight section. The reciprocal of this will be called the *length ratio* which is therefore the length of a straight section when the total length of the body is taken to be 2 units. In Table 6 the width and length ratios are given for different values of r_1/v_0. The corresponding value of the transonic similarity parameter

$(1-M_1^2)/\{(\gamma+1)\delta\}^{\frac{2}{3}}$ is also given for convenience of reference. Here M_1 is the Mach number at infinity and γ is taken to be 1·4.

As might have been anticipated from the transonic similarity theory the width and length ratios are dependent only on the values of the transonic similarity parameter. However, the ratio of the width to the length of the body is determined only when M_1 and δ are known separately.

FIG. 3. Typical profile for $M_1 = 0{\cdot}82$.

A typical profile is shown to scale in Fig. 3. It corresponds to a (total) wedge angle of 10° in a flow for which the Mach number at infinity is 0·82.

This research has been sponsored in part by the Air Force Office of Scientific Research of the Air Research and Development Command, U.S. Air Force, under contract AF 61(514)–1170, through the European Office A.R.D.C.

REFERENCES

1. G. GUDERLEY and H. YOSHIHARA, *J. Aero. Sci.* **17** (1950) 723.
2. J. D. COLE, *J. Math. Phys.* **30** (1951) 79.
3. J. B. HELLIWELL and A. G. MACKIE, *J. Fluid Mech.* **3** (1957) 93.
4. A. ROSHKO, Nat. Adv. Comm. Aero., Wash., Tech. Note 3168, 1954.
5. L. TRILLING, *Z. angew. Math. Phys.* **4** (1953) 358.
6. D. RIABOUCHINSKY, *Proc. Lond. Math. Soc.* **19** (1921) 206.
7. P. GERMAIN and M. LIGER, *C.R. Acad. Sci.* **234** (1952) 1846.
8. A. ERDÉLYI (ed.), *Tables of Integral Transforms*, vol. 2 (McGraw-Hill, 1954).
9. M. LIGER, O.N.E.R.A. Publ. 64, 1953.

ON THE ABSOLUTE MINIMUM WEIGHT DESIGN OF FRAMED STRUCTURES†

By JACQUES HEYMAN‡
(*Engineering Laboratories, Cambridge University*)

[Received 11 June 1958]

SUMMARY

If the cross-section of the members of a frame is varied continuously so that the 'strength' of the frame follows the bending moment diagram, then, provided the design is carried out in a certain way, the frame will have absolute minimum material consumption. This theorem is proved separately here, although for plastic design the theorem is a special case of the general principles given by Drucker and Shield (**1**, **2**). However, this special theorem applies equally well to certain completely elastic structures.

The theorem is applied to determine the minimum weight of some simple continuous beam systems, and a trial and error 'relaxation' technique is developed. These designs are compared with more practical designs in which the cross-section of the members varies discontinuously.

1. Introduction

THE calculation of absolute minimum weight of a structure is of interest to the designer, since he is able to estimate penalties in weight and cost should he depart, for practical reasons, from this minimum. It is inconvenient, for example, to vary the cross-section of steel members continuously, and abrupt changes in cross-section may imply the use of only a few per cent more material. [Simple comparative examples are given below.] Reinforced concrete may be 'shaped' more easily than steelwork; here again, the designer can balance the cost of complicated formwork against the saving in material for the minimum weight design.

The term 'strength' of a member will be left undefined for the moment. For the purpose of the following arguments, however, it may be of help to think of the strength of a member as the full plastic moment (for plastic design), or as the limiting elastic moment in which the yield stress is just reached in the outer fibres (elastic design). A more detailed discussion of strength, and the way in which a given strength can be achieved practically, is given below.

† The results presented in this paper were obtained in the course of research sponsored by the Office of Naval Research under Contract Nonr-562(10) with Brown University.

‡ Fellow of Peterhouse, Lecturer in Engineering, University of Cambridge. Visiting Professor, Brown University, 1957–8.

2. Basic principles

For a frame of given dimensions acted upon by given (fixed) loads, it is possible (if the frame is redundant) to construct infinitely many equilibrium bending moment distributions. Suppose that for one such distribution the bending moment at a generic cross-section is M_0, and that the size of the member at that cross-section is such that the strength is also $|M_0|$. Although strength has not been defined, it will be assumed that if a frame has strength $|M_0|$ (variable), then the total weight of the frame is given, to some scale, by

$$W = \int |M_0|\, dx, \tag{1}$$

where the integration extends over the length of all members. The implications of equation (1) will be discussed later.

A given function $|M_0|$ will be called a *design* of the frame. Of the infinitely many designs corresponding to the infinitely many equilibrium bending moment distributions, one will have minimum weight. This minimum weight design will be denoted $|M_0^*|$.

Consider now a deflected form of the structure defined by displacements y from the original position. The curvature κ of any cross-section is given as usual by the second derivative of deflexion with respect to distance along the member, i.e. $\kappa = d^2y/dx^2$. A deflected form y will be called *compatible* with a design $|M_0|$ if $\operatorname{sgn} M_0 = \operatorname{sgn} \kappa$ everywhere; that is, if sagging bending moments are denoted positive, the curvature is positive at a cross-section where a positive moment acts, and negative at a section of hogging bending moment.

The following theorem holds: *If, for the given loads, a design $|M_0^*|$ can be found that is compatible with a deflected form of the structure having constant absolute curvature, then the design $|M_0^*|$ has minimum weight.*

This theorem is a special case of the general theorem of Drucker and Shield (**1**, **2**) for the continuum. However, the general theorem applies only to plastic structures; the following proof of the special theorem is valid for elastic as well as for plastic frames.

Suppose concentrated loads P and distributed loads p are applied to the frame, these being in equilibrium with the set of bending moments M_0^*. Further, suppose that for this design $|M_0^*|$ the deflexions y of the frame are compatible with curvatures $\pm\kappa$, where κ is a constant. By virtual work,

$$\overline{W} = \int py\, dx + \sum Py = \int M_0^* \kappa\, dx. \tag{2}$$

Now, since $(\operatorname{sgn} M_0^*) = (\operatorname{sgn} \kappa)$, the quantity $\overline{W}$ is given from (2) as

$$\overline{W} = \int |M_0^*||\kappa|\, dx = |\kappa| \int |M_0^*|\, dx = |\kappa| W^*, \tag{3}$$

using equation (1). Thus the weight W^* of the putative minimum weight design is $\overline{W}/|\kappa|$.

Consider any other design $|M_0|$, where, of course, M_0 is in equilibrium with the loads P and p. By virtual work again,

$$\overline{W} = \int py\,dx + \sum Py = \int M_0 \kappa\,dx. \quad (4)$$

Thus from (3) and (4),

$$W^* = \int M_0 \frac{\kappa}{|\kappa|}\,dx \leqslant \int |M_0| \left|\frac{\kappa}{|\kappa|}\right| dx \quad (5)$$

since M_0 and κ are not necessarily compatible. Now $\kappa/|\kappa| = \pm 1$; thus (5) gives

$$W^* \leqslant \int |M_0|\,dx = W. \quad (6)$$

Thus W^* cannot exceed the weight of any other design, and hence is the minimum weight.

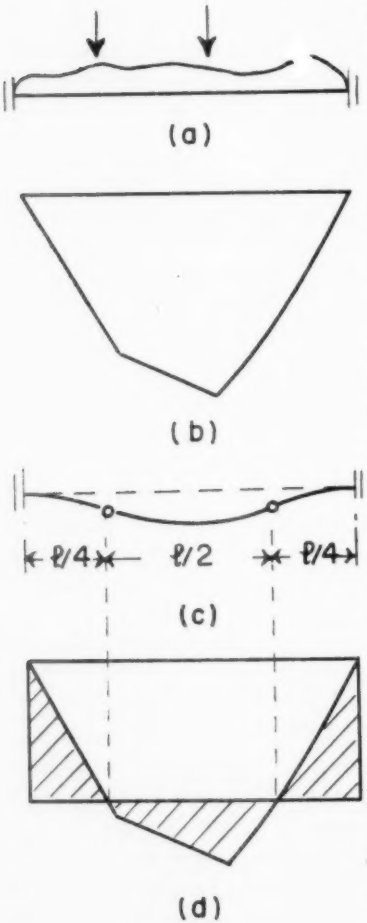

FIG. 1

The theorem can be illustrated simply by reference to a fixed-ended beam, Fig. 1. Suppose the loads in Fig. 1 (*a*) act downwards, for simplicity, so that the 'free' bending moment diagram is of the non re-entrant form in Fig. 1 (*b*). [Re-entrant bending moment diagrams lead to complications; these are discussed below.] The infinitely many equilibrium distributions may be constructed by superimposing on this free bending moment diagram a straight reactant line due to the end fixing moments. Now the minimum weight theorem states that the beam can take up a deflected form with constant curvature; simple geometrical considerations show that arcs of constant curvature can be combined only in the way shown in Fig. 1 (*c*). Over the central half of the beam there is an arc of positive curvature, and the two end portions, of lengths $l/4$, have constant negative curvature. This deflexion diagram is symmetrical, and is the only one which satisfies the theorem, being completely

independent of the applied loads. From the theorem, the sign of the bending moment must be positive in the central half of the beam, and negative at the ends, to correspond with the signs of the curvatures. The constant curvature arcs must therefore join at inflexion points, and the reactant line is fixed as in Fig. 1 (*d*). The shaded diagram gives the strength of the beam for minimum weight; note that this strength becomes zero at the inflexion points, so that the final minimum weight design is statically determinate (consisting of a simply supported central portion of length $l/2$ with two end cantilevers).

In constructing the deflexion diagram, Fig. 1 (*c*), it has been assumed that discontinuities of slope do not occur at the inflexion points.

LEMMA. *The deflected form of the minimum weight design consists of arcs of constant curvature. These arcs must join with no discontinuity of slope.*

Suppose there is a deflected form of the minimum weight beam for which discontinuities in slope θ occur at the inflexion points. Consider a design $|M_0^{**}|$ identical with $|M_0^{*}|$ (the minimum weight design), except that in the neighbourhood of the inflexion points $M_0^{**} \neq 0$. Thus the design $|M_0^{**}|$ is too 'strong', and

$$W^{**} > W^{*}. \tag{7}$$

Now, as before,

$$\overline{W} = |\kappa| W^{*} = |\kappa| W^{**} + \sum |M_0^{**}.\theta|, \tag{8}$$

the last term representing the work done at the discontinuities. From (8), $W^{**} < W^{*}$, which contradicts (7). Thus the lemma is established.

3. Simple designs

It was seen that the minimum weight design of a fixed-ended beam is independent of the loading system, provided the loads all act vertically downwards. The same is true of a propped cantilever; geometrical considerations show that the point of inflexion must always occur at a distance $l/\sqrt{2}$ from the prop (Fig. 2). This independence of the minimum weight design on the loading system holds for only the simplest problems.

Consider, for example, the two span beam with one redundancy sketched in Fig. 3 (*a*). The bending moment diagram will be of the general form shown in Fig. 3 (*b*), where the single redundancy has been taken as the moment M at the internal support. As sketched, it will be seen that there are two inflexion points distant a_1 and a_2 from the internal support. [Most loading conditions, but not all, will imply two inflexion points for the minimum weight design. Attention will be confined for the moment to the case illustrated.] From the theorem, the deflected form of the minimum weight design is as sketched in Fig. 3 (*c*), with hinges at the two

sections defined by a_1 and a_2. [Note that this structure now has one degree of freedom, compared with the just statically determinate structure of Fig. 1 (*c*).] Now a_1 and a_2 are not uniquely determined from purely geometrical considerations of the deflected form. General expressions are given below; it may be noted here that the constant curvature condition gives only one relationship between a_1 and a_2. Some other equation must

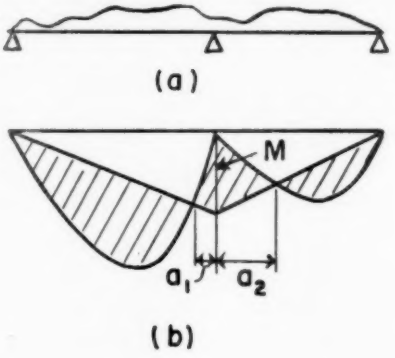

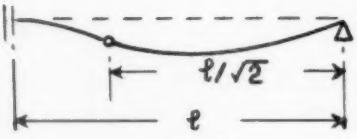

FIG. 2

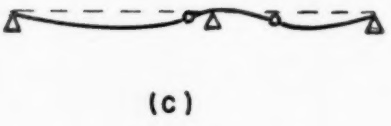

FIG. 3

therefore be found to solve the problem; this equation is furnished by inspection of Fig. 3 (*b*). It will be seen that a_1 and a_2 are related by the actual shape of the free bending moment diagram. This implies that the loading conditions must be used to find the minimum weight design, and this is no longer independent of the loads as it was for the single span fixed ended beam.

It will now be demonstrated (but not proved rigorously) that it is always possible to construct a proper minimum weight deflexion curve, i.e. one consisting of arcs of constant curvature. Consider a portion of a continuous beam between two supports, and suppose that the free bending moment diagram is drawn and a reactant line superimposed. Now an arc of constant curvature is specified by two arbitrary constants; if there is no inflexion point in the bending moment diagram, the known deflexions at the supports (zero for simplicity) will enable the two constants to be calculated. If the free bending moment diagram is re-entrant, so that

there may exist inflexion points, a similar argument may be used. Between one end of the beam and the first inflexion point, an arc of constant curvature may be specified in terms of one unknown constant (the other constant being determined by the condition $\delta = 0$ at the end support). By continuity of slope and deflexion at the first inflexion point, the arc of reverse curvature between the first and second inflexion points is then uniquely determined in terms of the one unknown constant. Thus each arc may be constructed until the other end of the beam is reached; at the other end, the condition $\delta = 0$ enables the unknown constant to be calculated.

Suppose now one extra internal support is provided for the span considered. One extra condition must be satisfied at this support ($\delta = 0$, say). But the extra support has introduced one extra redundancy into the problem; this means that the reactant line can be adjusted with one degree of freedom in order that the extra deflexion condition is satisfied. Similarly, a fixed end to a beam introduces one extra geometrical condition ($\theta = 0$), but one redundancy is also introduced.

For every example of a framed structure, the degrees of freedom of the reactant line (i.e. the degree of redundancy) will always enable a minimum weight deflexion curve to be constructed.

4. Slope-inflexion equations

A relaxation method is developed in the next section which 'balances' angles of rotation at supports. For this purpose, certain elementary solu-

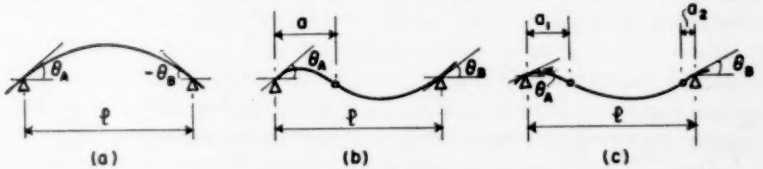

FIG. 4

tions are required, and the most common cases are illustrated in Fig. 4. In Fig. 4 (*a*) a single span is bent into constant curvature with no inflexion points; one inflexion point occurs in Fig. 4 (*b*), and two in Fig. 4 (*c*). Taking the constant curvature κ equal to unity, the following expressions may be obtained for the angles of rotation at the supports:

No inflexion points: $$\theta_A = \frac{l}{2}, \qquad \theta_B = -\frac{l}{2}. \tag{9a}$$

One inflexion point:
$$\theta_A = \frac{l}{2} - \frac{(l-a)^2}{l}, \qquad \theta_B = \frac{l}{2} - \frac{a^2}{l}. \tag{9b}$$

Two inflexion points:
$$\theta_A = \frac{l}{2} - \frac{(l-a_1)^2}{l} + \frac{a_2^2}{l}, \qquad \theta_B = -\frac{l}{2} + \frac{(l-a_2)^2}{l} - \frac{a_1^2}{l}. \tag{9c}$$

It will be seen that if the positions of the inflexion points are known, the angles at each end of a span may be calculated immediately from equations (9). Since the positions of the inflexion points depend, in general, on the bending moment diagram, no general solutions are possible except for the trivial cases of single-span beams. [For example, a single-span fixed-ended beam has $\theta_A = \theta_B = 0$; equations (9c), assuming two inflexion points, give $a_1 = a_2 = l/4$.]

5. Numerical example

The problem shown in Fig. 5 will be solved numerically to illustrate the relaxation technique. A continuous beam has supports at intervals of

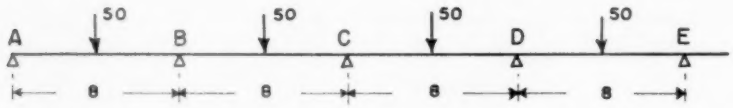

FIG. 5

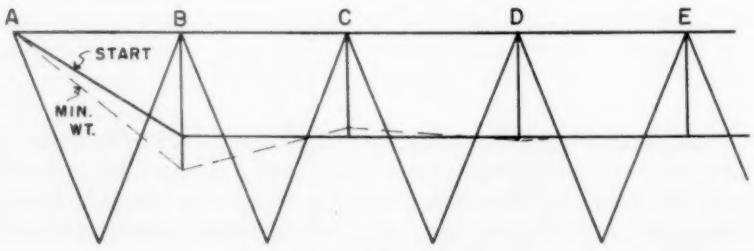

FIG. 6

8 units, each span carrying a central concentrated load of 50 units; the minimum weight design is required. The problem is started by constructing the free bending moment diagram, and superimposing a guessed

reactant line, as in Fig. 6. For this problem, the height of the free bending moment diagrams is 100 units, and the values of the reactant moments at the internal supports have each been taken as 50. These starting moments are shown in Table 1. From Fig. 6 the values of a_1 and a_2 (see Fig. 4 (*c*)) may be read off, and the rotations θ computed for each end of the separate spans by means of equations (9 c). The rotations agree except at support B, where there is a discontinuity in slope of 1·12. The value of M_B is adjusted to make the slope continuous at B; it will be seen that increasing M_B from 50 to 64 causes the discontinuity to decrease from 1·12 to —0·04. A discontinuity is introduced by this process at support C; moment M_C must be adjusted, and the work proceeds until all discontinuities are small. The final reactant line for minimum weight is shown in Fig. 6.

This method can of course be used for any system of loads; the free bending moment diagram is drawn, and the values a_1 and a_2 defining the inflexion points read off for the current position of the reactant line.

6. The 'strength' of frames

The minimum weight designs proposed above can be achieved with either entirely elastic or completely plastic frames; in both cases it is assumed that a suitable load factor is incorporated in the loads.

Examining first an entirely elastic structure, it will be seen that the conditions of the basic theorem will be satisfied if (1) the yield stress is just reached in the extreme fibres at all cross-sections, (2) the members have constant depth, and (3) the width of the (rectangular) cross-section is adjusted so that the moment of resistance at each section equals the design bending moment. Condition (1) is one of the strength criteria; all sections are fully stressed. Since all cross-sections have equal maximum stress, the requirement of condition (2), that all members have the same depth, ensures that constant curvatures are developed. Condition (3) completes the strength criterion and ensures that the weight of the members is a linear function of the moment of resistance, as implied by equation (1).

These three conditions could be almost exactly fulfilled in practice with materials like wood, or like pre-stressed concrete; note that condition (3) implies that the width of the members is zero at the inflexion points, so that some practical adjustment must be made at these sections. The three conditions could be satisfied reasonably closely with an I section steel beam, the flanges being curtailed continuously or in discrete steps. The linear weight criterion of equation (1) would not be satisfied so closely with this type of design.

TABLE 1

	A	*B*	*C*	*D*	*E*
Start	0	50	50	50	50
	$a_1 = 0$	$a_2 = 1{\cdot}6$ | $a_1 = a_2 = 2$	$a_1 = a_2 = 2$	$a_1 = a_2 = 2$	
θ		1·12 | 0	0 | 0	0 | 0	0 | 0
		1·12	0	0	0
Adjust M_B	0	64	50	50	50
	$a_1 = 0$	$a_2 = 1{\cdot}94$ | $a_1 = 2{\cdot}39$	$a_2 = 2{\cdot}15$		
θ		0·60 | 0·64	−0·44 | 0	0 | 0	0 | 0
		−0·04	−0·44	0	0
Adjust M_C	0	64	45	50	50
		$a_1 = 2{\cdot}34$	$a_2 = 1{\cdot}98$ | $a_1 = 1{\cdot}85$	$a_2 = 1{\cdot}95$	
θ		0·60 | 0·49	−0·15 | −0·25	0·15 | 0	0 | 0
		0·11	0·10	0·15	0
Adjust M_B, M_D	0	65	45	51	50
	$a_1 = 0$	$a_2 = 1{\cdot}96$ | $a_1 = 2{\cdot}36$	$a_2 = 2{\cdot}00$ | $a_1 = 1{\cdot}85$	$a_2 = 1{\cdot}98$ | $a_1 = 2{\cdot}03$	$a_2 = 2{\cdot}01$
θ		0·56 | 0·52	−0·20 | −0·24	0·10 | 0·05	−0·03 | 0
		0·04	0·04	0·05	−0·03

Suppose now that the material used exhibits an elastic-ideal plastic stress-strain curve, a condition closely approximated by structural mild steel. If the full plastic moment of each cross-section defines the 'strength' of that cross-section, then all sections of the structure must be fully plastic in order that the minimum weight theorem be satisfied. Since curvatures can have any values under these conditions, the curvature condition of the theorem will be satisfied automatically. Thus the only practical problem with a fully plastic design in steel is the actual variation of the cross-section to follow the minimum weight bending moment diagram; the theoretical problem is to make this variation in such a way that the linear weight condition is satisfied. Again, these conditions can be satisfied reasonably closely if I beams with curtailed flanges are used.

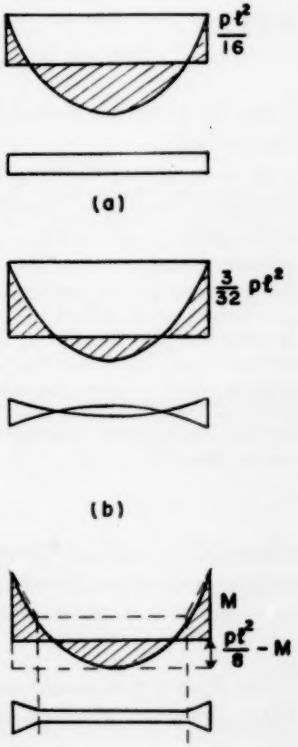

FIG. 7

7. Practical designs

In practice it will not be possible to vary the cross-section of a member continuously, or even discontinuously at more than a few sections. It is of interest, therefore, to examine the consequences of using prismatic members over some, at least, of the length of the members, and, in particular, to estimate the weight penalty involved in such modified designs. As an illustration, only the example of the fixed-ended beam will be discussed.

Fig. 7 (*a*) shows the collapse bending moment diagram if a prismatic beam is used to carry the uniformly distributed load p. M_0 is constant at the value $pl^2/16$, and the weight, from equation (1), is

$$W = \frac{pl^3}{16} = 2\frac{pl^3}{32}. \qquad (10\,a)$$

Fig. 7 (*b*) shows the bending moment distribution for minimum weight

design, the inflexion points occurring at quarter span; M_0 is given by

$$M_0 = \left| \frac{3}{32} l^2 - \frac{lx}{2} + \frac{x^2}{2} \right| p$$

leading to the minimum weight

$$W = \frac{pl^3}{32}. \tag{10 b}$$

Thus the prismatic beam uses just double the material of the minimum weight beam.

A more practical design is shown in Fig. 7 (*c*). A prismatic central portion of the beam connects two linearly tapering end portions. Thus, if the moment M in Fig. 7 (*c*) has the value $\frac{3}{32}pl^2$ (corresponding to the minimum weight bending moment distribution), the prismatic central portion has $M_0 = \frac{1}{32}pl^2$, and the corresponding weight is

$$W = 1{\cdot}29\frac{pl^3}{32}. \tag{10 c}$$

The central prismatic portion has length $l/\sqrt{2}$. In fact, if M is chosen as $5pl^2/48$, a relative minimum weight design is obtained for the type of beam sketched in Fig. 7 (*c*):

$$W = 1{\cdot}23\frac{pl^3}{32}. \tag{10 c) \textit{bis}}$$

Finally, Horne (**3**) has given the weight of a beam of the shape sketched in Fig. 7 (*d*); the relative minimum for this shape is

$$W = 1{\cdot}56\frac{pl^3}{32}. \tag{10 d}$$

These figures give an indication of the economies which may be achieved if non-prismatic members are used.

REFERENCES

1. D. C. Drucker and R. T. Shield, *Design for Minimum Weight.* Proc. 9th Internat. Congr. Appl. Mech., Brussels.
2. —— —— 'Bounds on minimum weight design', *Quart. App. Math.* **15** (1957) 269.
3. M. R. Horne, *Determination of the Shape of Fixed-Ended Beams for Maximum Economy according to the Plastic Theory.* Final Report, IABSE, 4th Congress, Cambridge and London, 1953.

THE GENERATION OF TORSIONAL STRESS WAVES IN A CIRCULAR CYLINDER

By R. P. N. JONES† (*University of Sheffield*)

[Received 11 June 1958]

SUMMARY

A general solution in series form is obtained for problems in which torsional waves are generated in a bar of circular section as a result of given initial conditions, or given external stresses. The solution is in effect an extension of the Pochhammer–Chree theory of harmonic wave propagation, and it satisfies exactly the elasticity equations and the boundary conditions. A particular problem is considered in which there is a suddenly applied torque in the form of a distributed shear force acting circumferentially on the surface of the bar. In this problem the displacements at the surface are given satisfactorily by the elementary theory at large distances along the bar, except near the wave front, where the convergence of the series is slow. The derived series for stress and velocity at the surface of the bar do not converge satisfactorily. An alternative solution in terms of waves of distortion in an infinite medium is discussed.

1. Introduction

In the elementary theory of torsional vibration of a uniform bar of circular section, it is assumed that each cross-section undergoes a pure rotation ϕ_0 about the axis of the bar. This assumption leads to a simple wave equation, viz.

$$\frac{\partial^2 \phi_0}{\partial t^2} = c^2 \frac{\partial^2 \phi_0}{\partial z^2} \tag{1}$$

in which the axis Oz lies along the axis of the bar and $c^2 = \mu/\rho$, where ρ is the density and μ the modulus of rigidity. It may be shown that this solution satisfies exactly the equations of motion of an elastic solid and the boundary conditions on the free surface of the bar. However, in the Pochhammer–Chree theory of harmonic wave propagation (see Kolsky (**1**) for references) it is shown that additional types of torsional wave motion are possible, in which the displacements over the cross-section are of more complicated form, having one or more nodal circles. To determine the importance of these higher modes of wave-motion, and the limitations of the elementary theory, it is necessary to consider the generation of torsional disturbances by a given initial motion, or given external stresses. A general method of obtaining exact solutions to such problems is described in this paper.

† Now at the Engineering Department, Cambridge.

2. Solution of equation of motion

It is convenient to use cylindrical coordinates (r, θ, z) with the z-axis lying along the axis of the bar. If the corresponding displacement components are denoted by (u, v, w), then, in the case of torsional motion, u and w vanish everywhere, and v is independent of θ. With these simplifications, the equations of motion of an isotropic elastic medium (**2**) reduce to the single equation

$$\frac{\partial^2 v}{\partial t^2} = c^2\left[\frac{\partial^2 v}{\partial z^2} + \frac{\partial^2 v}{\partial r^2} + \frac{1}{r}\frac{\partial v}{\partial r} - \frac{v}{r^2}\right]. \tag{2}$$

All stress-components are zero except $\sigma_{\theta z}$, $\sigma_{r\theta}$ which are given by the equations

$$\sigma_{\theta z} = \mu \frac{\partial v}{\partial z}, \tag{3}$$

$$\sigma_{r\theta} = \mu r \frac{\partial}{\partial r}\left(\frac{v}{r}\right). \tag{4}$$

If the surface of the cylinder is free from stress, the boundary condition to be satisfied is that

$$[\sigma_{r\theta}]_{r=a} = 0, \tag{5}$$

where a is the radius of the cross-section.

It has been stated above that (2) and (5) are satisfied by the elementary solution

$$v = r\phi_0(z, t) \equiv v_0 \tag{6}$$

where ϕ_0 satisfies (1). It may be verified that another solution of (2) satisfying the boundary condition (5) is

$$v = aJ_1(K_n r)\phi_n(z, t) \equiv v_n \tag{7}$$

where n denotes a positive integer, J_1 denotes the Bessel function of the first kind, ϕ_n satisfies the equation

$$\frac{\partial^2 \phi_n}{\partial t^2} = c^2 \frac{\partial^2 \phi_n}{\partial z^2} - c^2 K_n^2 \phi_n, \tag{8}$$

and $K_n a$ is the nth non-zero root of

$$\frac{\partial}{\partial a}\left[\frac{1}{a}J_1(Ka)\right] = 0, \tag{9}$$

that is,

$$J_2(Ka) = 0. \tag{10}$$

The first nine roots of (10) are given by Jahnke and Emde (**3**). In particular

$$K_1 a = 5{\cdot}136, \quad K_2 a = 8{\cdot}417, \quad K_3 a = 11{\cdot}620, \quad K_n a \simeq (n+\tfrac{3}{4})\pi$$

when n is large.

The Pochhammer–Chree theory deals with the propagation of harmonic waves. Solutions of this type may be obtained by putting

$$\phi_n = \exp[ik(z - Vt)], \tag{11}$$

where k is the wave number and V the phase velocity. The case $n = 0$ corresponds to wave propagation in the fundamental mode, which is dispersionless ($V = c$), whilst the solutions for $n = 1, 2,...$ correspond to the higher modes of torsional wave propagation given by the Pochhammer–Chree theory, in which

$$V^2 = c^2\left(1+\frac{K_n^2}{k^2}\right). \tag{12}$$

It will be assumed that the general solution of (2) satisfying the boundary condition (5) may be expressed as an expansion in terms of the characteristic solutions (6) and (7), i.e.

$$v = \sum_{n=0}^{\infty} v_n = r\phi_0 + a\sum_{n=1}^{\infty} \phi_n J_1(K_n r), \tag{13}$$

where ϕ_0 and ϕ_n satisfy (1) and (8). This general solution may be regarded as an extension of the Pochhammer–Chree theory of torsional wave propagation. The first term of the series is of course the solution given by the elementary theory.

3. Initial value problem for bar of infinite length

Consider a bar of infinite length in which the initial displacement and velocity are given by the equations

$$\left.\begin{aligned} v &= f_1(r,z) \\ \frac{\partial v}{\partial t} &= f_2(r,z) \end{aligned}\right\}. \tag{14}$$

Assuming that (13) may be differentiated term by term, the initial conditions (14) give

$$f_1(r,z) = r\phi_0(z,0) + a\sum_{n=1}^{\infty} J_1(K_n r)\phi_n(z,0), \tag{15}$$

$$f_2(r,z) = r\dot{\phi}_0(z,0) + a\sum_{n=1}^{\infty} J_1(K_n r)\dot{\phi}_n(z,0), \tag{16}$$

where dots denote differentiation with respect to t. It may be shown that the characteristic functions $J_1(K_n r)$ satisfy the following orthogonal properties:

$$\int_0^a J_1(K_n r) r^2\, dr = 0, \tag{17}$$

$$\int_0^a J_1(K_n r) J_1(K_m r) r\, dr = 0 \quad (n \neq m). \tag{18}$$

By use of these properties equations (15) and (16) may be solved for $\phi_0(z,0)$, etc. Thus

$$\phi_0(z,0) = \frac{4}{a^4}\int_0^a f_1(r,z)r^2\,dr, \tag{19}$$

$$\phi_n(z,0) = \frac{1}{P_n a}\int_0^a f_1(r,z)J_1(K_n r)r\,dr, \tag{20}$$

where

$$P_n = \int_0^a [J_1(K_n r)]^2 r\,dr = \tfrac{1}{2}[aJ_1(K_n a)]^2. \tag{21}$$

Similar expressions are obtained for $\dot{\phi}_0(z,0)$, $\dot{\phi}_n(z,0)$. The solution is completed by solving (1) and (8) with the given initial-value functions $\phi_0(z,0)$, etc. The solutions are

$$\phi_0(z,t) = \tfrac{1}{2}\phi_0(z+ct,0)+\tfrac{1}{2}\phi_0(z-ct,0)+\frac{1}{2c}\int_{z-ct}^{z+ct}\dot{\phi}_0(\xi,0)\,d\xi, \tag{22}$$

$$\phi_n(z,t) = \frac{1}{2c}\frac{\partial}{\partial t}\int_{z-ct}^{z+ct} J_0(K_n\sigma)\phi_n(\xi,0)\,d\xi+\frac{1}{2c}\int_{z-ct}^{z+ct} J_0(K_n\sigma)\dot{\phi}_n(\xi,0)\,d\xi, \tag{23}$$

where

$$\sigma^2 = (ct)^2-(z-\xi)^2.$$

4. Bars of semi-infinite or finite length

When the bar does not extend from $z = -\infty$ to $z = +\infty$ it is necessary to satisfy additional boundary conditions on the ends of the bar. In the simple cases where the end of the bar is either 'free' ($\sigma_{\theta z} = 0$), or 'fixed' ($v = 0$), solutions satisfying the boundary conditions may be obtained from the infinite bar solution by the method of images. If, in the infinite bar problem, the initial displacement and velocity are even functions of z, then considerations of symmetry show that there is no stress at the section $z = 0$ (unless an external torque is applied at that section) and the conditions at $z = 0$ are those of a free end. Similarly, if the initial displacement and velocity are odd functions of z, the conditions at $z = 0$ are those of a fixed end. A similar method may be used to discuss the reflections of waves at a fixed or free end, and in either case it may be shown that the reflected wave is of the same form as the incident wave. At a free end the displacements of the reflected and incident waves are of the same sign; at a fixed end they are of opposite sign.

An important problem is that in which stress waves are generated in a semi-infinite bar ($z > 0$) by the application of shear stress $\sigma_{\theta z}$ on the end $z = 0$. Let the given applied stress be

$$[\sigma_{\theta z}]_{z=0} = f_3(r,t). \tag{24}$$

Assuming differentiability of (13) we have

$$\frac{1}{\mu}f_3(r,t) = r\phi_0'(0,t)+a\sum_{n=1}^{\infty} J_1(K_n r)\phi_n'(0,t), \tag{25}$$

where primes denote differentiation with respect to z. By use of (17) and (18) we obtain

$$\phi_0'(0,t) = \frac{4}{\mu a^4}\int_0^a f_3(r,t)r^2\,dr, \tag{26}$$

$$\phi_n'(0,t) = \frac{1}{\mu P_n a}\int_0^a f_3(r,t)J_1(K_n r)r\,dr. \tag{27}$$

If ϕ_n and $\dot{\phi}_n$ are initially zero everywhere, the solutions of (1) and (8) are, for $ct < z$,

$$\phi_0 = \phi_n = 0$$

and for $ct > z$

$$\phi_0(z,t) = -c\int_0^{t-z/c}\phi_0'(0,\tau)\,d\tau, \tag{28}$$

$$\phi_n(z,t) = -c\int_0^{t-z/c} J_0(K_n s)\phi_n'(0,\tau)\,d\tau, \tag{29}$$

where

$$s^2 = c^2(t-\tau)^2-z^2. \tag{30}$$

The solution given by (28) and (29) exhibits a wave front at $z = ct$. By differentiating these equations and proceeding to the limit $ct = z+0$, we obtain

$$\phi_n'\left(z,\frac{z}{c}\right) = \phi_n'(0,0), \tag{31}$$

$$\dot{\phi}_n\left(z,\frac{z}{c}\right) = \dot{\phi}_n(0,0) = -c\phi_n'(0,0), \tag{32}$$

and therefore ϕ' and $\dot{\phi}$ are constant at the wave front. It follows that the distributions of stress and velocity across the section of the bar at the wave front are constant and equal to those obtaining at $z = 0$, $t = 0$, i.e.

$$[\sigma_{\theta z}]_{z=ct} = f_3(r,0), \tag{33}$$

$$[\dot{v}]_{z=ct} = -\frac{1}{\sqrt{(\mu\rho)}}f_3(r,0). \tag{34}$$

5. Bar with external torque applied at surface

The general solution given above will now be applied to a problem where stress waves are generated by the sudden application of an external torque at the surface of the bar. Consider first a semi-infinite bar, $z > 0$, and let there be a shear stress over the section $z = 0$ given by the equations

$$\left.\begin{aligned}\sigma_{\theta z} &= 0, \quad 0 \leqslant r < a-h\\ \sigma_{\theta z} &= ArH(t), \quad a-h \leqslant r \leqslant a\end{aligned}\right\}, \tag{35}$$

where $H(t)$ is the unit step-function and A is a constant, given by the equation

$$A = -\frac{2T_0}{\pi[a^4-(a-h)^4]}, \tag{36}$$

where T_0 is the resultant torque of the stresses (35). From (26) and (27) we obtain

$$\phi_0'(0,t) = -\frac{2T_0}{\pi\mu a^4}, \tag{37}$$

$$\phi_n'(0,t) = -\frac{A(a-h)^2 J_2[K_n(a-h)]}{\mu a K_n P_n}. \tag{38}$$

By proceeding to the limit $h = 0$ we obtain the case where the external torque is applied in the form of a line shear force, of magnitude $T_0/2\pi a^2$ per unit length, acting around the circumference $r = a$ at $z = 0$. The solution of this problem will also apply (for $z > 0$) to an infinite bar with an external torque $2T_0 H(t)$ applied at $r = a$, $z = 0$.

In the limit $h = 0$, (38) becomes

$$\phi_n'(0,t) = -\frac{T_0}{\pi\mu a^4 J_1(K_n a)}, \tag{39}$$

and from (28), (29), we have, for $ct > z$,

$$\phi_0(z,t) = \frac{2B}{a^2}(ct-z), \tag{40}$$

$$\phi_n(z,t) = \frac{Bc}{a^2 J_1(K_n a)} \int_0^{t-z/c} J_0(K_n s)\, d\tau, \tag{41}$$

where

$$B = \frac{T_0}{\pi a^2 \mu} \tag{42}$$

and s is defined by (30).

The displacement at any point on the surface of the bar is given by the equation

$$[v]_{r=a} = \sum_{n=0}^{\infty} [v_n]_{r=a} \tag{43}$$

in which, for $ct > z$,

$$[v_0]_{r=a} = \frac{2B}{a}(ct-z), \tag{44}$$

$$[v_n]_{r=a} = \frac{Bc}{a} \int_0^{t-z/c} J_0(K_n s)\, d\tau. \tag{45}$$

For large values of n it may be shown that

$$[v_n]_{r=a} \sim \frac{B}{\pi c^2 t}(2a\alpha)^{\frac{1}{2}}(n+\tfrac{3}{4})^{-\frac{1}{2}}\sin(\pi\beta) \tag{46}$$

where

$$\alpha^2 = (ct)^2 - z^2, \tag{47}$$

and
$$\beta = (n+\tfrac{3}{4})\frac{\alpha}{a} - \frac{1}{4}. \tag{48}$$

The series (43) is absolutely convergent, although at small or moderate

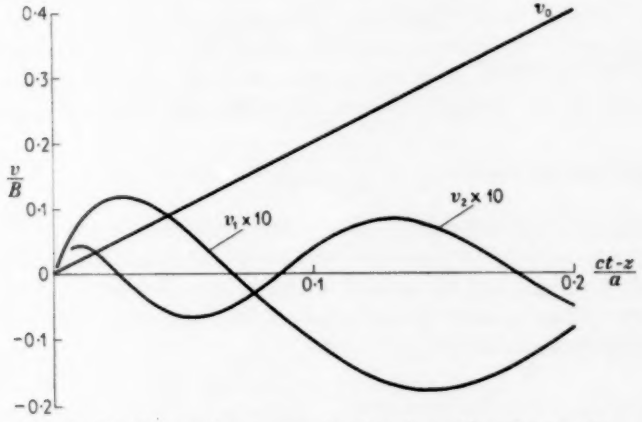

FIG. 1. Displacement components at surface of bar for $z = 4a$.

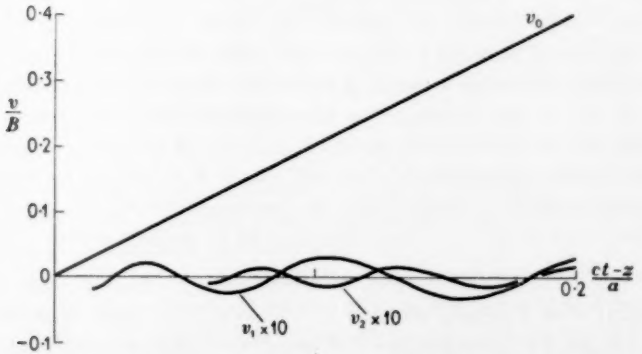

FIG. 2. Displacement components at surface of bar for $z = 40a$.

values of z/a, and in the region of the principal wave front, the convergence is too slow for satisfactory computation. However, for large values of z/a the terms $v_1, v_2, \ldots$ are small, and the displacement is given fairly accurately by v_0 only, except at the wave front. This is illustrated in Figs. 1 and 2, which show the displacement components v_0, v_1, v_2, at two positions on the surface of the bar, for $z = 4a$ and $z = 40a$. The components v_1 and

v_2 are in each case plotted to a scale ten times as large as that of v_0. By differentiation of (44) and (45) we have

$$[\dot{v}_0]_{r=a} = \frac{2Bc}{a}, \tag{49}$$

$$[\dot{v}_n]_{r=a} = \frac{Bc}{a} J_0(K_n \alpha). \tag{50}$$

For large values of n

$$[\dot{v}_n]_{r=a} \sim \frac{Bc}{\pi} \sqrt{\left(\frac{2}{a\alpha}\right)} (n+\tfrac{3}{4})^{-\frac{1}{2}} \cos(\pi\beta) \tag{51}$$

and therefore the series

$$\sum_{n=0}^{\infty} [\dot{v}_n]_{r=a} \tag{52}$$

does not converge absolutely. If $\alpha \neq 2am$, where m is any positive integer, the terms may be bracketed into groups having alternately positive and negative signs, and the series is conditionally convergent. If $\alpha = 2am$, the series diverges, since all terms are of the same sign for $n \to \infty$. The series also diverges at $ct = z+0$, since

$$\lim_{ct \to z+0} [\dot{v}_n]_{r=a} = \frac{Bc}{a}. \tag{53}$$

A similar discussion applies to the series

$$\sum_{n=0}^{\infty} [v'_n]_{r=a}. \tag{54}$$

The divergence of (52) and (54) at $ct = z+0$ may be inferred from equations (33) and (34). The shear stresses $\sigma_{\theta z}$ at $z = ct$ are the same as those applied at $z = 0$, $t = 0$, and consist of a line shear force acting around $r = a$. The shear stress and velocity at $r = a$, $z = ct$, are therefore infinite.

To avoid the divergence of (52) and (54) it is necessary to allow h in (38) to remain finite. Alternatively, in the case of the infinite bar, the line shear force at $r = a$, $z = 0$, may be replaced by a shear stress

$$\sigma_{r\theta} = T_0/2\pi a^2 \epsilon$$

distributed over a surface element $r = a$, $|z| < \epsilon$, in which case the solution is obtained by integration with respect to z. Either of these modifications is sufficient to ensure the absolute convergence of the two series.

6. Wave solutions

An alternative to the Pochhammer–Chree theory for uniform bars is to consider the propagation of waves of dilatation and distortion, and their reflections at the surface of the bar. This method has been discussed qualitatively by Kolsky (4) for the problem of longitudinal wave-propagation. A similar discussion may be applied to the problem considered in

the preceding section. In the case of torsional motion, only waves of distortion are present, and, because of axial symmetry, it is sufficient to consider wave-propagation in the plane $\theta = 0$ only.

In Fig. 3, P is any point on the surface of the bar (in the plane $\theta = 0$), and O_1, O_2 are points lying on the circle of application of the external torque $r = a$, $z = 0$. Two waves of distortion will arrive at P via the direct paths $O_1 P$, $O_2 P$, the displacements associated with the two waves being of opposite sign, since the shear forces at O_1 and O_2 are in opposite directions. Subsequently, reflected waves will arrive at P via paths such

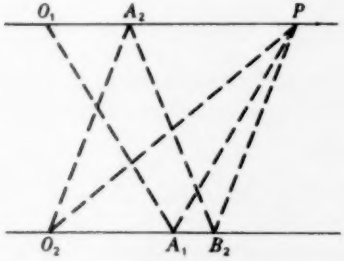

FIG. 3

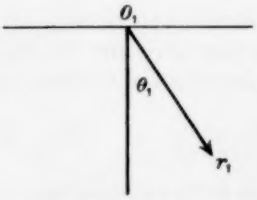

FIG. 4

as $O_1 A_1 P$, $O_2 A_2 B_2 P$, and so on. At each point of reflection the displacements of the incident wave are parallel to the free surface, and the reflected wave consists of a single wave of distortion, with angle of reflection equal to the angle of incidence. The arrival times of the direct and reflected waves are given by the equation

$$\alpha = 2ma, \tag{55}$$

where α is defined by (47), and $m = 0$ or a positive integer. The divergence of the series (52) and (54) is thus associated with the arrival of direct and reflected wave-fronts at the point P.

An approximate expression for the displacements near the surface of the bar at the first wave front may be obtained by neglecting the curvature of the surface, and (in the case of the infinite bar) considering the problem of a semi-infinite elastic solid. Choosing new cylindrical coordinates (r_1, θ_1, z_1) as in Fig. 4, let the solid be bounded by the plane $\theta_1 = \pm\frac{1}{2}\pi$. A line shear force, of magnitude $T_0 H(t)/\pi a^2$ per unit length, acts along the line $O_1 z_1$. If the displacement components are denoted by (u_1, v_1, w_1), it will be assumed that u_1 and v_1 vanish and that w_1 is independent of θ_1 and z_1; w_1 is then given by the single equation of motion

$$\frac{\partial^2 w_1}{\partial t^2} = c^2\left[\frac{\partial^2 w_1}{\partial r_1^2} + \frac{1}{r_1}\frac{\partial w_1}{\partial r_1}\right]. \tag{56}$$

All stress components vanish except σ_{rz} which is given by

$$\sigma_{rz} = \mu \frac{\partial w_1}{\partial r_1}. \tag{57}$$

It may be verified that the solution

$$w_1 = 0 \quad (ct < r_1),$$

$$w_1 = \frac{T_0}{\pi^2 a^2 \mu} \cosh^{-1}\left(\frac{ct}{r_1}\right) \quad (ct > r_1) \tag{58}$$

satisfies (56) and also the loading condition

$$\lim_{r_1 \to 0} [-\pi r_1 \sigma_{rz}] = \frac{T_0}{\pi a^2} H(t). \tag{59}$$

Transforming to the original coordinates and notation, we have an approximate expression for the displacements at the surface of the bar in the neighbourhood of the first wave front, viz.

$$[v]_{r=a} \simeq \frac{B}{\pi} \cosh^{-1}\left(\frac{ct}{z}\right) \quad (ct > z). \tag{60}$$

It is to be expected that this approximate wave-solution will be satisfactory only when the disturbance is confined to the outer layers of the bar, i.e. when α is small compared with a. Equation (60) therefore applies only in the region of the first wave front, for small or moderate values of z/a. In these circumstances the convergence of the series solution (43) is poor, and a numerical comparison of the two solutions is difficult. The solutions are plotted in Fig. 5 for $z = 4a$ and values of $(ct-z)/a$ up to 4×10^{-3}. At the maximum value of the abscissa the disturbance at $z = 4a$ will have spread to a radial depth of $0{\cdot}18a$ approximately. In the case of the series solution three curves are given, representing the sums to one, four, and ten terms. In view of the approximations involved, agreement between the two solutions is reasonable.

7. Conclusions

The generalized Pochhammer–Chree theory of torsional waves given in this paper shows that the importance of the higher modes of wave propagation depends greatly on the manner in which the waves are generated. Only in the particular case where the initial conditions or the applied stresses themselves conform to the elementary theory will the higher modes be absent.

When torsional waves are generated by shear stresses at the end of a bar, the higher modes are important at the wave front, as well as at the end where the stresses are applied, and the elementary theory is unsatis-

factory in these regions. The example considered in the paper is an extreme case in which there are suddenly applied stresses in the form of line shear forces around the circumference at the end of the bar. In this example the displacements are given satisfactorily by the elementary theory at large distances along the bar, except near the wave front, but neither the elementary theory nor the generalized Pochhammer–Chree theory gives a satisfactory solution for the stresses or velocity, since the

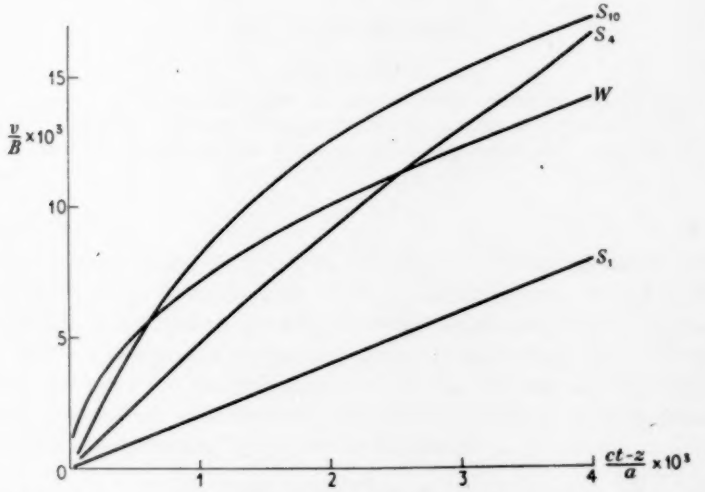

FIG. 5. Displacement at surface of bar for $z = 4a$. W = approximate wave solution (60). S_m = sum to m terms of series solution (43).

series fail to converge at certain points. In this case an alternative solution in terms of waves of distortion is desirable. However, it is probable that the generalized Pochhammer–Chree theory will be adequate for the calculation of stress and velocity in less severe cases, where the external stresses are distributed over a finite area, or are applied gradually.

There is little experimental evidence available on torsional waves, apart from that obtained by Davies and Owen (**5**), (**6**), with a torsional pressure-bar. In these experiments, torsional waves were generated in a long bar by the application of a torsional impact at the mid-point, and the waves were observed by measuring surface displacement at a considerable distance along the bar. These measurements showed no evidence of the excitation of the higher modes, a result which is in agreement with the conclusions of the present paper.

REFERENCES

1. H. Kolsky, *Stress Waves in Solids* (Oxford, 1953), 65.
2. A. E. H. Love, *The Mathematical Theory of Elasticity* (Cambridge, 1927), 288.
3. E. Jahnke and F. Emde, *Funktionentafeln* (Dover Publications, 1945), 168.
4. H. Kolsky, *Phil. Mag.* **45** (1954) 712.
5. R. M. Davies and J. D. Owen, *Proc. Roy. Soc.* A, **204** (1950) 17.
6. J. D. Owen, Ph.D. Thesis, University of Wales, Aberystwyth (1950).

A NOTE ON THE APPROXIMATE CALCULATION OF THE TEMPERATURE DISTRIBUTION IN AN INCOMPRESSIBLE LAMINAR BOUNDARY LAYER OVER A HEATED PLANE SURFACE

By D. E. BOURNE (*University of Sheffield*)

[Received 24 July 1958]

SUMMARY

The analysis of an earlier paper (**1**) is completed by evaluating in terms of Whittaker functions approximate expressions, in the form of definite integrals, for the temperature distribution in a laminar boundary layer over a heated plane surface.

1. Introduction

It has been demonstrated by Davies and Bourne (**1**) that the temperature distribution in an incompressible laminar boundary layer over a heated semi-infinite plane surface can conveniently be calculated by an approximate method based on a power law representation of the exact velocity profile. Consider the particular case, when the mainstream velocity U_0 is constant and the difference between the mainstream temperature T_0 and surface temperature T_1 is given by the series

$$T_1 - T_0 = \sum_{n=0}^{\infty} a_n x^n, \tag{1}$$

where x denotes distance from the leading edge of the surface and the a_n are constants. Then the temperature T in the boundary layer is given by

$$T - T_0 = \sum_{n=0}^{\infty} a_n x^n X_n(\xi), \tag{2}$$

where the variable ξ is defined by

$$\xi = \frac{1}{2}\left(\frac{U_0}{\nu x}\right)^{\frac{1}{2}} y, \tag{3}$$

y denotes the normal distance from the surface, ν is the kinematic coefficient of viscosity, and the functions $X_n(\xi)$ are expressed as certain integrals. In the case $n = 0$ the integral was shown (**1**) to be expressible in terms of a Pearson I-function (**2**), but for $n > 0$ no reduction was found possible.

It is the purpose of this note to complete the analysis by showing that in general the integrals are expressible in terms of Whittaker functions (**3**, p. 304).

2. Reduction of the integrals

Denoting the velocity component, in the boundary layer, parallel to the surface by U, the velocity profile is represented (**1**) approximately by the formula

$$U/U_0 = b\xi^{\beta}, \tag{4}$$

where b, β are constants. The functions $X_n(\xi)$ are then given (**1**, equation (47))† by

$$X_n(\xi) = \pi^{-1}\mu(\sin\mu\pi)(1+2n)B_n\{\mu, 1+2n\mu\}I_n, \tag{5}$$

where B_n is a beta function,

$$\mu = (1+\beta)/(2+\beta), \tag{6}$$

and

$$I_n = \int_0^1 (1-u)^{-\mu}u^{\mu(1+2n)-1}\exp\left\{\frac{-2b_1\sigma\xi^{2+\beta}}{(1+\beta)(2+\beta)(1-u)}\right\}du, \tag{7}$$

σ being the Prandtl number. I_n is the integral to be evaluated.

We write

$$\frac{2b_1\sigma\xi^{2+\beta}}{(1+\beta)(2+\beta)} = \eta, \tag{8}$$

and changing the independent variable to $v = \eta u/(1-u)$, the integral becomes

$$I_n = e^{-\eta}\eta^{-\mu(1+2n)}\int_0^{\infty} v^{\mu(1+2n)-1}\left(1+\frac{v}{\eta}\right)^{-1-2\mu n}e^{-v}\,dv. \tag{9}$$

Setting

$$\mu(1+2n)-1 = -k-\tfrac{1}{2}+l; \qquad -1-2\mu n = k-\tfrac{1}{2}+l,$$

i.e.

$$k = -\mu(2n+\tfrac{1}{2}); \qquad l = \tfrac{1}{2}(\mu-1), \tag{10}$$

we have

$$I_n = e^{-\eta}\,\eta^{-\mu(1+2n)}\int_0^{\infty} v^{-k-\frac{1}{2}+l}\left(1+\frac{v}{\eta}\right)^{k-\frac{1}{2}+l}e^{-v}\,dv, \tag{11}$$

and using the definition of the Whittaker function $W_{k,l}(\eta)$ given by Whittaker and Watson (**3**, p. 340) this may be written

$$I_n = e^{-\frac{1}{2}\eta}\eta^{-\mu(1+2n)-k}\Gamma(\tfrac{1}{2}-k+l)W_{k,l}(\eta). \tag{12}$$

Substituting k, l from (10), we find from (5) and (11) that

$$X_n(\eta) = \pi^{-1}\mu(\sin\mu\pi)(1+2n)B_n\{\mu, 1+2n\mu\}\times$$
$$\times e^{-\frac{1}{2}\eta}\eta^{-\frac{1}{2}\mu}\Gamma(\mu+2\mu n)W_{-\mu(2n+\frac{1}{2}),\frac{1}{2}(\mu-1)}(\eta). \tag{13}$$

The result may be simplified by expanding the beta function in terms of gamma functions and using the relation $\pi^{-1}(\sin\mu\pi)\Gamma(\mu) = \{\Gamma(1-\mu)\}^{-1}$

† An error in that result is corrected here.

(3, p. 239); after substituting from (6) and (8) we find

$$X_n(\xi) = \left\{\Gamma\left(\frac{1}{2+\beta}\right)\right\}^{-1}\Gamma\left\{1+\frac{2n(1+\beta)}{(2+\beta)}\right\}\left\{\frac{2b_1\sigma}{(1+\beta)(2+\beta)}\right\}^{-(1+\beta)/2(2+\beta)}\times$$

$$\times\xi^{-\frac{1}{2}(1+\beta)}\exp\left\{\frac{-b_1\sigma\xi^{2+\beta}}{(1+\beta)(2+\beta)}\right\}W_{\frac{(4n+1)(1+\beta)}{2(2+\beta)},\frac{1}{2(2+\beta)}}\left\{\frac{2b_1\sigma\xi^{2+\beta}}{(1+\beta)(2+\beta)}\right\}. \quad (14)$$

This is the required result.

It is noted that the result, mentioned earlier, that the function $X_0(\xi)$ is expressible in terms of a (tabulated) Pearson I-function, follows easily from (14) (cf. 3, p. 341, noting that $W_{k,m}(z) = W_{k,-m}(z)$).

REFERENCES

1. D. R. Davies and D. E. Bourne, *Quart. J. Mech. Appl. Math.* **9** (1956) 457.
2. K. Pearson, *Tables of the Incomplete Gamma Function* (London, H.M.S.O., 1922).
3. E. T. Whittaker and G. N. Watson, *Modern Analysis* (Cambridge, 1946).

DIFFUSION OF IONS IN A STATIC F_2 REGION

By J. E. C. GLIDDON

(*Queen Mary College, Mile End Road, London, E.* 1)

[Received 20 November 1958]

SUMMARY

The vertical diffusion of ions under the action of gravity and of a rate of electron loss which decreases exponentially with height is shown to correspond to heat conduction in a rod with a heat-source distribution and radiation from the lateral surface. Electron density is determined as a time-periodic function of the height and is expressed in the form of an infinite series.

1. Notation

z	height above a reference level.
t	time in seconds measured from sunrise.
ϕ	time in radians measured from sunrise.
$k = t/\phi$	$(= 1{\cdot}37 \times 10^4)$ number of seconds in a radian.
$N = N(z, t)$	electron density.
n	number-density of neutral molecules.
q	rate of ion-production.
T	temperature of the atmosphere.
$D = D(z, t)$	coefficient of diffusion.
H	scale height.
z_0	height above reference level of maximum ion-production.
$K = K(z)$	coefficient of attachment.

2. Introduction

It is now generally believed that the rate of electron loss in the F_2 region of the ionosphere is of the attachment type (that is, proportional to the electron density) and is also controlled by the downward diffusion of ions. In their discussion of this problem, Ferraro and Özdogan (**1**) assumed that the loss coefficient, K, of the electrons was constant. This assumption was made to simplify the analysis and also because at that time it appeared that the molecular density of the air at the level of the F_2 region was such as to make diffusion the main controlling factor. However, it has been pointed out by Ratcliffe *et al.* (**2**) that, as was shown by Bates and Massey (**3**), under certain circumstances the loss coefficient K is not constant but proportional to the local molecular density of oxygen (O_2) so that it decreases exponentially with height. The object of the present paper is

to give an analytical solution of the diffusion equation for the case when K is of the form suggested by Ratcliffe and his co-workers, namely,

$$K = 10^{-4}\exp\left(\frac{300-h}{50}\right)\text{sec}^{-1}. \tag{1}$$

The application to ionospheric problems will be reserved for a later paper. In particular, the calculations of Ferraro and Özdogan will need some revision in the light of new satellite data which indicate that the density in the F_2 region is about 10 times greater than the value which had been derived from an analysis of rocket data. The new estimate of the molecular density is, moreover, in accord with that which had previously been inferred on theoretical grounds (**4**, **5**).

3. Statement of the problem

The equation governing diffusion of ions in the ionosphere is (**1**)

$$\frac{\partial N}{\partial t} = q - KN + D\left(\frac{\partial^2 N}{\partial z^2} + \frac{3}{2H}\frac{\partial N}{\partial z} + \frac{N}{2H^2}\right). \tag{2}$$

In this equation q is taken to be the Chapman function

$$\begin{aligned} q &= q_0\exp\left[1 - \frac{z-z_0}{H} - \text{cosec}\,\phi\exp\left(-\frac{z-z_0}{H}\right)\right] \qquad (0 \leqslant \phi \leqslant \pi) \\ &= 0 \qquad\qquad (\pi \leqslant \phi \leqslant 2\pi). \end{aligned} \tag{3}$$

In accordance with equation (1) we shall denote by z_0 the height of maximum ion production and write, without loss of generality,

$$kK = \beta\exp\left(-\frac{z-z_0}{H}\right), \tag{4}$$

where β is a constant.

The coefficient of diffusion D may be expressed in the form b/n where b is a function of n and T. For the temperatures obtaining in the F_2 region, however, the variation of b with n and T may be ignored. We shall further assume that the density of neutral molecules is given by

$$n = n_0\exp\left(-\frac{z-z_0}{H}\right); \tag{5}$$

then making use of (5), we first transform (2) by the substitutions

$$\zeta^2 = \exp\left(-\frac{z-z_0}{H}\right), \tag{6}$$

and

$$N = v\zeta. \tag{7}$$

The transformed equation is

$$\frac{\partial v}{\partial t} = q\zeta^{-1} - Kv + \frac{b}{4n_0H^2}\frac{\partial^2 v}{\partial \zeta^2}. \tag{8}$$

It will be noted from equation (8) that the transformed problem is identical with that of heat conduction in a rod with radiation from the lateral surface and a heat-source distribution $q\zeta^{-1}$.

In equation (8) we now write

$$t = k\phi, \qquad n_0 H^2/kb = \gamma, \tag{9}$$

and

$$4(\beta\gamma)^{\frac{1}{2}}\zeta^2 = x^2; \tag{10}$$

then making use of (3) and (4) we obtain

$$\frac{\partial^2 v}{\partial x^2} - \left(\frac{\gamma}{\beta}\right)^{\frac{1}{2}} \frac{\partial v}{\partial \phi} - \tfrac{1}{4}x^2 v = -\tfrac{1}{2}kq_0 e(\gamma^{\frac{1}{2}}\beta^{-\frac{1}{2}}x)\exp\left\{-x^2\frac{\operatorname{cosec}\phi}{4(\beta\gamma)^{\frac{1}{2}}}\right\}. \tag{11}$$

We require a solution of this equation which is periodic in ϕ, with period 2π. Although there are no physical boundaries, we shall see below that the behaviour of v at $x = 0$ (infinite height) must be specified. It is required also that $N \to 0$ when $x \to \infty$.

4. Solution of the equation

The homogeneous equation corresponding to (11) is separable. Thus, inserting $v = V(x)\Phi(\phi)$ into the homogeneous equation we find that

$$\Phi = e^{-(\gamma/\beta)^{\frac{1}{2}}\nu\phi}, \tag{12}$$

and that V satisfies the differential equation

$$\frac{d^2V}{dx^2} + (\nu - \tfrac{1}{4}x^2)V = 0, \tag{13}$$

where ν is the real or complex separation constant.

Solutions of the equation (13) are the parabolic functions $D_{\nu-\frac{1}{2}}(x)$. Now the functions

$$D_n(x) \quad (n = 0, 1, 2, 3, \ldots) \tag{14}$$

form a complete set of orthogonal functions in the interval $-\infty < x < \infty$. They are connected with the Hermite polynomials

$$H_n(x) = (-1)^n e^{x^2}\frac{d^n}{dx^n}(e^{-x^2}) \tag{15}$$

by the equation

$$D_n(x) = 2^{-\frac{1}{2}n}e^{-\frac{1}{4}x^2}H_n(x/\sqrt{2}). \tag{16}$$

Any arbitrary function $\psi(x)$ defined in the interval $-\infty < x < \infty$ and satisfying suitable conditions can be expanded in a series of the form

$$\psi(x) = \sum_{n=0}^{\infty} a_n D_n(x). \tag{17}$$

In the present case neither v nor the function on the right of (11) have been defined for negative values of x. However, we postulate that, at a great height ($z \to \infty$, $x \to 0$),

$$v = O(x). \tag{18}$$

This implies that the electron-density N and the rate of ion-production q are of the same order of smallness at great height. Since for all n, $D_{2n}(x)$ is $O(1)$ and $D_{2n+1}(x)$ is $O(x)$ when $x \to 0$, it follows that if v can be expanded in a series of the form (17), only functions of odd order $D_{2n+1}(x)$ can be present. The definition of the function $x\exp\{-x^2\operatorname{cosec}\phi/4(\beta\gamma)^{\frac{1}{2}}\}$ can now be completed by continuation as an odd function in the interval $-\infty < x \leqslant 0$. Finally, the requirement that $N \to 0$ when $x \to \infty$ is satisfied by all $D_n(x)$.

We therefore write

$$v = \sum_{n=0}^{\infty} f_{2n+1}(\phi) D_{2n+1}(x) \tag{19}$$

and

$$xe^{-ax^2} = \sum_{n=0}^{\infty} g_{2n+1}(\phi) D_{2n+1}(x) \tag{20}$$

where

$$a = (\operatorname{cosec}\phi)/4(\beta\gamma)^{\frac{1}{2}} \tag{21}$$

and

$$g_{2n+1}(\phi) = \frac{1}{(2\pi)^{\frac{1}{2}}(2n+1)!} \int_{-\infty}^{\infty} xe^{-ax^2} D_{2n+1}(x)\, dx. \tag{22}$$

Substituting (19) and (20) into (11) we find

$$\sum_{n=0}^{\infty} f_{2n+1}(\phi) D''_{2n+1}(x) - (\gamma/\beta)^{\frac{1}{2}} \sum_{n=0}^{\infty} f'_{2n+1}(\phi) D_{2n+1}(x) - \tfrac{1}{4} \sum_{n=0}^{\infty} x^2 f_{2n+1}(\phi) D_{2n+1}(x)$$
$$= \sum_{n=0}^{\infty} -\tfrac{1}{2} k q_0 e(\gamma^{\frac{1}{2}}\beta^{-\frac{1}{2}}) g_{2n+1}(\phi) D_{2n+1}(x).$$

Then, making use of the relation

$$D''_{2n+1}(x) - \tfrac{1}{4}x^2 D_{2n+1}(x) = -(2n+\tfrac{3}{2}) D_{2n+1}(x),$$

we have

$$\sum_{n=0}^{\infty} \{(2n+\tfrac{3}{2}) f_{2n+1}(\phi) + (\gamma/\beta)^{\frac{1}{2}} f'_{2n+1}(\phi)\} D_{2n+1}(x)$$
$$= \sum_{n=0}^{\infty} \tfrac{1}{2} k q_0 e(\gamma^{\frac{1}{2}}\beta^{-\frac{1}{2}}) g_{2n+1}(\phi) D_{2n+1}(x).$$

Equating coefficients of $D_{2n+1}(x)$ gives

$$f'_{2n+1}(\phi) + (2n+\tfrac{3}{2})(\beta/\gamma)^{\frac{1}{2}} f_{2n+1}(\phi) = \tfrac{1}{2} k q_0 e(\beta\gamma)^{-\frac{1}{2}} g_{2n+1}(\phi). \tag{23}$$

We now require a solution of equation (23) which is periodic in ϕ with period 2π. The solution required is easily seen to be

$$f_{2n+1}(\phi) = C\Big\{ \int_0^{\phi} g_{2n+1}(\alpha) \exp\{-(2n+\tfrac{3}{2})(\beta/\gamma)^{\frac{1}{2}}(\phi-\alpha)\}\, d\alpha +$$
$$+ [\exp\{(4n+3)(\beta/\gamma)^{\frac{1}{2}}\pi\} - 1]^{-1} \int_0^{\pi} g_{2n+1}(\alpha) \exp\{-(2n+\tfrac{3}{2})(\beta/\gamma)^{\frac{1}{2}}(\phi-\alpha)\}\, d\alpha \Big\} \tag{24}$$

where

$$C = \tfrac{1}{2} k q_0 e(\beta\gamma)^{-\frac{1}{2}}, \tag{25}$$

and the upper limit in the second integral is π on account of the definition (3). Hence the required periodic solution is given by

$$v = \sum_{n=0}^{\infty} f_{2n+1}(\phi) D_{2n+1}(x) \tag{26}$$

and therefore

$$N = \zeta \sum_{n=0}^{\infty} f_{2n+1}(\phi) D_{2n+1}\{2(\beta\gamma)^{\frac{1}{2}}\zeta\}. \tag{27}$$

5. Convergence of the solution

It is possible by elementary methods to evaluate the integral in equation (22) in finite terms. Omitting the algebraic details, we find

$$g_{2n+1}(\phi) = \frac{(-1)^n}{2^n n!}\left(\frac{2\sin\phi}{\kappa+\sin\phi}\right)^{\frac{3}{2}}\left(\frac{\kappa-\sin\phi}{\kappa+\sin\phi}\right)^n \tag{28}$$

where

$$\kappa = (\beta\gamma)^{-\frac{1}{2}}. \tag{29}$$

We now examine the behaviour of $f_{2n+1}(\phi)$ as $n \to \infty$. We write

$$f_{2n+1}(\phi) = \frac{(-1)^n C}{2^n n!}[I_{2n+1}(\phi)+(1-\exp\{-(4n+\tfrac{3}{2})\mu\pi\})^{-1}J_{2n+1}(\phi)], \tag{30}$$

where we have written

$$\mu = (\beta/\gamma)^{\frac{1}{2}}. \tag{31}$$

The integrals $I_{2n+1}(\phi)$ and $J_{2n+1}(\phi)$ can be expressed as Laplace integrals,

$$I_{2n+1}(\phi) = \int_0^{\phi} h_1(\alpha) e^{n h_2(\alpha)}\, d\alpha \tag{32}$$

and

$$J_{2n+1}(\phi) = \int_0^{\pi} h_1(\alpha) e^{n\{h_2(\alpha)-2\pi\}}\, d\alpha, \tag{33}$$

where

$$h_1(\alpha) = \left(\frac{2\sin\alpha}{\kappa+\sin\alpha}\right)^{\frac{3}{2}} e^{-\frac{1}{2}\mu(\phi-\alpha)} \tag{34}$$

and

$$h_2(\alpha) = \log\left(\frac{\kappa-\sin\alpha}{\kappa+\sin\alpha}\right) - 2\mu(\phi-\alpha). \tag{35}$$

It is easy to show that $h_2(\alpha)$ can have a stationary value within the range of integration only if $\gamma > \beta+\beta^{-1}$ or, since β is essentially positive, if $\gamma > \frac{1}{2}$. The values of γ we contemplate using are $\leqslant \frac{1}{2}$ and for such values $h_2(\alpha)$ is negative and monotonic increasing. When $\gamma = \frac{1}{2}$, $h_2(\alpha)$ has a minimum at the end-point $\alpha = 0$. The major contribution to the integral $I_{2n+1}(\phi)$, when n is large, comes from the neighbourhood of the upper limit. Accordingly, we expand $h_1(\alpha)$ and $h_2(\alpha)$ in ascending powers of $\phi-\alpha$ and integrate term by term. We find

$$I_{2n+1} \sim e^{n h_2(\phi)}\left[-\frac{h_1(\phi)/h_2'(\phi)}{n} + \frac{h_1'(\phi)/\{h_2'(\phi)\}^2 - h_1(\phi)h_2''(\phi)/\{h_2'(\phi)\}^3}{n^2} + \ldots\right] \tag{36}$$

where $h_1'(\phi)$ means the value of $dh_1(\phi-\alpha)/d\alpha$ when $\alpha = 0$, etc. The dominant term is

$$F(\phi)\left(\frac{\kappa-\sin\phi}{\kappa+\sin\phi}\right)^n \frac{1}{2n} \tag{37}$$

where

$$F(\phi) = \left(\frac{2\sin\phi}{\kappa+\sin\phi}\right)^{\frac{3}{2}}\left(\mu-\frac{\kappa\cos\phi}{\kappa^2-\sin^2\phi}\right)^{-1}. \tag{38}$$

The integral $J_{2n+1}(\phi)$ can be dealt with in a similar manner and we find

$$J_{2n+1}(\phi) \sim e^{-2n\pi} I_{2n+1}(\phi). \tag{39}$$

Now the asymptotic behaviour of $D_{2n+1}(x)$, as $n \to \infty$ for fixed x, is given by (6),

$$D_{2n+1}(x) \sim \frac{(-1)^n}{2^{n+\frac{1}{2}}} \frac{\Gamma(2n+2)}{\Gamma(n+\frac{3}{2})} [\sin(2n+\tfrac{3}{2})^{\frac{1}{2}}x + O(n^{-\frac{1}{2}})]. \tag{40}$$

Hence, from (24) and (40),

$$f_{2n+1}(\phi)D_{2n+1}(x) \sim \frac{C}{2^n n!} F(\phi)\left(\frac{\kappa-\sin\phi}{\kappa+\sin\phi}\right)^n \frac{1}{2n}\frac{1}{2^{n+\frac{1}{2}}}\frac{\Gamma(2n+2)}{\Gamma(n+\frac{3}{2})}\times$$
$$\times[\sin(2n+\tfrac{3}{2})^{\frac{1}{2}}x + O(n^{-\frac{1}{2}})].$$

Making use of Stirling's formula, this can be written

$$f_{2n+1}(\phi)D_{2n+1}(x) \sim \frac{C}{\sqrt{(2\pi)}} F(\phi)\left(\frac{\kappa-\sin\phi}{\kappa+\sin\phi}\right)^n \frac{\sin(2n+\frac{3}{2})^{\frac{1}{2}}x}{n}\left\{\left(\frac{n+\frac{1}{2}}{n}\right)^{n+\frac{1}{2}} e^{-\frac{1}{2}}\right\} \tag{41}$$

where the bracketed function of n tends to unity as $n \to \infty$.

It can be seen that the solution is uniformly convergent and that the convergence can be expected to be rapid in the neighbourhood of $\phi = \frac{1}{2}\pi$ (mid-day) but slow in the neighbourhood of $\phi = 0$ and $\phi = \pi$ (sunrise and sunset).

6. Uniqueness of the solution

If there are two time-periodic solutions v_1 and v_2 of equation (11) which satisfy the conditions of vanishing at $x = 0$ and $x = \infty$ then $v = v_1 - v_2$ will satisfy the homogeneous equation corresponding to (11) and will likewise vanish at $x = 0$ and $x = \infty$.

Now it can be seen from (12) and (13) that a purely harmonic solution with time-factor $e^{in\phi}$ (n integral) must be of the form

$$v = \mathrm{re}\, e^{in\phi}\{A D_{\nu-\frac{1}{2}}(x) + B D_{\nu-\frac{1}{2}}(-x)\}, \tag{42}$$

where A and B are arbitrary complex constants, $\nu = -i(\gamma/\beta)^{\frac{1}{2}}n$, and $D_{\nu-\frac{1}{2}}(x)$, $D_{\nu-\frac{1}{2}}(-x)$ are independent solutions of (13).

The condition of vanishing at $x = 0$ can be satisfied by taking $B = -A$, but the general asymptotic solution of $D_{\nu-\frac{1}{2}}(-x)$ (6) shows that the behaviour of $D_{\nu-\frac{1}{2}}(-x)$ at $x = \infty$ requires $B = 0$. It follows that $v = 0$ is the only solution satisfying all the conditions.

Acknowledgement

My thanks are due to Professor V. C. A. Ferraro who suggested this problem and who has generously discussed it with me on many occasions.

REFERENCES

1. V. C. A. Ferraro and I. Özdogan, 'The effect of diffusion on the vertical distribution of ionisation in a quiet F region', *J. Atmos. Terr. Phys.* **12** (1958) 140–9.
2. J. A. Ratcliffe, E. R. Schmerling, C. S. G. K. Setty, and J. O. Thomas, 'The rates of production and loss of electrons in the F region of the ionosphere', *Phil. Trans.* **248** (1956) 621.
3. D. R. Bates and H. S. W. Massey, *Proc. Roy. Soc.* **A, 192** (1948), 1.
4. V. C. A. Ferraro, 'Diffusion of ions in the ionosphere', *Terr. Mag.* **50** (1945) 215.
5. D. F. Martyn, *Australian J. Physics.* **9** (1956) 161.
6. *Higher Transcendental Functions*, vol. 2. Bateman MS. project (McGraw-Hill, 1953).

USE OF GREEN'S FUNCTION IN THE SOLUTION OF IONOSPHERIC DIFFUSION PROBLEMS

By J. E. C. GLIDDON

(*Queen Mary College, Mile End Road, London, E.* 1)

[Received 4 December 1958]

SUMMARY

The mathematical analogy between diffusion of ions in the ionosphere and heat conduction in a rod is used to solve the problem of diffusion with an attachment-type law of electron loss. The solution for the case of a constant loss coefficient is obtained in terms of Green's function for the semi-infinite conducting solid. For the case of a loss coefficient which decreases exponentially with height a generalized heat-source is derived and the problem is solved in terms of the corresponding Green's function.

1. Introduction

In a previous paper (**1**), it was shown that the equation governing diffusion of ions in the F_2 region of the ionosphere was reducible to the equation of heat conduction in a rod with radiation taking place from the lateral surface. This comparison will now be used to derive solutions of the diffusion problem in terms of the Green's function for the two cases when the loss coefficient K is (i) constant, (ii) of the form $\beta\zeta^2$, where β is a constant and ζ is related to the space variable.

2. Statement of the problem

It has been shown in (**1**) that the electron density $N(\zeta, \phi)$ in the F_2 region of the ionosphere is given by

$$N = \zeta v, \tag{1}$$

where v satisfies the equation

$$\frac{\partial^2 v}{\partial \zeta^2} - 4\gamma \frac{\partial v}{\partial \phi} - 4\gamma k K v = -4\gamma k q \zeta^{-1}. \tag{2}$$

In this equation ζ is related to the space variable (corresponding to height above a fixed level), ϕ is the time measured in radians from sunrise, $1/\gamma$ is proportional to the diffusion coefficient, K is the loss coefficient of electrons, k is the number of seconds in a radian, and

$$\begin{aligned} q &= q_0 e \zeta^2 e^{-\zeta^2 \operatorname{cosec} \phi} \qquad (0 \leqslant \phi \leqslant \pi), \\ &= 0 \qquad\qquad\qquad\quad (\pi \leqslant \phi \leqslant 2\pi), \end{aligned} \tag{3}$$

is the rate of ion-production.

It is required to find the solution of (2) which is periodic in ϕ with period 2π and which vanishes when $\zeta = 0$ and when $\zeta = \infty$.

3. Green's function for the case when K is constant

When K is constant the 'radiation' term $-4\gamma kKv$ can be removed from (2) by the substitution

$$v = ue^{-kK\phi}. \tag{4}$$

The function $u(\zeta, \phi)$ then satisfies the heat-conduction equation

$$L(u) = \frac{\partial^2 u}{\partial \zeta^2} - 4\gamma \frac{\partial u}{\partial \phi} = -4\gamma kq\zeta^{-1}e^{kK\phi}. \tag{5}$$

The boundary conditions to be satisfied by u are

$$u(0, \phi) = 0 \tag{6}$$

and

$$\lim_{\zeta \to \infty} u(\zeta, \phi) = 0, \tag{7}$$

while in place of the usual initial-value condition we have the condition of time-periodicity,

$$u(\zeta, \phi + 2m\pi) = u(\zeta, \phi) \quad (m = 1, 2, 3, \ldots). \tag{8}$$

Green's function for this problem can be found directly by reflecting a unit heat source at $\zeta = \zeta_0$ and time $\phi = \phi_0$ in the boundary $\zeta = 0$. Thus,

$$G(\zeta, \phi | \zeta_0, \phi_0) = \pi^{-\frac{1}{2}} \left(\frac{\gamma}{\phi_0 - \phi}\right)^{\frac{1}{2}} \left[\exp\left\{-\frac{\gamma(\zeta - \zeta_0)^2}{\phi_0 - \phi}\right\} - \exp\left\{-\frac{\gamma(\zeta + \zeta_0)^2}{\phi_0 - \phi}\right\}\right]. \tag{9}$$

The equation satisfied by G is the adjoint to (5), namely,

$$M(G) = \frac{\partial^2 G}{\partial \zeta^2} + 4\gamma \frac{\partial G}{\partial \phi} = 0. \tag{10}$$

Green's theorem corresponding to (5) is then given by

$$\iint \{GL(u) - uM(G)\}\, d\phi d\zeta = \iint -4\gamma kGq\zeta^{-1}e^{kK\phi}\, d\phi d\zeta, \tag{11}$$

where the integration is extended over the infinite rectangle

$$-2n\pi \leqslant \phi \leqslant \phi_0 - \epsilon, \qquad 0 \leqslant \zeta \leqslant \infty. \tag{12}$$

and the limit is taken when $\epsilon \to 0$. Integrating the left-hand side of (11) we obtain

$$\int_{-2n\pi}^{\phi_0 - \epsilon} \left[G\frac{\partial u}{\partial \zeta} - u\frac{\partial G}{\partial \zeta}\right]_{\zeta=0}^{\zeta=\infty} d\phi - 4\gamma \int_0^\infty [Gu]_{-2n\pi}^{\phi_0 - \epsilon} d\zeta$$
$$= \int_{-2n\pi}^{\phi_0 - \epsilon} \int_0^\infty -4\gamma kGq\zeta^{-1}e^{kK\phi}\, d\phi d\zeta. \tag{13}$$

The first integral on the left vanishes by virtue of (6), (7), and (9). On letting $\epsilon \to 0$ we obtain

$$u(\zeta_0, \phi_0) - \int_0^\infty G(\zeta, -2n\pi \mid \zeta_0, \phi_0) u(\zeta_0, -2n\pi)\, d\zeta$$

$$= k \int_0^{\phi_0} e^{kK\phi}\, d\phi \int_0^\infty G(\zeta, \phi \mid \zeta_0, \phi_0) q\zeta^{-1}\, d\zeta +$$

$$+ \sum_{m=1}^{n} k \int_0^{2\pi} e^{kK(\phi - 2m\pi)}\, d\phi \int_0^\infty G(\zeta, \phi - 2m\pi \mid \zeta_0, \phi_0) q\zeta^{-1}\, d\zeta. \quad (14)$$

Here we have made use of the periodicity of q and it may be noted that the limits $(0, 2\pi)$ with respect to ϕ can be replaced by $(0, \pi)$ according to (3).

We now evaluate the integrals on the right-hand side of (14). We have

$$k \int_0^\infty G(\zeta, \phi \mid \zeta_0, \phi_0) q\zeta^{-1}\, d\zeta = k q_0 e\pi^{-\frac{1}{2}} \int_0^\infty \left(\frac{\gamma}{\phi_0 - \phi}\right)^{\frac{1}{2}} \exp\left(\frac{-\gamma\zeta_0^2}{\phi_0 - \phi}\right) \times$$

$$\times \left[\zeta \exp\left\{-\zeta^2\left(\frac{\gamma}{\phi_0 - \phi} + \operatorname{cosec}\phi\right) + \frac{2\gamma\zeta_0}{\phi_0 - \phi}\zeta\right\} -\right.$$

$$\left. - \zeta \exp\left\{-\zeta^2\left(\frac{\gamma}{\phi_0 - \phi} + \operatorname{cosec}\phi\right) - \frac{2\gamma\zeta_0}{\phi_0 - \phi}\zeta\right\}\right] d\zeta. \quad (15)$$

Integration can be effected with the help of the error-function integrals giving

$$\int_0^\infty t e^{-a^2t^2 + bt}\, dt - \int_0^\infty t e^{-a^2t^2 - bt}\, dt = \frac{b}{2a^3} e^{b^2/4a^2}\left\{\operatorname{erfc}\left(-\frac{b}{2a}\right) + \operatorname{erfc}\left(\frac{b}{2a}\right)\right\}$$

$$= \pi^{\frac{1}{2}} \frac{b}{2a^3} e^{b^2/4a^2}. \quad (16)$$

Applying this result to the right-hand side of (15) we have

$$k \int_0^\infty G(\zeta, \phi \mid \zeta_0, \phi_0) q\zeta^{-1}\, d\zeta = k q_0 e\zeta_0 \left(1 + \frac{\phi_0 - \phi}{\gamma} \operatorname{cosec}\phi\right)^{-\frac{3}{2}} \times$$

$$\times \exp\left\{-\frac{\zeta_0^2 \operatorname{cosec}\phi}{1 + [(\phi_0 - \phi)/\gamma]\operatorname{cosec}\phi}\right\}. \quad (17)$$

Similar results are obtained for the remaining integrals on the right of (14) by writing $\phi - 2m\pi$ in place of ϕ. Also, letting $n \to \infty$ and using the periodicity of $u(\zeta, \phi)$, we see that the integral on the left of (14) tends

uniformly to zero. Finally, interchanging ζ_0, ϕ_0 and ζ, ϕ we obtain the required result,

$$u(\zeta,\phi) = kq_0 e\zeta \int_0^{\phi} \Delta_0^{-\frac{1}{2}} \exp\left\{kK\phi_0 - \frac{\zeta^2}{\Delta_0}\operatorname{cosec}\phi_0\right\} d\phi_0 +$$

$$+ kq_0 e\zeta \sum_{n=1}^{\infty} \int_0^{\pi} \Delta_n^{-\frac{1}{2}} \exp\left\{kK(\phi_0 - 2n\pi) - \frac{\zeta^2\operatorname{cosec}\phi_0}{\Delta_n}\right\} d\phi_0 \quad (18)$$

where $$\Delta_n = 1 + \frac{\phi - \phi_0 + 2n\pi}{\gamma}\operatorname{cosec}\phi_0 \quad (n = 0, 1, 2, \ldots). \quad (19)$$

The electron density N, as given by (1), (4), and (18), agrees with the result previously obtained by Ferraro and Özdogan (**2**).

4. Green's function for the case when $kK = \beta\zeta^2$

When the loss coefficient decreases exponentially with the height we write (**1**),

$$kK = \beta\zeta^2, \quad (20)$$

where β is constant. Equation (2) is then transformed by the substitutions

$$4(\beta\gamma)^{\frac{1}{2}}\zeta^2 = x^2, \quad (21)$$

and

$$\left(\frac{\beta}{\gamma}\right)^{\frac{1}{2}}\phi = \tau. \quad (22)$$

Writing, for convenience,

$$\kappa = (\beta\gamma)^{-\frac{1}{2}}, \quad (23)$$

$$\mu = \left(\frac{\beta}{\gamma}\right)^{\frac{1}{2}} \quad (24)$$

we obtain

$$\frac{\partial^2 v}{\partial x^2} - \frac{\partial v}{\partial \tau} - \tfrac{1}{4}x^2 v = -\tfrac{1}{2}kq_0 e\gamma^{\frac{1}{2}}\beta^{-\frac{1}{2}} x e^{-\frac{1}{4}\kappa x^2 \operatorname{cosec}(\tau/\mu)}. \quad (25)$$

The differential equation to be satisfied by the Green's function G is

$$\frac{\partial^2 G}{\partial x^2} + \frac{\partial G}{\partial \tau} - \tfrac{1}{4}x^2 G = \delta(\tau_0 - \tau)\delta(x - x_0). \quad (26)$$

In the first place we require the solution of this equation, in the range $-\infty < x < \infty$, which vanishes at $x = \pm\infty$. Assuming an expansion for G in terms of parabolic functions $D_n(x)$, we write

$$G(x, \tau \mid x_0, \tau_0) = \sum_{n=0}^{\infty} p_n(\tau) D_n(x). \quad (27)$$

Substituting this series into (26) we find, after simplification,

$$\sum_{n=0}^{\infty} \{p_n'(\tau) - (n + \tfrac{1}{2})p_n(\tau)\} . D_n(x) = \delta(\tau_0 - \tau)\delta(x - x_0). \quad (28)$$

Multiplying both sides of (28) by $D_n(x)$ and integrating from $-\infty$ to ∞ we find that

$$p_n'(\tau)-(n+\tfrac{1}{2})p_n(\tau) = \delta(\tau_0-\tau)\frac{D_n(x_0)}{(2\pi)^{\frac{1}{2}}n!}, \tag{29}$$

whence

$$p_n(\tau) = \frac{1}{(2\pi)^{\frac{1}{2}}n!}e^{-(n+\frac{1}{2})(\tau_0-\tau)}D_n(x_0) \tag{30}$$

and so, formally,

$$G(x,\tau\,|\,x_0,\tau_0) = \frac{1}{(2\pi)^{\frac{1}{2}}}\sum_{n=0}^{\infty}\frac{1}{n!}e^{-(n+\frac{1}{2})(\tau_0-\tau)}D_n(x_0)D_n(x). \tag{31}$$

Again $G(x,\tau\,|\,x_0,\tau_0)$ can be expressed in closed form by use of the series of products of Hermite polynomials, viz.

$$\sum_{n=0}^{\infty}\frac{(\frac{1}{2}z)^n}{n!}H_n(x)H_n(y) = (1-z^2)^{-\frac{1}{2}}\exp\left\{\frac{2xyz-(x^2+y^2)z^2}{1-z^2}\right\}. \tag{32}$$

From (31) and (32), with the aid of the relation

$$D_n(x) = 2^{-\frac{1}{2}n}e^{-\frac{1}{4}x^2}H_n(x/\sqrt{2}), \tag{33}$$

we find that

$$G(x,\tau|x_0,\tau_0) = \{4\pi\sinh(\tau_0-\tau)\}^{-\frac{1}{2}}\exp\left\{-\frac{(x^2+x_0^2)\cosh(\tau_0-\tau)-2xx_0}{4\sinh(\tau_0-\tau)}\right\}. \tag{34}$$

It is easily verified that

$$\lim_{\tau\to\tau_0}\int_0^{\infty}G(x,\tau\,|\,x_0,\tau_0)\,dx = 1, \tag{35}$$

so that (34) is the analogue of the unit heat source used in Section 3. Also, as in the previous section, the Green's function which vanishes when $x = 0$ is given by reflecting (34) in $x = 0$, that is, returning now to the use of ϕ, ϕ_0,

$$G(x,\phi\,|\,x_0,\phi_0)-G(x,\phi\,|\,-x_0,\phi_0). \tag{36}$$

The solution of (25) is now obtained as in section 3, Green's theorem being of precisely similar form. We find that

$$v(x_0,\phi_0) = \tfrac{1}{2}kq_0e\beta^{-\frac{1}{2}}\gamma^{\frac{1}{2}}\lim_{n\to\infty}\int_{-2n\pi}^{\phi_0}\mu\,d\phi\int_0^{\infty}xe^{-\frac{1}{4}\kappa x^2\operatorname{cosec}\phi}\times$$
$$\times\{G(x,\phi\,|\,x_0,\phi_0)-G(x,\phi\,|\,-x_0,\phi_0)\}\,dx,$$

or

$$v(x_0,\phi_0)$$
$$= \tfrac{1}{2}kq_0e(\beta\gamma)^{-\frac{1}{2}}\int_0^{\phi_0}d\phi\int_0^{\infty}xe^{-\frac{1}{4}\kappa x^2\operatorname{cosec}\phi}\{G(x,\phi\,|\,x_0,\phi_0)-G(x,\phi\,|\,-x_0,\phi_0)\}\,dx+$$
$$+\tfrac{1}{2}kq_0e(\beta\gamma)^{-\frac{1}{2}}\times$$
$$\times\sum_{n=1}^{\infty}\int_0^{\pi}\int_0^{\infty}xe^{-\frac{1}{4}\kappa x^2\operatorname{cosec}\phi}\{G(x,\phi-2n\pi\,|\,x_0,\phi_0)-G(x,\phi-2n\pi\,|\,-x_0,\phi_0)\}\,dx. \tag{37}$$

We find with the help of (16) that

$$\int_0^\infty xe^{-\frac{1}{4}\kappa x^2 \operatorname{cosec}\phi}\{G(x,\phi \mid x_0,\phi_0)-G(x,\phi \mid -x_0,\phi_0)\}\,dx$$

$$= x_0\Delta^{-\frac{1}{2}}(\phi_0,\phi)\exp\left\{-\frac{x_0^2}{4}\frac{\Gamma(\phi_0,\phi)}{\Delta(\phi_0,\phi)}\right\} \quad (38)$$

where

$$\Gamma(\phi_0,\phi) = \kappa \operatorname{cosec}\phi \cosh\mu(\phi_0-\phi)+\sinh\mu(\phi_0-\phi), \quad (39)$$

$$\Delta(\phi_0,\phi) = \kappa \operatorname{cosec}\phi \sinh\mu(\phi_0-\phi)+\cosh\mu(\phi_0-\phi). \quad (40)$$

In a similar way we can express the integrals under the summation sign in (37) in the form

$$\int_0^\pi x_0\{\Delta(\phi_0,\phi-2n\pi)\}^{-\frac{1}{2}}\exp\left\{-\frac{x_0^2}{4}\frac{\Gamma(\phi_0,\phi-2n\pi)}{\Delta(\phi_0,\phi-2n\pi)}\right\}d\phi. \quad (41)$$

Finally, interchanging x_0, ϕ_0 and x, ϕ we have

$$v(x,\phi) = \tfrac{1}{2}kq_0\,e(\beta\gamma)^{-\frac{1}{2}}\int_0^\phi x\{\Delta(\phi,\phi_0)\}^{-\frac{1}{2}}\exp\left\{-\frac{x^2}{4}\frac{\Gamma(\phi,\phi_0)}{\Delta(\phi,\phi_0)}\right\}d\phi_0+$$

$$+\tfrac{1}{2}kq_0\,e(\beta\gamma)^{-\frac{1}{2}}\sum_{n=1}^\infty\int_0^\pi x\{\Delta(\phi,\phi_0-2n\pi)\}^{-\frac{1}{2}}\exp\left\{-\frac{x^2}{4}\frac{\Gamma(\phi,\phi_0-2n\pi)}{\Delta(\phi,\phi_0-2n\pi)}\right\}d\phi_0. \quad (42)$$

5. Proof of equivalence of the two solutions obtained for the case $kK = \beta\zeta^2$

We now show that the solution obtained in section 4 is equivalent to the solution obtained previously in (**1**).

The series form (31) of the Green's function shows that

$$G(x,\phi \mid x_0,\phi_0)-G(x,\phi \mid -x_0,\phi_0)$$

$$= \frac{2}{(2\pi)^{\frac{1}{2}}}\sum_{n=0}^\infty \frac{1}{(2n+1)!}e^{-(2n+\frac{1}{2})\mu(\phi_0-\phi)}D_{2n+1}(x_0)D_{2n+1}(x). \quad (43)$$

Using this form in (37) we have

$$v(x_0,\phi_0) = \tfrac{1}{2}kq_0\,e(\beta\gamma)^{-\frac{1}{2}}\sum_{n=0}^\infty\frac{2}{(2\pi)^{\frac{1}{2}}}\frac{D_{2n+1}(x_0)}{(2n+1)!}\int_0^{\phi_0}e^{-(2n+\frac{1}{2})\mu(\phi_0-\phi)}\,d\phi\times$$

$$\times\int_0^\infty xe^{-\frac{1}{4}\kappa x^2\operatorname{cosec}\phi}D_{2n+1}(x)\,dx+\tfrac{1}{2}kq_0\,e(\beta\gamma)^{-\frac{1}{2}}\sum_{n=0}^\infty\sum_{s=1}^\infty\frac{2}{(2\pi)^{\frac{1}{2}}}\frac{D_{2n+1}(x_0)}{(2n+1)!}\times$$

$$\times\int_0^\pi e^{-(2n+\frac{1}{2})\mu(\phi_0-\phi+2s\pi)}\,d\phi\int_0^\infty xe^{-\frac{1}{4}\kappa x^2\operatorname{cosec}\phi}D_{2n+1}(x)\,dx. \quad (44)$$

In the notation of (1) we have

$$g_{2n+1}(\phi) = \frac{2}{(2\pi)^{\frac{1}{2}}} \frac{1}{(2n+1)!} \int_0^\infty x e^{-\frac{1}{2}\kappa x^3 \operatorname{cosec}\phi} D_{2n+1}(x)\, dx, \tag{45}$$

so that (44) may be written

$$v(x_0, \phi_0) = \tfrac{1}{2} k q_0 e (\beta\gamma)^{-\frac{1}{2}} \sum_{n=0}^{\infty} D_{2n+1}(x_0) \int_0^{\phi_0} g_{2n+1}(\phi) e^{-(2n+\frac{1}{2})\mu(\phi_0 - \phi)}\, d\phi +$$

$$+ \tfrac{1}{2} k q_0 e (\beta\gamma)^{-\frac{1}{2}} \sum_{n=0}^{\infty} \sum_{s=1}^{\infty} D_{2n+1}(x_0) \int_0^{\pi} g_{2n+1}(\phi) e^{-(2n+\frac{1}{2})\mu(\phi_0 - \phi + 2s\pi)}\, d\phi. \tag{46}$$

Rearranging and interchanging x, ϕ, with x_0, ϕ_0, we have

$$v(x, \phi) = \tfrac{1}{2} k q_0 e (\beta\gamma)^{-\frac{1}{2}} \sum_{n=0}^{\infty} \left\{ \int_0^{\phi} g_{2n+1}(\phi_0) e^{-(2n+\frac{1}{2})\mu(\phi - \phi_0)}\, d\phi_0 + \right.$$

$$\left. + \int_0^{\pi} \sum_{s=1}^{\infty} \{e^{-(4n+3)\mu\pi}\}^s \cdot g_{2n+1}(\phi_0) e^{-(2n+\frac{1}{2})\mu(\phi - \phi_0)}\, d\phi_0 \right\} D_{2n+1}(x)$$

or, inserting the value of $\sum_{s=1}^{\infty} \{e^{-(4n+3)\mu\pi}\}^s$,

$$v(x, \phi) = \tfrac{1}{2} k q_0 e (\beta\gamma)^{-\frac{1}{2}} \sum_{n=0}^{\infty} \left\{ \int_0^{\phi} g_{2n+1}(\phi) e^{-(2n+\frac{1}{2})\mu(\phi - \phi_0)}\, d\phi_0 + \right.$$

$$\left. + [e^{(4n+3)\mu\pi} - 1]^{-1} \int_0^{\pi} g_{2n+1}(\phi_0) e^{-(2n+\frac{1}{2})\mu(\phi - \phi_0)}\, d\phi_0 \right\} D_{2n+1}(x). \tag{47}$$

This agrees with the result obtained in (1) when written in the form

$$v(x, \phi) = \sum_{n=0}^{\infty} f_{2n+1}(\phi) D_{2n+1}(x). \tag{48}$$

Acknowledgement

It is a great pleasure to record my thanks to Professor V. C. A. Ferraro for many helpful discussions in the preparation of this paper.

REFERENCES

1. J. E. C. Gliddon, 'Diffusion of ions in a static F_2 region,' *Quart. J. Mech. Appl. Math.* **12** (1959) 340–6.
2. V. C. A. Ferraro and I. Özdogan, 'The effect of diffusion on the vertical distribution of ionisation in a quiet F region', *J. Atmos. Terr. Phys.* **12** (1958) 140–9.

ON THE DEPTH OF BODIES PRODUCING LOCAL MAGNETIC ANOMALIES

By R. A. SMITH

(*Durham Colleges in the University of Durham*)

[Received 17 April 1958]

SUMMARY

Some inequalities relating to magnetism are proved and their relevance to the interpretation of local anomalies in the earth's magnetic field is discussed. From observations of the resolved part, in any one direction, of the earth's magnetic field, these inequalities could be used to calculate (subject to certain hypotheses) a maximum possible value for the depth below the earth's surface of the top surface of the magnetized body producing the anomaly.

1. Introduction

In this paper some inequalities are derived which may be of use in discussing the results of surveys of local anomalies in the earth's magnetic field. The problem of interpretation, which is to determine the nature and structure of the magnetized bodies causing the anomaly, is complicated by the fact that the distribution of dipoles which will produce a given field at the earth's surface is not unique. The methods normally used in discussing this problem (see (**1**), (**2**), (**3**)) draw on information from other sources, often geological, to form a rough model and then adjust the characteristics of this model to fit the observed anomaly. When there is only little information available from other sources not much can be said with confidence about the body causing the anomaly. It is in such situations as this that the method described below might be of use. It produces some useful information about the body but requires only light assumptions to be made about it. The method can be applied to the readings of surveys using either a vertical magnetometer or a total field (airborne) magnetometer. The analogous problem for gravity anomalies has been discussed by Bullard and Cooper (**4**) and by Bott and Smith (**5**) but neither of these methods can be used for the study of magnetic anomalies.

The writer is indebted to Dr. M. H. P. Bott for suggesting the problem to him and for much helpful advice on various aspects of geophysical prospecting.

2. Summary and discussion of the results

Take a system of rectangular cartesian axes $Oxyz$ with the y-axis pointing vertically upwards and the other axes in the plane of the earth's

surface. Let **v** be any fixed vector and let $A(x,z)$ denote the resolved part parallel to **v** of the magnetic field produced at the point $(x,0,z)$ by a finite magnetized body B which lies beneath the earth's surface. The body B will be said to have *parallel magnetization* if the intensity of magnetization **I** has the same direction† and sense at every point of B though its magnitude $|\mathbf{I}|$ may vary from point to point. We prove the following results:

THEOREM 1. *If the finite body B has parallel magnetization and lies wholly underneath the plane* $y = -h\ (h > 0)$ *then*

$$h^2 \int_{-\infty}^{+\infty} [f(x)]^2\,dx \leqslant \tfrac{1}{2} \int_{-\infty}^{+\infty} [F(x)]^2\,dx, \tag{2.1}$$

where

$$f(x) = \int_{-\infty}^{+\infty} A(x,z)\,dz, \tag{2.2}$$

and

$$F(x) = \int_{-\infty}^{x} f(t)\,dt. \tag{2.3}$$

Also

$$hV(F^2) \leqslant 2^{\frac{1}{2}} \int_{-\infty}^{+\infty} [F(x)]^2\,dx, \tag{2.4}$$

where $V(F^2)$ *denotes the total variation of the function* $[F(x)]^2$ *over the range* $-\infty < x < +\infty$.

The number $V(F^2)$ is easily calculated from a graph or table of the function by means of the relation $V(F^2) = 2(M-m)$, where M denotes the sum of all the maximum values of $[F(x)]^2$ and m denotes the sum of all its minimum values.

THEOREM 2. *If the finite body B has parallel magnetization and lies underneath all three of the planes* $y = -h$, $y = 3^{\frac{1}{2}}x$, $y = -3^{\frac{1}{2}}x$, *then*

$$h^2 \int_{-\infty}^{+\infty} \left[\frac{df}{dx}\right]^2 dx \leqslant 3 \int_{-\infty}^{+\infty} [f(x)]^2\,dx, \tag{2.5}$$

and

$$hV(f^2) \leqslant 3^{\frac{1}{2}}.2 \int_{-\infty}^{+\infty} [f(x)]^2\,dx, \tag{2.6}$$

where $f(x)$ *is given by* (2.2) *and* $V(f^2)$ *denotes the total variation of the function* $[f(x)]^2$ *over the range* $-\infty < x < +\infty$.

The number $V(f^2)$ can be evaluated in the manner described above for $V(F^2)$.

If the vector **v** is taken to point vertically downwards, then $A(x,z)$ is the magnetic anomaly at the point $(x,0,z)$ due to B, as obtained from the

† The vector **I** is not required to have the same direction as the vector **v** of course.

readings of a vertical magnetometer. If the magnetic ground field of the earth can be regarded as constant in both magnitude and direction over the region considered and the vector **v** is taken parallel to this ground field, then, to the first order, $A(x,z)$ is the magnetic anomaly at the point $(x,0,z)$ as obtained from the readings of a total field magnetometer provided that this anomaly is small. If the function $A(x,z)$ is completely known, the integrals in (2.1), (2.4), (2.5), and (2.6) can all be evaluated. Any one of these inequalities then provides a maximum possible value for the depth below the earth's surface of the top surface of the body B. The actual depth h can be any value less than or equal to this maximum. It should be noticed that in proving the theorems no assumptions are made about the shape of the body. The inequalities (2.1) and (2.5) are 'best possible' in the sense that the equality sign is actually attained when the body B degenerates into a single dipole lying in the plane $y = -h$. Our method of proof suggests that (2.4) and (2.6) are not best possible in this sense. For the case when the body B is a single dipole it can be shown that they overestimate its depth by 12 per cent and 33 per cent respectively. The hypotheses of Theorem 2 require that the body B lie underneath a wedge of angle 60° formed by the planes $y = \pm 3^{\frac{1}{2}}x$. This is a serious restriction on the usefulness of the result. It is not clear from our method of proof that this is the bluntest wedge under which the inequalities (2.5) and (2.6) are valid but it can be shown that (2.5) is not valid if the wedge angle is increased to 82°.

A body B^* will be described as *two-dimensional and extended parallel to the z-axis* if it can be regarded as a bundle of uniform, linear, dipoles each of which lies parallel to the z-axis and the body extends to infinity in both directions. Both the intensity of magnetization **I** inside such a body and the magnetic field **H** produced by it, are functions of x and y only and are everywhere perpendicular to the z-axis. The magnetic anomaly $A(x)$ which is the resolved part parallel to **v** of the field **H** at the point $(x,0,z)$, is clearly a function of x only. Theorems 1 and 2 cannot be applied as they stand to two-dimensional bodies since the integral in (2.2) is then always divergent. For such bodies the following result will be shown to hold:

THEOREM 3. *If the body B^* has parallel magnetization, lies underneath the plane $y = -h$, and is a two-dimensional body extended parallel to the z-axis, then the inequalities* (2.1) *and* (2.4) *are both true if $f(x)$ is taken to mean $A(x)$, and $F(x)$ is given by* (2.3). *If, in addition, B^* lies underneath both the planes $y = \pm 3^{\frac{1}{2}}x$, then the inequalities* (2.5) *and* (2.6) *are also true with this meaning for $f(x)$.*

All these results assume that the body producing the anomaly has parallel magnetization. Whilst this will never be satisfied exactly, experimental evidence (see (**6**)) indicates that it is a fairly good approximation to the state of magnetization in most igneous rock masses. In proving Theorem I, no assumption is made about the orientation of the coordinate axes in the plane of the earth's surface. In practice, however, it is desirable that the z-axis should not be taken parallel or nearly parallel to the direction of magnetization **I**. As explained at the end of section 5, any deviations from the hypothesis of parallel magnetization can be expected to produce a more marked effect on the results when **I** is nearly parallel to the z-axis. In general **I** will be inclined to the horizontal plane at an appreciable angle and then no caution will be necessary in choosing the direction of the axes in the earth's surface.

The procedure in this paper will be to prove Theorem 3 first and then to deduce Theorems 1 and 2 by a simple extension of it. The key to this extension is the following result:

THEOREM 4. *Let* $\mathbf{H}(x,y,z)$ *be the magnetic field produced at the point* (x,y,z) *by a simple dipole situated at the point* (ξ,η,ζ), *whose moment is the vector* $\mathbf{M} = (\lambda,\mu,\nu)$. *If we write*

$$\mathbf{H}^*(x,y) = \int_{-\infty}^{+\infty} \mathbf{H}(x,y,z)\,dz, \tag{2.7}$$

then $\mathbf{H}^*$ *is equal to the magnetic field produced at the point* (x,y,z) *by a uniform linear dipole which passes through the point* (ξ,η,ζ), *lies parallel to the* z*-axis, extends to infinity in both directions, and has for its moment per unit length the vector* $\mathbf{M}^* = (\lambda,\mu,0)$.

It should be noticed how this result is used in section 5 to extend Theorem 3. Any other method which may be found for estimating the depth of two-dimensional bodies from observations of the magentic anomalies produced by them, can clearly be extended in the same way to produce a method applicable to three-dimensional bodies.

3. Preliminary calculations

In this section some preliminary results are proved.

LEMMA 1. *If* X *and* Y *are real and* $X \geqslant 2h > 0$, *then*

$$(2h)^{-2}\,\mathrm{re}(X+iY)^{-1} \geqslant \mathrm{re}(X+iY)^{-3}.$$

Proof. If $\tan\theta = Y/X$, then $X+iY = Xe^{i\theta}/\cos\theta$. Hence,

$$(2h)^{-2}\,\mathrm{re}(X+iY)^{-1} - \mathrm{re}(X+iY)^{-3} = (2h)^{-2}\,\mathrm{re}(X^{-1}\cos\theta\, e^{-i\theta}) - \\ -\mathrm{re}(X^{-3}\cos^3\theta\, e^{-3i\theta})$$

$$= \frac{\cos^2\theta}{4h^2X}\left[1 - \left(\frac{2h}{X}\right)^2 \cos\theta\cos 3\theta\right]$$

$$\geqslant 0.$$

LEMMA 2. *If X and Y are real, $X \geqslant 2h > 0$ and $|Y| \leqslant X\tan\frac{1}{6}\pi$, then*

$$(2h)^{-2}\,\mathrm{re}(X+iY)^{-3} \geqslant \mathrm{re}(X+iY)^{-5}.$$

Proof. If $Y/X = \tan\theta$, it may be supposed that $|\theta| \leqslant \frac{1}{6}\pi$ since $|Y|/X \leqslant \tan\frac{1}{6}\pi$. When this is so, $\cos 3\theta \geqslant 0$ and $\cos 3\theta \geqslant \cos 5\theta$. The proof of Lemma 2 now proceeds like that of Lemma 1 and it is omitted here.

LEMMA 3. *Let $\phi(z) = S(z)/T(z)$, where $S(z)$ and $T(z)$ are polynomials in z and the degree of $T(z)$ exceeds that of $S(z)$ by 2 or more. If $\phi(z)$ is analytic at all points of the real axis, then*

$$\int_{-\infty}^{+\infty} \phi(x)\,dx = 2\pi i\rho,$$

where the integral is taken along the real axis and ρ denotes the sum of the residues of $\phi(z)$ at its poles in the half-plane $\mathrm{im}\,z > 0$. If there are no poles in this half-plane, then $\rho = 0$.

This result is a special case of a well-known theorem in the calculus of residues.

LEMMA 4. *Let $z = x+iy$ and let $a_1, a_2, \ldots, a_n, b_1, b_2, \ldots, b_n$ be complex constants with $\mathrm{im}\,a_r < 0$ for all r. If*

$$Q(z) = \sum_{r=1}^{n} \frac{b_r}{z-a_r}, \tag{3.1}$$

then

$$\int_{-\infty}^{+\infty} \left|\frac{d^pQ}{dz^p}\right|^2 dx = 2\pi(2p)! \sum_{r=1}^{n}\sum_{s=1}^{n} \frac{b_r\bar{b}_s}{[ia_r - i\bar{a}_s]^{2p+1}}, \tag{3.2}$$

where the integral is taken along the real axis and $\bar{a}_s$, $\bar{b}_s$ denote the complex conjugates of a_s, b_s respectively.

Equation (3.2) is true for $p = 0$ provided that in this case d^pQ/dz^p is taken to mean Q and $0! = 1$.

Proof. If the bar denotes the complex conjugate then

$$\int_{-\infty}^{+\infty} \left|\frac{d^pQ}{dz^p}\right|^2 dx = \int_{-\infty}^{+\infty} \left\{\frac{d^pQ}{dz^p}\right\}\left\{\overline{\frac{d^pQ}{dz^p}}\right\} dx$$

$$= \int_{-\infty}^{+\infty} \left\{\sum_{r=1}^{n} \frac{(-1)^p p!\, b_r}{(x-a_r)^{p+1}}\right\}\left\{\sum_{s=1}^{n} \frac{(-1)^p p!\, \bar{b}_s}{(x-\bar{a}_s)^{p+1}}\right\} dx$$

$$= \sum_{r=1}^{n}\sum_{s=1}^{n} (p!)^2 b_r \bar{b}_s \int_{-\infty}^{+\infty} [(x-a_r)(x-\bar{a}_s)]^{-p-1}\, dx. \quad (3.3)$$

Now $[(z-a_r)(z-\bar{a}_s)]^{-p-1}$ is a rational function of z which is analytic on the real axis and everywhere in the upper half plane except at the point $z = \bar{a}_s$ where it has a pole of order $p+1$. Using Lemma 3 it can be shown that

$$\int_{-\infty}^{+\infty} [(x-a_r)(x-\bar{a}_s)]^{-p-1}\, dx = 2\pi(2p)!(p!)^{-2}(ia_r - i\bar{a}_s)^{-2p-1}.$$

Equation (3.2) is now obtained by substituting this value of the integral into (3.3).

LEMMA 5. *Let the function $Q(z)$ be as described in Lemma 4 and let $d^pQ/dz^p = U+iV$, where U and V are real. Then*

$$\int_{-\infty}^{+\infty} U^2\, dx = \tfrac{1}{2}\int_{-\infty}^{+\infty} \left|\frac{d^pQ}{dz^p}\right|^2 dx,$$

where the integrals are taken along the real axis.

Proof. If $$\phi(z) = \{d^pQ/dz^p\}^2 = (U+iV)^2$$

then $\phi(z)$ satisfies all the conditions of Lemma 3 and has no poles in the half-plane $\operatorname{im} z > 0$. It follows from Lemma 3 that

$$0 = \int_{-\infty}^{+\infty} \phi(x)\, dx$$

$$= \int_{-\infty}^{+\infty} (U^2 - V^2)\, dx + i\int_{-\infty}^{+\infty} 2UV\, dx.$$

It now follows from the real part of this equation that

$$\int_{-\infty}^{+\infty} U^2\, dx = \int_{-\infty}^{+\infty} V^2\, dx = \tfrac{1}{2}\int_{-\infty}^{+\infty} (U^2+V^2)\, dx.$$

4. Two-dimensional bodies

In this section Theorem 3 will be proved with the help of the following result:

LEMMA 6. *Consider a collection of n uniform, infinite, linear dipoles with moments $M_1, M_2, \ldots, M_n$ respectively, which are all extended parallel to the ζ-axis of a system of rectangular axes $O\xi\eta\zeta$ and cut the plane $\zeta = 0$ in the points $(\xi_1, \eta_1, 0), (\xi_2, \eta_2, 0), \ldots, (\xi_n, \eta_n, 0)$ respectively. Suppose further that η_r is negative for all r and that all the moment vectors of these dipoles point in the same direction, which is perpendicular to the ζ-axis and makes an angle α with the direction of the positive ξ-axis. Let* $\mathbf{v}$ *be a fixed vector whose direction cosines with respect to these axes are (λ, μ, ν), and let $A(x)$ denote the resolved part parallel to* $\mathbf{v}$ *of the magnetic field produced at the point $(x, 0, 0)$ by these linear dipoles. If $F(x) = \int_{-\infty}^{x} A(x)\,dx$, then*

$$\frac{1}{4\pi(2p)!(\lambda^2+\mu^2)} \int_{-\infty}^{+\infty} \left\{\frac{d^p F}{dx^p}\right\}^2 dx = \sum_{r=1}^{n} \sum_{s=1}^{n} M_r M_s \operatorname{re}[i\xi_r - i\xi_s - \eta_r - \eta_s]^{-2p-1}. \tag{4.1}$$

This is valid for $p = 0$ provided that in this case $d^p F/dx^p$ is taken to mean F and $0! = 1$.

Proof. The two-dimensional magnetic field produced by this collection of linear dipoles has a complex potential (see (7), p. 182) whose value at the point $(x, y, 0)$ is

$$W(z) = \sum_{r=1}^{n} \frac{2M_r e^{i\alpha}}{z - a_r}, \tag{4.2}$$

where $z = x+iy$ and $a_r = \xi_r + i\eta_r$. In terms of this complex potential, the resolved parts parallel to the coordinate axes of the field at the point $(x, y, 0)$ are

$$(-\operatorname{re} dW/dz,\ \operatorname{im} dW/dz,\ 0).$$

The resolved part parallel to $\mathbf{v}$ of the field at the point $(x, 0, 0)$ is therefore

$$A(x) = -\lambda \operatorname{re}\frac{dW}{dz} + \mu \operatorname{im}\frac{dW}{dz} = \operatorname{re}\left\{C\frac{dW}{dz}\right\},$$

where $C = -(\lambda + i\mu)$. It follows that

$$F(x) = \int_{-\infty}^{x} \operatorname{re}\left\{C\frac{dW}{dz}\right\} dx = \operatorname{re}\{CW(x)\},$$

since $W(x) \to 0$ as $x \to -\infty$. If $b_r = 2CM_r e^{i\alpha}$, then $CW(z)$ as given by (4.2) is identical with the function $Q(z)$ defined by (3.1) and so

$$F(x) = \operatorname{re} Q(x) \quad \text{and} \quad d^p F/dx^p = \operatorname{re}(d^p Q/dz^p).$$

From Lemmas 4 and 5 it now follows that

$$\int_{-\infty}^{+\infty} \left\{\frac{d^p F}{dx^p}\right\}^2 dx = \frac{1}{2}\int_{-\infty}^{+\infty} \left|\frac{d^p Q}{dz^p}\right|^2 dx$$

$$= \pi(2p)! \sum_{r=1}^{n}\sum_{s=1}^{n} \frac{b_r \bar{b}_s}{[ia_r - i\bar{a}_s]^{2p+1}}.$$

On substituting for a_r and b_r in this and remembering that M_r is real, we obtain

$$\int_{-\infty}^{+\infty} \left\{\frac{d^p F}{dx^p}\right\}^2 dx = (2p)!\, 4\pi |C|^2 \sum_{r=1}^{n}\sum_{s=1}^{n} \frac{M_r M_s}{[i\xi_r - i\xi_s - \eta_r - \eta_s]^{2p+1}}.$$

The result (4.1) follows on taking the real part of this equation.

Proof of Theorem 3. We shall prove Theorem 3 first for the case when the two-dimensional body B^* consists of the collection of n linear dipoles described in Lemma 6. If these linear dipoles all lie underneath the plane $\eta = -h$, then $\eta_r \leqslant -h$ for all r. If

$$i\xi_r - i\xi_s - \eta_r - \eta_s = X + iY, \tag{4.3}$$

then $X = -\eta_r - \eta_s \geqslant 2h > 0$. Lemma 1 now shows that

$$(2h)^{-2}\,\mathrm{re}(i\xi_r - i\xi_s - \eta_r - \eta_s)^{-1} \geqslant \mathrm{re}(i\xi_r - i\xi_s - \eta_r - \eta_s)^{-3},$$

for all r and s. It follows that

$$(2h)^{-2} \sum\sum M_r M_s\, \mathrm{re}(i\xi_r - i\xi_s - \eta_r - \eta_s)^{-1}$$

$$\geqslant \sum\sum M_r M_s\, \mathrm{re}(i\xi_r - i\xi_s - \eta_r - \eta_s)^{-3}.$$

If we substitute for the two sums from (4.1) this becomes

$$(2h)^{-2}\int_{-\infty}^{+\infty} F^2\, dx \geqslant \frac{1}{2}\int_{-\infty}^{+\infty} \left\{\frac{dF}{dx}\right\}^2 dx. \tag{4.4}$$

Since $f(x) = dF/dx$, this is the inequality (2.1).

The inequality (2.4) is now deduced from this. The total variation of F^2 is given by

$$V(F^2) = \int_{-\infty}^{+\infty} \left|\frac{d}{dx}(F^2)\right| dx$$

$$= 2\int_{-\infty}^{+\infty} \left|F\frac{dF}{dx}\right| dx.$$

Schwarz's inequality (see (8), p. 381), when applied to this integral, shows that

$$[V(F^2)]^2 \leqslant 4 \int_{-\infty}^{+\infty} F^2\,dx \int_{-\infty}^{+\infty} \left(\frac{dF}{dx}\right)^2 dx.$$

Substituting into the right-hand side from (4.4) we obtain

$$[V(F^2)]^2 \leqslant 2h^{-2}\left[\int_{-\infty}^{+\infty} F^2\,dx\right]^2.$$

The square root of this is (2.4).

It will now be assumed that the n linear dipoles described in Lemma 6 all lie underneath both the planes $\eta = \pm 3^{\frac{1}{2}}\xi$. Then, in addition to the inequality $\eta_r \leqslant -h$, we have $-\eta_r \geqslant 3^{\frac{1}{2}}|\xi_r|$ for all r. If $X+iY$ is given by (4.3) then as before $X \geqslant 2h > 0$ and also

$$X = -\eta_r - \eta_s \geqslant 3^{\frac{1}{2}}|\xi_r| + 3^{\frac{1}{2}}|\xi_s| \geqslant 3^{\frac{1}{2}}|\xi_r - \xi_s| = 3^{\frac{1}{2}}|Y|,$$

which is equivalent to $|Y| \leqslant X \tan \frac{1}{6}\pi$. Lemma 2 now shows that

$$(2h)^{-2}\,\mathrm{re}(i\xi_r - i\xi_s - \eta_r - \eta_s)^{-3} \geqslant \mathrm{re}(i\xi_r - i\xi_s - \eta_r - \eta_s)^{-5}$$

for all r and s. It follows that

$$(2h)^{-2} \sum\sum M_r M_s\,\mathrm{re}(i\xi_r - i\xi_s - \eta_r - \eta_s)^{-3} \geqslant \sum\sum M_r M_s\,\mathrm{re}(i\xi_r - i\xi_s - \eta_r - \eta_s)^{-5}.$$

On substitution for the two sums from (4.1) this becomes

$$\frac{(2h)^{-2}}{2!} \int_{-\infty}^{+\infty} \left(\frac{dF}{dx}\right)^2 dx \geqslant \frac{1}{4!} \int_{-\infty}^{+\infty} \left(\frac{d^2F}{dx^2}\right)^2 dx.$$

Since $f(x) = dF/dx$, this is the inequality (2.5). Finally, the inequality (2.6) is deduced from (2.5) in precisely the same way that (2.4) was obtained from (2.1).

Theorem 3 has now been proved for the case when the two-dimensional body B^* consists of a finite collection of linear dipoles as described in Lemma 6. A continuous two-dimensional body B^* can be subdivided into a large number of infinite magnetized rods which approximate to linear dipoles. The magnetic field of B^* can therefore be imitated as closely as we please by the field of a finite collection of linear dipoles for which the inequalities of Theorem 3 hold. These inequalities are therefore also true for the field of the continuous body B^*. This intuitive argument can be justified easily by appeal to the general convergence theorem of Lebesgue (see (8), p. 345). This completes the proof of Theorem 3.

5. Three-dimensional bodies

In this section Theorem 4 is proved and then used to extend Theorem 3.

Proof of Theorem 4. Let $\mathbf{i}$, $\mathbf{j}$, $\mathbf{k}$ denote unit vectors parallel to the coordinate axes. If $\mathbf{r} = (x, y, z)$ and $\mathbf{a} = (\xi, \eta, \zeta)$ then the magnetic field $\mathbf{H}$ of the simple dipole $\mathbf{M}$ is given by $\mathbf{H} = -\nabla\Omega$ where

$$\Omega = -\mathbf{M}.\underline{\nabla}|\mathbf{r}-\mathbf{a}|^{-1}$$

(see (7), p. 133). From (2.7),

$$\begin{aligned}\mathbf{H}^*(x,y) &= -\int_{-\infty}^{+\infty}\left(\mathbf{i}\frac{\partial}{\partial x}+\mathbf{j}\frac{\partial}{\partial y}+\mathbf{k}\frac{\partial}{\partial z}\right)\Omega(x,y,z)\,dz \\ &= -\left(\mathbf{i}\frac{\partial}{\partial x}+\mathbf{j}\frac{\partial}{\partial y}\right)\int_{-\infty}^{+\infty}\Omega(x,y,z)\,dz \\ &= -\nabla\Omega^*, \qquad (5.1)\end{aligned}$$

where

$$\begin{aligned}\Omega^* &= \int_{-\infty}^{+\infty}\Omega(x,y,z)\,dz \\ &= -\int_{-\infty}^{+\infty}\left(\lambda\frac{\partial}{\partial x}+\mu\frac{\partial}{\partial y}+\nu\frac{\partial}{\partial z}\right)|\mathbf{r}-\mathbf{a}|^{-1}\,dz \\ &= -\int_{-\infty}^{+\infty}\left(\lambda\frac{\partial}{\partial x}+\mu\frac{\partial}{\partial y}\right)|\mathbf{r}-\mathbf{a}|^{-1}\,dz.\end{aligned}$$

Since the integrand in the last integral contains the variables z and ζ as a function of $z-\zeta$ only, the integral can be rewritten as follows:

$$\begin{aligned}\Omega^*(x,y) &= -\int_{-\infty}^{+\infty}\left(\lambda\frac{\partial}{\partial x}+\mu\frac{\partial}{\partial y}\right)|\mathbf{r}-\mathbf{a}|^{-1}\,d\zeta \\ &= -\int_{-\infty}^{+\infty}\mathbf{M}^*.\nabla|\mathbf{r}-\mathbf{a}|^{-1}\,d\zeta, \qquad (5.2)\end{aligned}$$

where $\mathbf{M}^* = (\lambda, \mu, 0)$. Equation (5.2) shows that Ω^* is the potential of a linear dipole which lies parallel to the z-axis and has moment $\mathbf{M}^*$ per unit length. Equation (5.1) then shows that $\mathbf{H}^*$ is the field of this linear dipole. This completes the proof of Theorem 4.

Proof of Theorems 1 *and* 2. Let $\mathbf{H}(x, 0, z)$ be the total field produced at the point $(x, 0, z)$ by a collection of n simple dipoles with moments $\mathbf{M}_1$, $\mathbf{M}_2$,..., $\mathbf{M}_n$ respectively, which all lie underneath the plane $y = -h$. If $\mathbf{H}^*(x)$ is obtained from $\mathbf{H}(x, 0, z)$ as in (2.7) then Theorem 4 shows that $\mathbf{H}^*(x)$ is the field produced at the point $(x, 0, z)$ by a family of linear dipoles

whose moments per unit length are $\mathbf{M}_1^*$, $\mathbf{M}_2^*$,..., $\mathbf{M}_n^*$ respectively. These linear dipoles all lie parallel to the z-axis and underneath the plane $y = -h$ and if the vectors $\mathbf{M}_1$,..., $\mathbf{M}_n$ are all parallel, the same will be true of the vectors $\mathbf{M}_1^*$,..., $\mathbf{M}_n^*$. When this is so they form a two-dimensional body of the type envisaged in Theorem 3 and if $f(x)$ denotes the resolved part of $\mathbf{H}^*(x)$ parallel to the fixed vector $\mathbf{v}$, then $f(x)$ satisfies the inequalities (2.1) and (2.4). If it is assumed in addition that the n simple dipoles $\mathbf{M}_1$,..., $\mathbf{M}_n$ all lie underneath the planes $y = \pm 3^{\frac{1}{2}}x$, then the linear dipoles $\mathbf{M}_1^*$,..., $\mathbf{M}_n^*$ also satisfy this hypothesis and the function $f(x)$ satisfies the additional inequalities (2.5) and (2.6). The resolved part of equation (2.7) parallel to $\mathbf{v}$ is $f(x) = \int_{-\infty}^{+\infty} A(x, z)\, dz$, where $A(x, z)$ denotes the resolved part of $\mathbf{H}(x, 0, z)$ parallel to $\mathbf{v}$. This shows that $f(x)$ is the function defined by (2.2). Theorems 1 and 2 have now been proved for the case when the body B consists of a finite collection of simple dipoles all pointing in the same direction. The results can be extended to the case when B is a finite continuous body with parallel magnetization by the same argument as that used in the proof of Theorem 3.

6. Nearly parallel magnetization

Suppose now that the moments $\mathbf{M}_1$,..., $\mathbf{M}_n$ of the n simple dipoles referred to in the previous proof are not exactly parallel to each other but are very nearly so. Theorem 4 shows that each vector $\mathbf{M}_r^*$ is the orthogonal projection on the plane $z = 0$ of the corresponding vector $\mathbf{M}_r$. If the angle between $\mathbf{M}_r$ and $\mathbf{M}_s$ is small then the angle between their orthogonal projections $\mathbf{M}_r^*$ and $\mathbf{M}_s^*$ will also be small, *except in the case when* $\mathbf{M}_r$ *and* $\mathbf{M}_s$ *are nearly parallel to the z-axis*. If this possibility is excluded then the moments $\mathbf{M}_1^*$,..., $\mathbf{M}_n^*$ of the corresponding linear dipoles will also be very nearly parallel. For this reason it is important that in practical applications the z-axis should not be taken nearly parallel to the direction of magnetization.

REFERENCES

1. A. S. Eve and D. A. Keys, *Applied Geophysics*, 4th ed. (Cambridge, 1956), pp. 16–76.
2. S. Chapman and J. Bartels, *Geomagnetism*, 2nd ed. (Oxford, 1939), pp. 137–57.
3. V. Vaquier *et al.*, *Interpretation of Aeromagnetic Maps* (New York, 1951).
4. E. C. Bullard and R. I. B. Cooper, *Proc. Roy. Soc.* **A, 194** (1948) 332–47.
5. M. H. P. Bott and R. A. Smith, *Geophysical Prospecting*, **6** (1958) 1–10.
6. T. Nagata, *Rock-Magnetism* (Tokyo, 1953), 123–34 and 214.
7. C. A. Coulson, *Electricity* (Edinburgh, 1948).
8. E. C. Titchmarsh, *Theory of Functions*, 2nd ed. (Oxford, 1939).

ROUTH TEST FUNCTION METHODS FOR THE NUMERICAL SOLUTION OF POLYNOMIAL EQUATIONS

By C. MACK

(*British Cotton Industry Research Association, Manchester*, 20)

[Received 1 May 1958.—Revise received 27 August 1958]

SUMMARY

In this paper two iterative methods are developed for the numerical solution of polynomial equations with real coefficients. The first (the x) method is based upon a systematic application of Routh's test (**1**) for the number of zeros of a polynomial with positive real parts. The second (the a) method uses the test in a different manner to evaluate quadratic factors directly. The methods have certain desirable features: (i) they always converge, even from an arbitrary start, (ii) numerical checks can be used at each stage, and (iii) with modern fully automatic desk machines with retaining keys they are relatively quick. Some properties of Routh's test are proved and an algebraic proof of the test itself (and two proofs of the fundamental theorem of algebra) are also given.

1. Introduction

THE methods given in this paper are partly developed from the test function methods of Frazer and Duncan (**2**). They have the advantage over the latter of not requiring any preliminary investigation by trial and error to obtain a near approximation before converging rapidly; in fact they always converge, even from an arbitrary start, and so have also this advantage over methods such as Lin's (**3**) and Friedman's (**4**) which may fail to converge however close the first approximation used to start. Lin's method has been modified so as to give greater probability of convergence by Aitken (**5**). In the later stages of the application of the a and x methods inverse interpolation from a suitable test function enables rapid convergence to be achieved, especially if Aitken's (**6**) or Neville's (**7**) repeated linear interpolation form of Lagrangian interpolation is used.

In section 2 the x method is first described. This applies Routh's test directly, with suitable changes of origin, and determines first whether real and/or complex zeros are present. If real roots are shown to exist they are then found in the usual way, while complex roots are found from the calculations involved in applying Routh's test itself.

The a method is described in section 3 and owes its origin partly to a method for solving quartics given by Mack and Porter (**8**). It consists in finding quadratic factors of the polynomial directly and applying Routh's test in an indirect, but equally powerful, way to do this systematically.

Complex zeros are found by the a method with appreciably less computation than by the x method, while real zeros can be found by one extra calculation at each stage (or can be found in pairs as quadratic factors). For degrees of six and upward it is usually the more economical method particularly if all zeros are known to have real parts of the same sign, or if the first application of Routh's test shows this to be so.

The two methods may be combined in a number of ways. Thus one or two applications of the x method may be used to convert the equation into one whose real parts are all of one sign, whereupon the a method can be used to complete the solution. It will also be shown that some of the quantities needed in the a method are computed incidentally during the development of the x method, and time and labour may be saved by using them. The methods also combine well with Bairstow's (**9**) method of improving a quadratic factor which usually needs a three or four significant figure approximation to start with but then converges rapidly.

At present the method recommended by many computers is the root-squaring process due to Graeffe (**10**). This is difficult to use without making mistakes; as significant figures are usually lost, and complications arise if there are several complex zeros present though Olver (**11**) does give a technique which avoids the main cause of error. Such difficulties are avoided with the methods of the present paper.

The time required by a particular method is an important criterion of its usefulness and some average times are given in the text. The methods can also be programmed easily for calculation on electronic computers.

2. The x method

2.1. *Routh's test*

We begin by stating Routh's test (**1**). Suppose that

$$f(z) \equiv c_0 z^n + c_1 z^{n-1} + c_2 z^{n-2} + \ldots + c_{n-1} z + c_n \tag{1}$$

is a polynomial in z of degree n with real coefficients. Routh's test consists, essentially, in taking the two polynomials formed by the even and odd powers of $f(z)$, dividing that of higher degree (i.e. $c_0 z^n + c_2 z^{n-2} + \ldots \equiv f_0$, say) by the other ($c_1 z^{n-1} + c_3 z^{n-3} + \ldots \equiv f_1$, say), obtaining a remainder f_2, then dividing f_1 by f_2, which is of degree $n-2$, obtaining a remainder f_3, and so on until f_n, a constant, in fact equal to c_n as we shall see, is obtained. This h.c.f. process is analogous to the Sturm process for finding the number of real zeros. Then, as Routh (**1**) showed, the number of changes of sign in the coefficients of the leading (i.e. the highest power) term in each f_i equals the number of zeros of $f(z)$ with *positive* real parts (a proof is given in subsection **4**).

In the form of detached coefficients this process yields the array

$$
\begin{array}{cccccccccc}
c_0 & & c_2 & & c_4 & & c_6 & . & . & . \\
 & c_1 & & c_3 & & c_5 & & . & . & . \\
 & & c_2^{(2)} & & c_4^{(2)} & & c_6^{(2)} & & . & . \\
 & & & c_3^{(3)} & & c_5^{(3)} & & . & . & . \\
 & & & & & & . & . & . & \\
 & & & & & & c_{n-3}^{(n-3)} & & c_{n-1}^{(n-3)} & \\
 & & & & & & & c_{n-2}^{(n-2)} & & c_n^{(n-2)} \\
 & & & & & & & & c_{n-1}^{(n-1)} & \\
 & & & & & & & & & c_n^{(n)}
\end{array}
\tag{2}
$$

where, with $c_{2s} \equiv c_{2s}^{(0)}$, $c_{2s+1} \equiv c_{2s+1}^{(1)}$, the $c_{r+2s}^{(r)}$ satisfy the relation

$$c_{r+2s}^{(r)} = c_{r+2s}^{(r-2)} - \{c_{r-2}^{(r-2)}/c_{r-1}^{(r-1)}\}c_{r+2s+1}^{(r-1)} \tag{3}$$

provided $r+2s \leqslant n-1$. In the final column of (2), where $r+2s = n$, it can be seen that all terms are the same, that is

$$c_n^{(n)} = c_n^{(n-2)} = c_n^{(n-4)} = \ldots = c_n. \tag{4}$$

It is worth noting that each row of (2) is generated from the two rows immediately above it in the same way and, also, that labour can be saved in computing the rth row by first calculating $c_{r-2}^{(r-2)}/c_{r-1}^{(r-1)}$ and then retaining it as a multiplier.

The number of *changes* of sign in the sequence

$$c_0,\ c_1,\ c_2^{(2)},\ c_3^{(3)},\ldots,\ c_r^{(r)},\ldots,\ c_n^{(n)} \tag{5}$$

then gives the number of zeros of $f(z)$ with positive real parts.

A check on the accuracy of the calculation of the array (2) may be made from the following result: If $s^{(r)}$ is the sum of the rth row, i.e. if

$$s^{(r)} \equiv c_r^{(r)} + c_{r+2}^{(r)} + c_{r+4}^{(r)} + \ldots \tag{6}$$

then it can be seen from (3) that

$$s^{(r)} = s^{(r-2)} - \{c_{r-2}^{(r-2)}/c_{r-1}^{(r-1)}\}s^{(r-1)}. \tag{7}$$

2.2. *Description of the x method*

In the x method we change the origin from $z = 0$ to $z = x$, compute the new coefficients of $f(z)$ when expressed in powers of $(z-x)$, and then apply Routh's test to these coefficients. Thus, we first find the coefficients C_i, where

$$f(z) \equiv C_0(z-x)^n + C_1(z-x)^{n-1} + C_2(z-x)^{n-2} + \ldots + C_{n-1}(z-x) + C_n. \tag{8}$$

This can be done by repeated division of $f(z)$ by $z-x$. An alternative, and

quicker, method when retaining keys are available, is to compute them by calculating column by column the following array:

$$
\begin{array}{llllllll}
(c_1 \equiv)c_{1,0} & (c_2 \equiv)c_{2,0} & (c_3 \equiv)c_{3,0} & \cdot\ \cdot\ \cdot & (c_{n-1} \equiv)c_{n-1,0} & & (c_n \equiv)c_{n,0} & \\
c_{1,1} & c_{2,1} & c_{3,1} & \cdot\ \cdot\ \cdot & c_{n-1,1} & & c_{n,1}(\equiv C_n) & \\
c_{1,2} & c_{2,2} & c_{3,2} & \cdot\ \cdot\ \cdot & c_{n-1,2}(\equiv C_{n-1}) & & & \\
\cdot\ \cdot\ \cdot & \cdot\ \cdot\ \cdot & \cdot\ \cdot\ \cdot & \cdot\ \cdot\ \cdot & \cdot\ \cdot\ \cdot & \cdot\ \cdot\ \cdot & \cdot\ \cdot\ \cdot & \cdot\ \cdot\ \cdot \\
c_{1,n-2} & c_{2,n-2} & c_{3,n-2}(\equiv C_3) & & & & & \\
c_{1,n-1} & c_{2,n-1}(\equiv C_2) & & & & & & \\
c_{1,n}(\equiv C_1) & & & & & & & \qquad (9)
\end{array}
$$

where, with $c_{0,t} \equiv c_0$ and hence $C_0 \equiv c_{0,n+1} \equiv c_0$,

$$c_{s,t} = c_{s,t-1} + xc_{s-1,t} \quad (s = 1, 2, \ldots, n). \tag{10}$$

In words, each term in (9) is the sum of the one above and the product of the term to the left times x. Accuracy may be checked by using the relation

$$C_0 + C_1 + C_2 + \ldots + C_n = f(x+1) \tag{11}$$

which follows from (8) when $z = x+1$. In practice, it is convenient to sum $C_0 + C_2 + C_4 + \ldots$ and $C_1 + C_3 + \ldots$ separately as these sums are useful in checking the Routh's test calculation which follows.

Routh's test (see (2)) is now applied to the C_i. Denote the general term in the consequent array (2) by $C^{(r)}_{r+2s}$. Then the number of changes of sign, $\rho\{x\}$ say, in the sequence $C^{(r)}_r$ $(r = 0, 1, 2, \ldots, n)$, gives the number of zeros of $f(z)$ with real parts greater than x.

Once we have found x_1, x_2 such that $\rho\{x_1\} \neq \rho\{x_2\}$ then we know that at least one real part, x_0 say, lies in the range $[x_1, x_2]$, and further subdivision of this range will find x_0 as accurately as desired. We can, in fact, specify such a range without trial, for if z_1 is the zero of $f(z)$ with least modulus then

$$|z_1| \leqslant |c_n/c_0|^{1/n} \equiv X, \quad \text{say,} \tag{12}$$

and a real part must therefore lie in $[-X, X]$. Sometimes too it is known, or the first test (which is usually with $x = 0$) shows, that $\rho\{0\} = 0$ or n. In both these cases all real parts must have the same sign and, hence, one real part must lie between 0 and $-c_1/(nc_0)$, a range which may be narrower than $[0, X]$ or $[-X, 0]$.

A given range $[x_1, x_2]$ can be subdivided in half and Routh's test applied again, and so on. If no indication that the true real part x_0 is nearer one boundary than the other, this subdivision by half can be repeated a few times. Then it is usually possible by inverse interpolation from a suitable

test function to find x_0 with great rapidity of convergence. This we now discuss.

The procedure differs in the two cases of real and complex zeros. We consider these two cases separately. If $\rho\{x_1\}$ and $\rho\{x_2\}$ differ by an odd number it will be found (see subsection 4.1) that $f(x_1)$ and $f(x_2)$ have opposite signs. This is a well-known condition for a real zero to exist in $[x_1, x_2]$ and it can be found in the usual way. In the later stages of this process inverse interpolation from the values of $f(x)$ itself can be used.

If $\rho\{x_1\}$ and $\rho\{x_2\}$ differ by an even number some suitable point x_3 in the range $[x_1, x_2]$ is chosen and $\rho\{x_3\}$ found. Subdivision is carried on until a range is found in which either $\rho\{x\}$ changes by an odd number or $\rho\{x\}$ changes by two, whilst $f(x)$ remains unchanged in sign (or appears to do so). If $f(x)$ does not change sign in the interval then it will be found that at one and only one intermediate point x_0, $C_{n-1}^{(n-1)}$ (the penultimate quantity in the Routh test array (2)) will vanish. At this point it will also be found that

$$C_n^{(n-2)}/C_{n-2}^{(n-2)} = C_{n-1}^{(n-3)}/C_{n-3}^{(n-3)} \equiv y_0^2, \quad \text{say,} \tag{13}$$

where y_0^2 is positive. Finally, it can be said that $x_0 \pm iy_0$ are zeros of $f(z)$. It should be noted that it is possible for $f(z)$ to have two real zeros close together and that it is then sometimes difficult to be sure of the nature of the zeros until somewhat later in the proceedings. In such cases $C_n^{(n)} \equiv f(x)$ is usually rather small and this gives an indication of the possible existence of two close real zeros. Otherwise it is generally safe in the later stages to interpolate inversely from $C_{n-1}^{(n-1)}$ to determine x_0.

Sometimes there is a loss of significant figures in $C_{n-1}^{(n-1)}$ and then accuracy is gained by calculating the last three rows of the test array (2) as follows. Evaluate

$$C_{n-1}^{(n-3)}/C_{n-3}^{(n-3)} \equiv y_3^2, \quad \text{say,} \tag{14}$$

and

$$C_{n-2}^{(n-2)} = C_{n-2}^{(n-4)} - y_3^2 C_{n-4}^{(n-4)}, \qquad C_n^{(n-2)}/C_{n-2}^{(n-2)} \equiv y_2^2, \quad \text{say.} \tag{15}$$

Then inversely interpolate from $y_3^2 - y_2^2$ to make this quantity zero (at which point $y_3^2 = y_2^2 = y_0^2$). The relation

$$C_{n-1}^{(n-1)} \equiv (y_3^2 - y_2^2) C_{n-3}^{(n-3)} \tag{16}$$

will give this quantity or its sign if required.

Sometimes all the last three rows of (2) show loss of significant figures. Then accuracy is increased by finding y_4^2, y_5^2 satisfying

$$C_{n-4}^{(n-4)} y_4^4 - C_{n-2}^{(n-4)} y_4^2 + C_n^{(n-4)} = 0, \qquad C_{n-5}^{(n-5)} y_5^5 - C_{n-3}^{(n-5)} y_5^3 + C_{n-1}^{(n-5)} y_5 = 0 \tag{17}$$

and inversly interpolating from $y_5^2 - y_4^2$ to make this quantity zero (the values of y_4^2, y_5^2 close to y_0^2 are those chosen).

This loss of significant figures is usually caused by the presence of two pairs of conjugate complex zeros with real parts close together and the loss is usually more than compensated for by the fact that knowledge about *two* pairs of zeros is being found. In fact, in this case, the alternative values of y_4^2, y_5^2 in (17) are also found to be close to each other and inverse interpolation from their difference will often give a second possible value of x_0.

Bairstow's (**9**) method of improving a quadratic factor is, in general, a very economical way of proceeding once x_0 and y_0^2 have been found to three or four significant figures and it is probably better to use this method in the final stages, especially if six or more figures are required.

When a linear or quadratic factor has been found to sufficient accuracy it should be divided out of $f(z)$ and the reduced polynomial factorized.

Finally, it is perhaps worth pointing out the advantage of the present method over Frazer and Duncan's (**2**) methods. In their methods the test function $C_{n-1}^{(n-1)}$ (or this multiplied by some quantity) alone was used to find a true value of x_0. Unfortunately $C_{n-1}^{(n-1)}$ is a rational function of x and can change sign through an infinity. Thus, until a good first approximation making $C_{n-1}^{(n-1)}$ small has been obtained, the choice of the next value of x is uncertain and convergence cannot be guaranteed.

2.3. *Approximate times of solution*

If all zeros are complex and have real parts of the same sign then, to six-figure accuracy, a competent computer with a modern desk machine should be able to solve a quartic in under three-quarters of an hour, and a sextic in under two hours. Eighth or higher degree equations are best solved by the a method.

2.4. *Example*

We will now solve by the x method, the quartic

$$z^4+0{\cdot}935z^3+1{\cdot}280z^2+0{\cdot}425z+0{\cdot}265 = 0.$$

Now the case $x = 0$ for which $\rho\{0\} = 0$ shows that one x_0 must lie in the range $[0, -0{\cdot}935/4] = [0, -0{\cdot}233...]$, and this is a smaller range than $[0, -[c_n/c_0]^{1/n}]$.

The value $x = -0{\cdot}1$ is conveniently near the middle of this range. Again, $\rho\{-0{\cdot}1\} = 0$ but the value of $y_3^2 - y_2^2$ is small. Hence, linear inverse interpolation can probably be used and this suggests $x = -0{\cdot}126$. In fact, $\rho\{-0{\cdot}126\} = 2$ but $y_3^2 - y_2^2$ is much smaller and the remaining values of x were chosen by linear inverse interpolation. The results are summarized

as follows ($C_3^{(3)}$ is given in some cases; its value is not important but its sign is):

x	C_1	$C_2^{(2)}$	y_3^2	y_2^2	$y_3^2-y_2^2$	$C_3^{(3)}$	$\rho\{x\}$
0	0·9350	0·8255	0·4545	0·3210	0·1335	0·1102	0
−0·1	0·5350	0·6988	0·3607	0·3356	0·0251	0·0175	0
−0·126	0·4310	0·6994	0·3224	0·3291	−0·0067	−0·0029	2
−0·1205	0·45300	0·697441	0·331678	0·331136	0·000542	+	0
−0·120916	0·451336	0·697550	0·331005	0·330996	0·000009	+	0

Finally, inverse linear interpolation from the last two results gives $x_0 = -0{\cdot}120923$, $y_0^2 = 0{\cdot}330994$. The corresponding quadratic factor is $z^2-2x_0z+x_0^2+y_0^2 \equiv z^2+0{\cdot}241846z+0{\cdot}345616$.

Divided into the quartic it gives as quotient, $z^2+0{\cdot}693154z+0{\cdot}776747$, with zero remainder to six decimal place accuracy.

The stage $x = -0{\cdot}126$ is now given in full to show a convenient format:

$(c_0 \equiv)1{\cdot}0000$	$(c_1 \equiv)0{\cdot}9350$	$(c_2 \equiv)1{\cdot}2800$	$(c_3 \equiv)0{\cdot}4250$	$(c_4 \equiv)0{\cdot}2650$
	$(c_{1,1} =)0{\cdot}8090$	$(c_{2,1} =)1{\cdot}1781$	$(c_{3,1} =)0{\cdot}2766$	$(c_{4,1} =)0{\cdot}2301$
				$(= C_4)$
	$(c_{1,2} =)0{\cdot}6830$	$(c_{2,2} =)1{\cdot}0920$	$(c_{3,2} =)0{\cdot}1390$	
			$(= C_3)$	
$(C_0 =)1{\cdot}0000$	$(c_{1,3} =)0{\cdot}5570$	$(c_{2,3} =)1{\cdot}0218$		$0{\cdot}2301$
		$(= C_2)$		$(= C_4^{(1)})$
$(y_3^2 =)0{\cdot}3224$	$(c_{1,4} =)0{\cdot}4310$		$0{\cdot}1390$	
	$(= C_1)$		$(= C_3^{(1)})$	
$(y_2^2 =)0{\cdot}3291$		$0{\cdot}6994$		$0{\cdot}2301$
		$(= C_2^{(2)})$		$(= C_4^{(2)})$
$y_3^2-y_2^2 = -0{\cdot}0067$			$-0{\cdot}0029$	
			$(= C_3^{(3)})$	

3. The a method

3.1. *Description of the method*

This method consists essentially in factorizing $f(z)$ (see (**1**)) into quadratic factors of the form z^2-az+b, the computer choosing a numerical value of a then obtaining two equations for b and continuing until a value a_0 has been found such that these two equations have a common root b_0; $z^2-a_0z+b_0$ is then a factor of $f(z)$. We shall, however, deal only with the case in which n is even ($= 2m$, say), for if $f(z)$ is of odd degree a real linear factor can quickly be found and divided out.

Now, when $f(z)$ is divided by z^2-az+b there is a remainder of the form

$$R_1(b)z+R_0(b), \tag{18}$$

where the R_i, which are polynomials in b whose coefficients are polynomials in a, are given by

$$R_0(b) \equiv (-)^m[c_0b^m-r_{2,m-1}b^{m-1}+r_{4,m-2}b^{m-2}-\ldots+ \\ +(-)^{m-1}r_{2m-2,1}b+(-)^mc_{2m}], \tag{19}$$

$$R_1(b) \equiv (-)^{m-1}[r_{1,m}b^{m-1}-r_{3,m-1}b^{m-2}+r_{5,m-2}b^{m-3}-\ldots+(-)^{m-1}r_{2m-1,1}] \tag{20}$$

and the r_{ij} are generated from the array

$$\begin{array}{ccccccccccccc}
(c_1 \equiv)r_{1,0} & & (c_2 \equiv)r_{2,0} & & (c_3 \equiv)r_{3,0} & \cdots & (c_{2m-2} \equiv)r_{2m-2,0} & & (c_{2m-1} \equiv)r_{2m-1,0} \\
r_{1,1} & & r_{2,1} & & r_{3,1} & \cdots & r_{2m-2,1} & & r_{2m-1,1} \\
r_{1,2} & & r_{2,2} & & r_{3,2} & \cdots & & & \\
\cdots & \cdots & \cdots & \cdots & \cdots & \cdots & \cdots & \cdots & \cdots \\
r_{1,m-2} & & r_{2,m-2} & & r_{3,m-2} & & r_{4,m-2} & & r_{5,m-2} \\
r_{1,m-1} & & r_{2,m-1} & & r_{3,m-1} & & & & \\
r_{1,m} & & & & & & & &
\end{array} \tag{21}$$

according to the rule,

$$r_{t,u} = r_{t,u-1} + a r_{t-1,u} \tag{22}$$

with $c_0 \equiv r_{0,u}$. This result can be proved by induction without difficulty. In words the rule is simply that each r_{ij} is the sum of the term above and the product of a and the term to the left. In fact the r_{ij} are identical with the c_{ij} of (9) if $a = x$, but there are fewer (about half) of them for the same value of n. It can be seen that if a test using a value of x has been carried out, then from the resulting c_{ij} it is possible to obtain the values of r_{ij}, for a having the same value as x, without further work; and in fact this combination of the x and a methods is sometimes useful.

Accuracy can be checked by using one of the relations

$$f(1) = R_1(a-1) + R_0(a-1), \qquad f(-1) = -R_1(-a-1) + R_0(-a-1) \tag{23}$$

which can be seen to hold from the fact that $z^2 - az + b$ is zero if $z = 1$, $b = a-1$, or $z = -1$, $b = -a-1$.

When the r_{ij} have been computed the h.c.f. of the two polynomials (19) and (20) is found. This can be done by applying Routh's test to the C_i where

$$C_0 = c_0, \quad C_1 = r_{1,m}, \quad C_2 = r_{2,m-1}, \quad C_3 = r_{3,m-1}, \quad C_4 = r_{4,m-2},$$
$$C_5 = r_{5,m-2}, \quad C_{2m-2} = r_{2m-2,1}, \quad C_{2m-1} = r_{2m-1,1}, \quad C_{2m} = c_{2m}. \tag{24}$$

The aim is to find $a = a_0$, say, such that the $C_{n-1}^{(n-1)}$ of (2) is zero, when, simultaneously,

$$C_n^{(n-2)} / C_{n-2}^{(n-2)} = C_{n-1}^{(n-3)} / C_{n-3}^{(n-3)} \equiv b_0, \quad \text{say.} \tag{25}$$

Further (see section 4) it can then be said that $R_0(b_0) = R_1(b_0) = 0$ and hence, that

$$z^2 - a_0 z + b_0$$

is a factor of $f(z)$. In fact a_0 may be found in a systematic manner by noting the number of changes of sign $\rho[a]$ say, of the $C_r^{(r)}$ in the Routh test array (2) derived from the C_i of (24). Once a_1 and a_2 have been found such that $\rho[a_1] \neq \rho[a_2]$ then (see section 4) a true value of a_0 must lie in $[a_1, a_2]$. Further it can be shown (see section 4) that $\rho[-\infty] = 2m$ and $\rho[+\infty] = 0$,

so that ranges $[a_1, a_2]$ exist. It does not seem possible to specify such a range initially, in general, except in the important cases when $\rho[0] = 0$ or $2m$. In either case it can be proved (section 4) that $\rho[-c_1/(mc_0)] \neq \rho[0]$. In other cases one or two trials will usually establish such a range, or by one or two applications of the x method, a change of origin will be found which will convert $f(z)$ to a polynomial all of whose zeros have negative real parts.

As in the x method, there may be loss of significant figures in $C_{n-1}^{(n-1)}$ and then the last few rows of (2) can be calculated as follows: Evaluate

$$b_3 \equiv C_{n-1}^{(n-3)}/C_{n-3}^{(n-3)}, \qquad C_{n-2}^{(n-2)} \equiv C_{n-2}^{(n-4)} - b_3 C_{n-4}^{(n-4)}, \tag{26}$$

$$b_2 \equiv C_n^{(n-2)}/C_{n-2}^{(n-2)}, \qquad C_{n-1}^{(n-1)} \equiv (b_3 - b_2) C_{n-3}^{(n-3)}. \tag{27}$$

Inverse interpolation from $b_3 - b_2$ can be used to find the value of a for which $b_3 = b_2 = b_0$.

It should be noted that if $\rho[a_1] = \rho[a_2]$ there may nevertheless be true values of a_0 in $[a_1, a_2]$ and that this can occur if there are more than two real zeros of $f(z)$. In this respect the a method differs from the x method.

The number of calculations per stage in the a method is lower, however, and it fits in with Bairstow's method (**9**) somewhat more easily (this is certainly to be recommended once four figures have been obtained if $n = 8$ or more). Finally, though it might appear that real zeros can only be found in the form of quadratic factors by the a method, real zeros can be found in the usual manner if, in computing the r_{ij}, we perform the one additional calculation

$$f(a) = c_{2m} + a r_{2m-1,1}. \tag{28}$$

3.2. *Approximate times of solution*

If all zeros are complex and have real parts of the same sign then to six-figure accuracy a quartic can usually be solved in half an hour, a sextic in an hour and a quarter and an eighth degree in two hours and a quarter.

Example. We now solve the following sextic equation

$$z^6 + 3{\cdot}31z^5 + 7{\cdot}71z^4 + 10{\cdot}94z^3 + 10{\cdot}94z^2 + 6{\cdot}70z + 2{\cdot}68 = 0.$$

Here $\rho[0] = 0$; hence, an a_0 lies in $[0, -3{\cdot}31/3 = -1{\cdot}10...]$. We choose for our second value of a, $-0{\cdot}6$ ($-0{\cdot}55$ would be more logical but $0{\cdot}6$ simplified the arithmetic slightly), and $b_3 - b_2$ is found to be much smaller than for $a = 0$ though $\rho[a]$ is still zero. The next trial value of a is therefore $-0{\cdot}7$ and $\rho[a]$ is 2. The value $a = -0{\cdot}64$ seems plausible and from

this stage onwards inverse Lagrangian interpolation was used. The following is a summary of the main results:

a	0	$-0{\cdot}6$	$-0{\cdot}7$	$-0{\cdot}64$	$-0{\cdot}645600$	$-0{\cdot}64556200$
c_1	3·3100	1·5100	1·2100	1·3900	1·373200	1·37331400
$C^{(2)}$	4·4050	1·9047	1·5382	1·7597	1·739160	1·73929883
b_2	1·1051	0·9894	0·8119	0·9438	0·935856	0·93591222
b_3	0·6621	0·9392	0·9100	0·9368	0·935904	0·93591110
b_3-b_2	0·4430	0·0502	$-0{\cdot}0981$	0·0070	$-0{\cdot}000048$	0·00000112
$\rho[a]$	0	0	2	0	2	0

Interpolation finally gives $a_0 = -0{\cdot}64556286$, $b_0 = 0{\cdot}93591094$ and division of the sextic by $z^2-a_0z+b_0$ gives

$$z^4+2{\cdot}66443714z^3+5{\cdot}05602740z^2+5{\cdot}18363175z+2{\cdot}86352033$$

with remainder $-0{\cdot}00000004z-0{\cdot}00000000$. The stage $a = -0{\cdot}7$ is now set out in full to show the format.

$(c_0 =)1{\cdot}0000$	$(c_1 =)3{\cdot}3100$	$(c_2 =)7{\cdot}7100$	10·9400	10·9400	6·7000	2·6800
	$(r_{1,1} =)2{\cdot}6100$	$(r_{2,1} =)5{\cdot}8830$	6·8219	6·1647	2·3847	
$(C_0 =)1{\cdot}0000$	$(r_{1,2} =)1{\cdot}9100$	$(r_{2,2} =)4{\cdot}5460$	3·6397	6·1647		2·6800
$C_0/C_1 = 0{\cdot}8264$	$(r_{1,3} =)1{\cdot}2100$		3·6397		2·3847	
	$(= C_1)$					
$C_1/C_2^{(2)} = 0{\cdot}7866$		1·5382		4·1940		2·6800
		$(= C_2^{(2)})$		$(= C_4^{(2)})$		
$b_3(= 0{\cdot}2766/0{\cdot}3407) = 0{\cdot}8119,$			0·3407		0·2766	
$b_2(= 2{\cdot}6800/2{\cdot}9451) = 0{\cdot}9100,$				2·9451		2·6800
$b_3-b_2 \quad = -0{\cdot}0981.$						

The a method can now be applied to the quartic quotient. We know that an a_0 (of this quartic) must lie in 0, $-2{\cdot}6644.../2$ since all real parts of zeros are negative. Further, the work on the sextic suggests that a_0 is (algebraically) less than $-0{\cdot}7$. Hence $a = -1{\cdot}0$ seems a convenient value to try and $\rho[-1{\cdot}0]$ is found to be 2. Hence $a = -0{\cdot}84$ is next tried (b_3 and b_2 are very close here), then $a = -0{\cdot}83$, and from this stage onward inverse interpolation can be used.

After a_0 and b_0 have been found to about four-figure accuracy, say, by the application of Lagrangian inverse interpolation using three or four values of a near the suspected value of a_0, Bairstow's method of improving a quadratic factor can be used. Indeed if the computer is familiar with these techniques, their combination is a very efficient way of using the a method.

4. Properties of, and proof of Routh's test (and the fundamental theorem of algebra)

4.1. *Examination of the causes of change in $\rho\{x\}$ and the accuracy needed in its calculation.*

Now the C_i, the coefficients of powers of $z-x$ in the expression (8) for $f(z)$, can be seen to be polynomials in x and therefore always finite. The

$C^{(r)}_{r+2s}$ of the Routh test array (2) calculated from the C_i are, however, rational functions with $C^{(r-1)}_{r-1}$ in their denominators, and hence may have infinities. We now consider what happens when $C^{(r)}_r$ goes through a zero. Applying the relation (3) we see that

$$C^{(r+1)}_{r+1+2s} = C^{(r-1)}_{r+1+2s} - \{C^{(r-1)}_{r-1}/C^{(r)}_r\}C^{(r)}_{r+2s+2}; \tag{29}$$

$$C^{(r+2)}_{r+2+2s} = C^{(r)}_{r+2+2s} - C^{(r)}_{r+2s+4}C^{(r)}_r/C^{(r)}_{r+2} + O(C^{(r)}_r)^2; \tag{30}$$

$$C^{(r+3)}_{r+3+2s} = C^{(r+1)}_{r+3+2s} - \{C^{(r+1)}_{r+1}/C^{(r+2)}_{r+2}\}C^{(r+2)}_{r+4+2s}. \tag{31}$$

Now we see that as $C^{(r)}_r$ goes through a zero, the $C^{(r+1)}_{r+1+2s}$ go through an infinity, but that the $C^{(r+2)}_{r+2+2s}$ are finite and so are the $C^{(r+3)}_{r+3+2s}$; for when we substitute for the $C^{(r+1)}_{r+1+2s}$ in (31) we find the terms in $1/C^{(r)}_r$ cancel. Hence, since rows of (2) are generated from the two rows above, all subsequent rows in (2) are finite, in general, unless a higher $C^{(i)}_i$ is simultaneously zero with $C^{(r)}_r$.

Now, (29) shows that as $C^{(r)}_r$ goes from -0 to $+0$, $C^{(r+1)}_{r+1}$ goes from $+$ to $-C^{(r-1)}_{r-1}C^{(r)}_{r+2}\,\infty$ and $C^{(r+2)}_{r+2}$ does not change sign. Considering all possible combinations of sign of $C^{(r-1)}_{r-1}$, $C^{(r)}_{r+2}$ we find that the numbers of changes of sign in the sequence $C^{(r-1)}_{r-1}$, $C^{(r)}_r$, $C^{(r+1)}_{r+1}$, $C^{(r+2)}_{r+2}$ does not alter as $C^{(r)}_r$ goes through a zero. Therefore $\rho\{x\}$ cannot alter, unless $r = n-1$ or n (in which cases $C^{(r+2)}_{r+2}$ is non-realizable).

If $C^{(n)}_n \equiv C_n \equiv f(x)$ goes through a zero then consideration of the possible change in signs shows that $\rho\{x\}$ can change by one only (if, simultaneously, $C^{(n-1)}_{n-1}$ is zero then a change of two is possible, $f(z)$ then having two coincident real zeros). If $C^{(n-1)}_{n-1} = 0$, and simultaneously, $C^{(n)}_n$ is non-zero and $C^{(n-2)}_n/C^{(n-2)}_{n-2}$ is positive, consideration of the possible signs shows that $\rho\{x\}$ changes by two as $C^{(n-1)}_{n-1}$ goes through its zero but does *not* change if the ratio $C^{(n-2)}_n/C^{(n-2)}_{n-2}$ is negative. Neither will $\rho\{x\}$ change if $C^{(n-1)}_{n-1}$ changes sign through an infinity, for then $C^{(n-2)}_{n-2}$ must go through a zero.

A consequence of the above argument is that a small error in calculating Routh's test will not affect $\rho\{x\}$ even if, say, $C^{(r)}_r$ is calculated to be $+\epsilon$ when it should be $-\eta$, both being small, unless $r = n-1$ or n. In such cases x is near the real part of a zero and greater accuracy is necessarily required.

Since the Routh test array (2) is derived from a process for finding the h.c.f. of two polynomials, i.e. the odd and even powers of $f(z)$ it follows that if, for $x = x_0$, $C^{(n-1)}_{n-1}$ is zero, then all polynomials

$$C^{(n-r)}_{n-r}\,y^r - C^{(n-r)}_{n-r+2}\,y^{r-2} + C^{(n-r)}_{n-r+4}\,y^{r-4} - \ldots \tag{32}$$

have some common factor, $y^2 - y_0^2$, say. In particular

$$C^{(n-2)}_{n-2}\,y_0^2 - C^{(n-2)}_n = 0, \qquad C^{(n-3)}_{n-3}\,y_0^3 - C^{(n-3)}_{n-1}\,y_0 = 0. \tag{33}$$

Also, putting $r = 0$ and 1 in (32), we see that

$$C_0 y_0^n - C_2 y_0^{n-2} + C_4 y_0^{n-4} - \ldots = 0, \qquad C_1 y_0^{n-1} - C_3 y_0^{n-3} + \ldots = 0. \quad (34)$$

Hence, if $z - x_0 = \pm i y_0$, then (8) and (34) show that $f(z)$ is zero. Thus a change in sign through a zero of $C_{n-1}^{(n-1)}$, and, hence a change of two in $\rho\{x\}$, is shown to be coincident with the existence of a pair of complex conjugate zeros.

Similar observations apply to the C_i of (24), with y^2 replaced by b. Here, as a goes through a_0, $C_{n-1}^{(n-1)}$ goes through a zero, $\rho[a]$ changes by two and $R_0(b)$ and $R_1(b)$ have a common factor $b - b_0$. Hence from (18) it follows that $f(z)$ divided by $z^2 - a_0 z + b_0$ gives a zero remainder.

4.2. *Negative terms in the Routh's test array*

If all zeros have negative real parts $f(z)$ is generated by factors of the form $(z+A)$ and $z^2 + Bz + C$ where A, B, C are necessarily positive. Hence, if c_0 is positive in $f(z)$ (see (1)) so are all the c_i. Conversely if one c_i is negative then $\rho\{0\} \neq 0$, and at least one of the $C_r^{(r)}$ must be negative also. Now each row of the array (2) is generated from the two rows immediately above, always in the same way. Hence, if in carrying out Routh's test to calculate $\rho\{x\}$ or $\rho[a]$ we find one of the terms in a row to be *negative* then necessarily one of the subsequent $C_r^{(r)}$ must be negative. Thus $\rho\{x\}$ cannot be zero, and, if this is what was wanted, no further work need be done.

4.3. *Proof of Routh's test (and the fundamental theorem of algebra)*

Now, if $c_0 = 1$, as $x \to \pm\infty$, the C_i of (8) can be seen to have the asymptotic values

$$C_0 = 1, \qquad C_i \sim \binom{n}{i} x^i.$$

Applying Routh's test to the C_i we find the terms in the array (2) have the general form

$$C_{2r+2s}^{(2r)} \sim \binom{n}{2r+2s} \times \times \frac{[(s+1)(s+2)\ldots(s+r)][(n+1)(n+3)\ldots(n+2r-1)]2^{r-1}x^{2r+2s}}{[(2r+2s+1)(2r+2s+3)\ldots(4r+2s-1)][n(n-2)(n-1)\ldots(n-2r+2)]}, \quad (35)$$

$$C_{2r+1+2s}^{(2r+1)} \sim \binom{n}{2r+2s+1} \times \times \frac{[(s+1)(s+2)\ldots(s+r)][(n+2)(n+4)\ldots(n+2r)]2^{r-1}x^{2r+2s+1}}{[(2r+2s+3)(2r+2s+5)\ldots(4r+2s+1)][(n-1)(n-3)\ldots(n-2r+1)]} \quad (36)$$

(these satisfy the relation (3) and have the right values when $r = 1$). Since, in any $C_j^{(i)}$, j is less than or equal to n, the coefficients of powers of x in (36) and (35) will be seen to be essentially positive. Hence, $C_r^{(r)}$ has the same sign as x^r, and so $\rho\{+\infty\} = 0$ and $\rho\{-\infty\} = n$. Hence, by 4.1, it follows that there exist at least n zeros of $f(z)$ which are, in general, distinct. It is well known that $f(z)$ cannot have more than n zeros and so it has exactly n. Then, if $\rho\{x_1\} = p$, it follows there are p real parts between x_1 and ∞, which proves Routh's test.

4.4. *The application of Routh's test to the a method and a further proof of the fundamental theorem of algebra*

Here, $n = 2m$, and the C_i of (26) can be seen from (23) to be polynomials in a, with asymptotic values, as $a \to \infty$,

$$C_0 = 1, \quad C_1 \sim \binom{m}{1}a, \quad C_2 \sim \binom{m}{2}a^2, \quad C_3 \sim \binom{m+1}{3}a^3,$$

$$C_4 \sim \binom{m+1}{4}a^4, \quad C_5 \sim \binom{m+2}{5}a^5, \quad \ldots. \tag{37}$$

The same argument as in 4.1 shows that since the C_i are finite, $\rho[a]$ can change only if $C_{2m-1}^{(2m-1)}$ or $C_{2m}^{(2m)}$ (calculated by (2) from the C_i) go through a zero. But $C_{2m}^{(2m)} = C_{2m} = c_{2m} =$ constant. So change can occur *only* if $C_{2m-1}^{(2m-1)}$ goes through a zero (and therefore will be by two).

Now the $C_j^{(i)}$ of (2) have the asymptotic values

$$C_{2r+2s}^{(2r)} \sim \binom{m+r+s}{2r+2s} \times$$

$$\times \frac{[(2m-1)(2m-3)\ldots(2m-2r-1)][s(s+1)\ldots(s+r-1)]a^{2r+2s}}{[(2r+2s+1)(2r+2s+3)\ldots(4r+2s-1)][m(m+1)\ldots(m+r-1)]}, \tag{38}$$

$$C_{2r+1+2s}^{(2r+1)} \sim \binom{m+r+s}{2r+2s+1} \times$$

$$\times \frac{[(2m+1)(2m+3)\ldots(2m+2r+1)][s(s+1)\ldots(s+r-1)]a^{2r+2s+1}}{[(2r+2s+3)(2r+2s+5)\ldots(4r+2s+1)][(m-1)(m-2)\ldots(m-r)]} \tag{39}$$

and hence the $C_r^{(r)}$ will have the same signs as a^r and so $\rho[+\infty] = 0$, $\rho[-\infty] = 2m$. Thus at least m factors of $f(z)$ with different a's exist (which incidentally again proves the fundamental theorem of algebra).

Now, if $\rho[0] = 0$, all real parts are negative. But (23) shows that $C_1 = c_1 + mac_0$. Hence if a is (algebraically) less than $-c_1/mc_0$, C_1 will be negative, and, hence, $\rho[-c_1/mc_0] \neq 0$. A similar argument holds when $\rho[0] = 2m$, which shows that $\rho[-c_1/mc_0] \neq 2m$.

REFERENCES

1. E. J. Routh, *Essay on the Stability of Motion* (Macmillan & Co., London, 1877).
2. R. A. Frazer and W. J. Duncan, *Proc. Roy. Soc.* A, **125** (1929) 68–82.
3. Shih-nge Lin, *J. Math. Phys.* **22** (1943) 60–77.
4. B. Friedman, *Commun. on Pure and App. Math.* **2** (1949), 195–201; see also Hartree (**12**) 201.
5. A. C. Aitken, *Quart. J. Mech. App. Math.* **8** (1955) 251–5.
6. —— *Proc. Edin. Math. Soc.* (2) **3** (1932) 56–76; see also Hartree (**12**) 84.
7. E. H. Neville, *J. Indian Math. Soc.* **20** (1934) 87–90; see also Hartree (**12**) 85.
8. C. Mack and A. Porter, *Phil. Mag.* **40** (1949) 578–85.
9. L. Bairstow, *Rep. Memor. Adv. Comm. Aero. Lond.* **154** (1914) 51–63.
10. C. H. Graeffe, *Die Auflösung der Hoheren Numerischen Gleichungen* (Zurich, 1837); see also Olver (**11**).
11. F. W. J. Olver, *Phil. Trans. Roy. Soc.* A, **244** (1952) 385–415.
12. D. R. Hartree, *Numerical Analysis* (Oxford, 1952).

DUAL FOURIER–BESSEL SERIES

By J. C. COOKE (*Farnborough*) *and*
C. J. TRANTER (*Royal Military College of Science, Shrivenham*)

[Received 9 June 1958]

SUMMARY

A method is given for determining the coefficients a_n in the 'dual' Fourier–Bessel series

$$\sum_{n=1}^{\infty} \alpha_n^p a_n J_\nu(\alpha_n r) = F(r) \quad (0 < r < 1),$$

$$\sum_{n=1}^{\infty} a_n J_\nu(\alpha_n r) = 0 \qquad (1 < r < a),$$

where $-1 \leqslant p \leqslant 1$, $F(r)$ is specified and α_n is a positive root of $J_\nu(\alpha_n a) = 0$. Such series arise in the solution of potential problems in which the application of a *finite* Hankel transform is appropriate and in which one of the boundary conditions is a 'mixed' one. As an illustration, the method is applied to find the potential due to an electrified circular disk situated inside an earthed coaxial infinite hollow cylinder. This shows that useful results can be obtained provided that the radius of the cylinder is sufficiently large.

1. Introduction

POTENTIAL problems in a semi-infinite medium in which different conditions hold over different parts of the same boundary can often be conveniently reduced by the use of a Hankel transform to the solution of a pair of dual integral equations. When the medium is confined within a circular cylinder or between a pair of parallel planes, such problems can be similarly reduced by the use of a *finite* Hankel transform to the determination of the coefficients in what may be termed 'dual' Fourier–Bessel series. In the physical problems so far considered, these dual series are of the form

$$\left.\begin{aligned} \sum_{n=1}^{\infty} \alpha_n^p a_n J_\nu(\alpha_n r) &= F(r) \quad (0 < r < 1) \\ \sum_{n=1}^{\infty} a_n J_\nu(\alpha_n r) &= 0 \qquad (1 < r < a) \end{aligned}\right\}, \tag{1}$$

where $-1 \leqslant p \leqslant 1$, $F(r)$ is specified, α_n is a positive root of $J_\nu(\alpha_n a) = 0$ and the coefficients a_n are to be determined.

The purpose of this note is to give a method for determining the coefficients a_n from equations (1). The solution given is formal only and the difficult question of convergence is not considered. The method used is similar to that previously used by one of us (1) in the case of dual integra equations and, under certain circumstances, the solution given is suitable

for computation purposes. As an illustration, we consider the problem of an electrified circular disc situated inside an earthed coaxial infinite hollow cylinder.

2. The reduction to a set of algebraical equations

It is sufficient for the purpose in view to take ν to be real and it follows from Tranter (**2**) that, if m is zero or a positive integer and $\nu > -1$,

$$\sum_{n=1}^{\infty} \frac{J_{\nu+2m+1+\frac{1}{2}p}(\alpha_n) J_\nu(\alpha_n r)}{\alpha_n^{1+\frac{1}{2}p} J_{\nu+1}^2(\alpha_n a)} = 0 \quad (1 < r < a).$$

By taking
$$a_n = \frac{1}{\alpha_n^{1+\frac{1}{2}p} J_{\nu+1}^2(\alpha_n a)} \sum_{m=0}^{\infty} b_m J_{\nu+2m+1+\frac{1}{2}p}(\alpha_n), \tag{2}$$

the second of equations (1) is therefore automatically satisfied.

The coefficients b_m have now to be chosen so that a_n satisfies the first of equations (1). Substituting from (2) and interchanging the order of the summations,

$$\sum_{m=0}^{\infty} b_m \sum_{n=1}^{\infty} \frac{J_{\nu+2m+1+\frac{1}{2}p}(\alpha_n) J_\nu(\alpha_n r)}{\alpha_n^{1-\frac{1}{2}p} J_{\nu+1}^2(\alpha_n a)} = F(r) \quad (0 < r < 1). \tag{3}$$

Now (**3**), if s is a positive integer or zero,

$$\frac{J_{\nu+2s+1+\frac{1}{2}p}(\alpha_n)}{\alpha_n^{1+\frac{1}{2}p}} = \frac{\Gamma(\nu+s+1)}{2^{\frac{1}{2}p}\Gamma(\nu+1)\Gamma(s+1+\frac{1}{2}p)} \int_0^1 r^{\nu+1}(1-r^2)^{\frac{1}{2}p} \mathscr{F}_s(1+\tfrac{1}{2}p+\nu, \nu+1, r^2) J_\nu(\alpha_n r)\, dr, \tag{4}$$

where

$$\mathscr{F}_s(1+\tfrac{1}{2}p+\nu, \nu+1, r^2) = {}_2F_1(-s, 1+\tfrac{1}{2}p+\nu+s;\ \nu+1;\ r^2)$$

is Jacobi's polynomial. Hence multiplying (3) by

$$r^{\nu+1}(1-r^2)^{\frac{1}{2}p} \mathscr{F}_s(1+\tfrac{1}{2}p+\nu,\ \nu+1,\ r^2),$$

integrating with respect to r between 0, 1, interchanging the order of integration and summation and use of (4) gives

$$\sum_{m=0}^{\infty} b_m \sum_{n=1}^{\infty} \frac{J_{\nu+2m+1+\frac{1}{2}p}(\alpha_n) J_{\nu+2s+1+\frac{1}{2}p}(\alpha_n)}{\alpha_n^2 J_{\nu+1}^2(\alpha_n a)} = E(\nu, s, p), \tag{5}$$

where, for brevity, we have written

$$E(\nu, s, p) = \frac{\Gamma(\nu+s+1)}{2^{\frac{1}{2}p}\Gamma(\nu+1)\Gamma(s+1+\frac{1}{2}p)} \int_0^1 r^{\nu+1}(1-r^2)^{\frac{1}{2}p} \mathscr{F}_s(1+\tfrac{1}{2}p+\nu, \nu+1, r^2) F(r)\, dr. \tag{6}$$

Equation (5) with $s = 0, 1, 2, 3,...$ provides a set of algebraical equations to determine the coefficients b_m. Once the values of b_m have been found from this set, the coefficients a_n can be evaluated from equation (2).

3. The iterative solution of the algebraical equations

The set of algebraical equations (5) can, under certain circumstances, be solved by an iterative process as follows. Provided ν is not a negative integer and that $\nu > -1-\frac{1}{2}p$, it is known (Tranter (**2**)) that, for all values of m and s under discussion here,†

$$\frac{2}{a^2}\sum_{n=1}^{\infty}\frac{J_{\nu+2m+1+\frac{1}{2}p}(\alpha_n)J_{\nu+2s+1+\frac{1}{2}p}(\alpha_n)}{\alpha_n^2 J_{\nu+1}^2(\alpha_n a)} = \frac{\delta_{m,s}}{2\nu+4s+2+p} + \\ +(-1)^{m+s}\frac{2}{\pi}\sin\tfrac{1}{2}p\pi\int_0^{\infty}\frac{K_\nu(t)}{tI_\nu(t)}I_{\nu+2m+1+\frac{1}{2}p}\left(\frac{t}{a}\right)I_{\nu+2s+1+\frac{1}{2}p}\left(\frac{t}{a}\right)dt, \quad (7)$$

where $\delta_{m,s} = 0$ when $m \neq s$ and $\delta_{m,s} = 1$ when $m = s$. Writing

$$L_{m,s}^{(\nu,p)} \\ = (-1)^{m+s+1}(2\nu+4s+2+p)\frac{2}{\pi}\sin\tfrac{1}{2}p\pi\int_0^{\infty}\frac{K_\nu(t)}{tI_\nu(t)}I_{\nu+2m+1+\frac{1}{2}p}\left(\frac{t}{a}\right)I_{\nu+2s+1+\frac{1}{2}p}\left(\frac{t}{a}\right)dt, \quad (8)$$

and substituting from (7) in (5), the algebraical equations to determine the coefficients b_m become

$$b_s - \sum_{m=0}^{\infty} b_m L_{m,s}^{(\nu,p)} = \frac{2}{a^2}(2\nu+4s+2+p)E(\nu,s,p) \quad (s = 0,1,2,3,...). \quad (9)$$

The iterative solution of this set of linear equations (which can be shown to converge if a is large enough although it is difficult to determine precise limits for this) is given by

$$b_s = \sum_{r=0}^{\infty} b_s^{(r)} \quad (s = 0,1,2,3,...), \quad (10)$$

where
$$b_s^{(0)} = \frac{2}{a^2}(2\nu+4s+2+p)E(\nu,s,p)$$

and
$$b_s^{(r)} = \sum_{m=0}^{\infty} L_{m,s}^{(\nu,p)} b_m^{(r-1)} \quad (r = 1,2,3,...) \quad (11)$$

† The particular case of $\nu = -\frac{1}{2}$, $p = -1$ is of some importance in practice. In this case the inequality $\nu > -1-\frac{1}{2}p$ does not hold but the result (7) remains valid except when $m = s = 0$. By modifying the analysis given in (**2**), it can be shown that the result for this case is

$$\frac{2}{a^2}\sum_{n=1}^{\infty}\frac{J_0^2(\alpha_n)}{\alpha_n^2 J_{\frac{1}{2}}^2(\alpha_n a)} = \log_e\left(\frac{8a}{\pi}\right) - 2\int_0^{\infty}\frac{I_0^2(t/a)-1}{t(e^{2t}+1)}dt.$$

4. The evaluation of $L_{m,s}^{(\nu,p)}$.

The theoretical determination of the coefficients a_n of the dual series (1) is contained in equations (2), (10), (11), (8) and in a practical problem, the chief difficulty lies in the computation of $L_{m,s}^{(\nu,p)}$. By expanding the Bessel functions of argument (t/a) in equation (8) in ascending powers of t/a, $L_{m,s}^{(\nu,p)}$ can be expressed as a series of descending powers of a with the aid of the integrals

$$M_n^{(\nu)} = \int_0^\infty \frac{t^n K_\nu(t)}{I_\nu(t)}\, dt. \tag{12}$$

These series are quite rapidly convergent if a is fairly large compared with unity.

TABLE 1

Values of $M_n^{(\nu)} = \int_0^\infty \frac{t^n K_\nu(t)}{I_\nu(t)}\, dt$

n \ ν	$-\frac{1}{2}$	0	$\frac{1}{2}$	1
0		1·36768		
1	0·64596		1·29193	
2		0·64689		2·50330
3	1·11570		1·27508	
4		2·06986		3·77139
5	5·80538		5·99265	
6		16·168		23·431
7	61·617		62·102	
8		231·69		302·29
9	1112·2		1114·4	
10		5286·6		

The values of ν occurring most frequently in practice are $\pm\frac{1}{2}$, 0, and 1 and the integrals $M_n^{(0)}$ have been evaluated by Knight (**4**) for $n = 0, 2, 4, 6, 8, 10$. These values, together with some of those for $M_n^{(1)}$ (which have been calculated in a similar manner) are given in Table 1. These integrals are laborious to compute and, to make the most of the method, Table 1 could be usefully extended to higher values of n. Useful approximating polynomials for $K_\nu(t)$, $I_\nu(t)$ when $\nu = 0$ and 1 have recently been given by Allen (**5**) and these should reduce the labour of extending this table should such a project be undertaken. Values for $M_n^{(-\frac{1}{2})}$ and $M_n^{(\frac{1}{2})}$ are also given in the table—these integrals can be expressed in terms of the Riemann zeta function and are easy to compute from a table of that function.

Some inequalities involving the integrals $M_n^{(\nu)}$ are useful in estimating the error when $L_{m,s}^{(\nu,p)}$ is computed by the above method. Knight (4) gives

$$M_{2n}^{(0)} < 2+\log_e 2-\gamma+\frac{\pi e^{-2}(2n+1)!}{2^{2n+1}} \tag{13}$$

where $\gamma = 0{\cdot}577215\ldots$ is Euler's constant. For $n > 3$, a better inequality is

$$M_{2n}^{(0)} < \frac{3{\cdot}15(2n)!}{2^{2n+1}}. \tag{14}$$

It can also be shown that, for $n > 1$,

$$M_{2n}^{(1)} < \frac{8(2n)!}{2^{2n+1}} \tag{15}$$

and it is almost certain that this can be improved upon.

As an example, using equation (8) and Table 1, it can be shown that

$$L_{0,0}^{(1,-1)} = \frac{6}{\pi}\int_0^\infty \frac{K_1(t)}{tI_1(t)} I_{\frac{1}{2}}^2\left(\frac{t}{a}\right) dt$$

$$= 0{\cdot}33818a^{-3}+0{\cdot}10190a^{-5}+0{\cdot}05426a^{-7}+0{\cdot}03457a^{-9},$$

with an error less than $\dfrac{0{\cdot}052}{a^{11}}\dfrac{a^2}{a^2-1}$.

5. An example

As an illustration, we consider the potential due to an electrified circular disk charged to unit potential and situated inside an earthed coaxial infinite hollow cylinder. An approximate solution to this problem has been given by Smythe (6) working by quite a different method. Using cylindrical coordinates (r, z), we take the disk as $z = 0$, $r < 1$ and the cylinder as $r = a$, $-\infty < z < \infty$. The potential V has to satisfy

$$\frac{\partial^2 V}{\partial r^2}+\frac{1}{r}\frac{\partial V}{\partial r}+\frac{\partial^2 V}{\partial z^2} = 0, \tag{16}$$

with $\quad V = 1,\ 0 < r < 1\text{:}\quad \dfrac{\partial V}{\partial z} = 0,\ 1 < r < a, \quad \text{when } z = 0, \tag{17}$

since there is symmetry about the plane $z = 0$, and

$$V = 0 \quad \text{when} \quad r = a, \qquad V \to 0 \quad \text{as} \quad |z| \to \infty. \tag{18}$$

If $\overline{V}$ is the *finite* Hankel transform (of order zero) of V, i.e. if

$$\overline{V} = \int_0^a rVJ_0(\alpha r)\, dr, \tag{19}$$

where α is a positive root of the equation $J_0(\alpha a) = 0$, then, by the usual procedure (see, for example, Tranter (7)), equations (16) and (18) lead to

$$\frac{\partial^2 \overline{V}}{\partial z^2} = \alpha^2 \overline{V}. \tag{20}$$

The solution of (20), finite at infinite axial distances is

$$\overline{V} = A(\alpha) e^{-\alpha |z|}, \tag{21}$$

where $A(\alpha)$ is a constant depending only on α. The inversion theorem appropriate to (19) then gives

$$V = \frac{2}{a^2} \sum_{n=1}^{\infty} \frac{A_n e^{-\alpha_n |z|} J_0(\alpha_n r)}{J_1^2(\alpha_n a)}. \tag{22}$$

Writing $\alpha_n A_n = a_n J_1^2(\alpha_n a)$ and substituting from (22) in the 'mixed' boundary condition (17), the coefficients a_n have to be found from

$$\left.\begin{aligned} \sum_{n=1}^{\infty} \alpha_n^{-1} a_n J_0(\alpha_n r) &= \tfrac{1}{2} a^2 \quad (0 < r < 1) \\ \sum_{n=1}^{\infty} a_n J_0(\alpha_n r) &= 0 \qquad (1 < r < a) \end{aligned}\right\}. \tag{23}$$

These are a special case ($\nu = 0$, $p = -1$, $F(r) = \frac{1}{2} a^2$) of the more general dual series already discussed.

The physical quantity of most interest in this problem is the electrostatic capacity of the system and here this is equal to the total charge on the disk. The surface density of charge on the disk is $(-\frac{1}{4}\pi)(\partial V/\partial z)_{z=0}$ and, taking into account both sides of the disk, the total charge is

$$-\frac{1}{2\pi} \int_0^1 2\pi r \left(\frac{\partial V}{\partial z}\right)_{z=0} dr.$$

Using equation (22) and the relation between A_n and a_n, this can be written

$$\frac{2}{a^2} \sum_{n=1}^{\infty} a_n \int_0^1 r J_0(\alpha_n r)\, dr, \quad \text{i.e.} \frac{2}{a^2} \sum_{n=1}^{\infty} \frac{a_n J_1(\alpha_n)}{\alpha_n},$$

if we assume it is legitimate to interchange the order of integration and summation. Putting $\nu = 0$, $p = -1$ in (2),

$$a_n = \frac{1}{\alpha_n^{\frac{1}{2}} J_1^2(\alpha_n a)} \sum_{m=0}^{\infty} b_m J_{2m+\frac{1}{2}}(\alpha_n)$$

and hence the capacity C, assuming an interchange in the order of the summations is permissible, is given by

$$C = \frac{2}{a^2} \sum_{m=0}^{\infty} b_m \sum_{n=1}^{\infty} \frac{J_{2m+\frac{1}{2}}(\alpha_n) J_1(\alpha_n)}{\alpha_n^{\frac{1}{2}} J_1^2(\alpha_n a)}. \tag{24}$$

Now it is known that, Tranter (**2**),

$$\frac{2}{a^2} \sum_{n=1}^{\infty} \frac{J_{2m+\frac{1}{2}}(\alpha_n) J_0(\alpha_n r)}{\alpha_n^{\frac{1}{2}} J_1^2(\alpha_n a)} = \int_0^{\infty} t^{\frac{1}{2}} J_{2m+\frac{1}{2}}(t) J_0(rt)\, dt,$$

so that, multiplication by r and integration with respect to r between 0 and 1 gives

$$\frac{2}{a^2} \sum_{n=1}^{\infty} \frac{J_{2m+\frac{1}{2}}(\alpha_n) J_1(\alpha_n)}{\alpha_n^{\frac{1}{2}} J_1^2(\alpha_n a)} = \int_0^{\infty} t^{-\frac{1}{2}} J_{2m+\frac{1}{2}}(t) J_1(t)\, dt.$$

From Watson (**8**) the infinite integral on the right vanishes except when $m = 0$ and then its value is $(2/\pi)^{\frac{1}{2}}$. Equation (24) then shows that the capacity is given by

$$C = \left(\frac{2}{\pi}\right)^{\frac{1}{2}} b_0. \tag{25}$$

With $\nu = 0$, $p = -1$, $F(r) = \frac{1}{2}a^2$, equation (6) gives

$$E(0, s, -1) = \frac{a^2}{2^{\frac{1}{2}}} \frac{\Gamma(s+1)}{\Gamma(s+\frac{1}{2})} \int_0^1 r(1-r^2)^{-\frac{1}{2}} \mathscr{F}_s(\tfrac{1}{2}, 1, r^2)\, dr.$$

Now $\mathscr{F}_0(\frac{1}{2}, 1, r^2) = 1$ and the orthogonality relation for the Jacobi polynomials (**9**) shows that

$$E(0, 0, -1) = \frac{a^2}{(2\pi)^{\frac{1}{2}}}, \qquad E(0, s, -1) = 0 \quad (s > 0),$$

and the first of equations (11) then gives

$$b_0^{(0)} = \left(\frac{2}{\pi}\right)^{\frac{1}{2}}, \qquad b_s^{(0)} = 0 \quad (s = 1, 2, 3, \ldots).$$

By expanding the Bessel functions of argument (t/a) in equation (8), it is apparent that $L_{m,s}^{(0,-1)}$ is of order $a^{-2m-2s-1}$ and, if we reject terms above a^{-5}, equations (11) and (25) yield

$$C = \left(\frac{2}{\pi}\right)^{\frac{1}{2}} b_0 = \frac{2}{\pi}\{1 - L_{0,0}^{(0,-1)}\}^{-1}. \tag{26}$$

Working as in section 4, it can be shown that

$$L_{0,0}^{(0,-1)} = \left(\frac{2}{\pi}\right)^2 \left[\frac{1{\cdot}36768}{a} + \frac{0{\cdot}21563}{a^3} + \frac{0{\cdot}09199}{a^5} + \ldots\right],$$

and these relations lead to values of the capacity of $2{\cdot}814/\pi$ when $a = 2$

and $2{\cdot}3255/\pi$ when $a = 4$. These results may be compared with Smythe's estimates that the capacity lies between $2{\cdot}807/\pi$ and $2{\cdot}818/\pi$ when $a = 2$ and between $2{\cdot}3253/\pi$ and $2{\cdot}3256/\pi$ when $a = 4$.

REFERENCES

1. C. J. Tranter, (*a*) *Quart. J. Mech. Appl. Math.* **3** (1950) 411 and **7** (1954) 317, or (*b*) *Integral Transforms in Mathematical Physics* (Methuen, 2nd edition, 1956), p. 111.
2. —— *Quart. J. of Math.* (Oxford) (in press).
3. See reference 1 (*a*), p. 318, or 1 (*b*), p. 113.
4. R. C. Knight, *Quart. J. of Math.* (Oxford) **7** (1936) 124.
5. E. E. Allen, *Math. Tables and Other Aids to Computation* **10** (1956) 162.
6. W. R. Smythe, *J. Appl. Phys.* **24** (1953) 773.
7. See reference 1 (*b*), pp. 88 et seq.
8. G. N. Watson, *Theory of Bessel Functions* (Cambridge, 1944), p. 403.
9. W. Magnus and F. Oberhettinger (translated by J. Wermer), *Special Functions of Mathematical Physics* (Chelsea Pub. Co., New York, 1949), p. 83.

DRAG FORCE ON A GOLF BALL IN FLIGHT AND ITS PRACTICAL SIGNIFICANCE

By D. WILLIAMS (*Royal Aircraft Establishment, Farnborough*)

[Received 25 April 1958]

SUMMARY

An experimental method of measuring the aerodynamic drag of a golf ball in free flight under typical playing conditions is described and the results obtained are discussed. The method depends on deriving a curve in which the 'carry' of the ball is plotted against initial ball velocity off the tee, so that only these two parameters need to be measured. A main conclusion is that the variation of the drag coefficient with Reynolds number is such as to make the drag vary linearly rather than as the square of the velocity (over the relevant speeds), with a consequent advantage to long hitters.

1. Introduction

THE forces acting on a golf ball in flight have been the subject of a number of investigations in the past. Of these probably the latest is that carried out by J. M. Davies (1) in 1949. Apart from presenting a comprehensive review of previous work, he describes in his paper a number of experiments carried out in the small wind tunnel of the B. F. Goodrich Co. The effect of various degrees of surface smoothness and of rotational velocity on the lift and drag of the ball were measured and some interesting results were obtained. Unfortunately, however, all the experiments were made at a constant tunnel speed of 105 ft/sec and therefore at a constant Reynolds number of 88,000. It was therefore not possible to estimate how the aerodynamic forces on the ball vary with the higher Reynolds numbers achieved in practice.

It is true, of course, that a fair amount of data on the drag of spheres of varying degrees of roughness over a wide range of Reynolds number already exists and is recorded in the standard textbooks. It is all based, however, on wind-tunnel tests on non-rotating spheres with a type of surface roughness very different from that of the conventional dimpled golf ball. But, although it would be hazardous to use this data for estimating the forces on a golf ball in free flight, it has amply demonstrated the interesting fact—and particularly interesting from the golfer's point of view—of the sudden and very marked drop in the drag coefficient at a certain critical Reynolds number.

It is now well known that this drop is due to the fact that the transition

from laminar to turbulent flow occurs earlier in the passage of the air over the ball, thereby narrowing the wake and reducing the drag.

Past experimental work has also shown that the smoother the surface of the sphere the more sudden the drop in the drag coefficient, and that, beyond a certain degree of roughness, the drop starts at a much lower speed and is distributed over a much wider speed range. Again it is difficult to translate the results of experiments on non-rotating spheres with particular types of roughness, in tunnels of a particular degree of turbulence, in terms of the spinning golf ball in free flight with its own peculiar type of surface roughness.

The ordinary handicap golfer's interest in this problem arises from his suspicion that the long drives achieved by the professional player are largely due to some peculiarity in the behaviour of the ball which he himself is unable to exploit but which he feels is 'just round the corner' if only he could achieve that little extra initial velocity. The matter is also of interest to the ruling body that governs the game, for if it were found that there is a critical speed which, if reached, gives the player something for nothing, so to speak, some action might be taken to obviate what might be considered an unfair advantage.

It was with such considerations in mind that the writer evolved a fairly reliable method of determining how the drag of a golf ball varies with its speed under typical playing conditions. To make the conditions typical, the ball must be struck by a lofted club-head similar to that of a driver so that, with typical back-spin, it follows the orthodox flight path of a good drive.

Two parameters alone need be measured—the initial velocity of the ball and its 'carry', i.e. the distance it covers before striking the ground. By plotting the 'carry' against the initial velocity a curve is obtained the tangent to which at any particular initial velocity gives the aerodynamic drag at that velocity.

It is claimed that this is not a 'rough-and-ready' method of obtaining the drag coefficient of a golf ball under typical playing conditions but a perfectly sound method that leads to results that are inaccurate only in so far as the two relevant parameters are inaccurately measured. This is the only reason for the use of the phrase 'fairly reliable'.

The necessary tests, which covered a range of carry extending from 150 to 230 yd, were carried out by Messrs. Dunlops (through the courtesy of Mr. S. G. Ball), and the data they obtained is plotted in Fig. 1. From this it is seen that, between the chosen limits of initial velocity, the curve is well represented by a straight line, so that the tangent to the curve is constant.

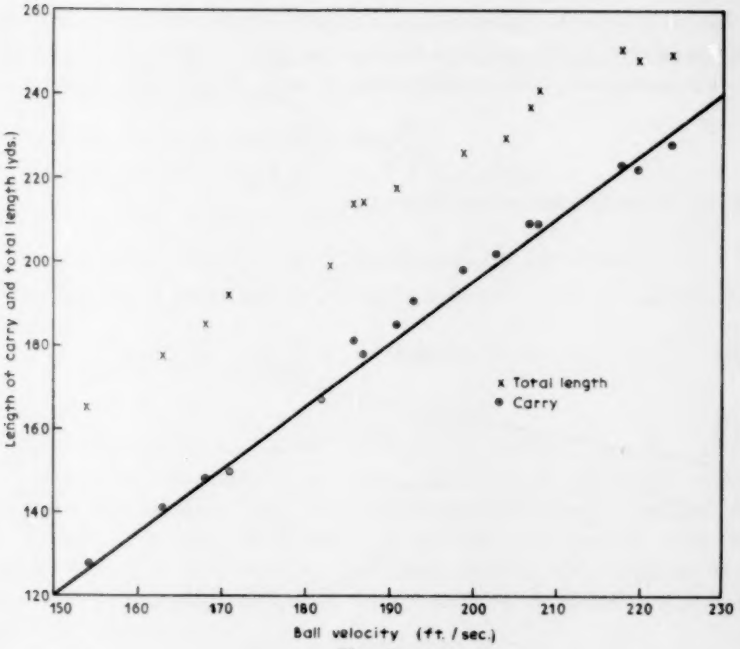

FIG. 1

2. The theoretical basis

Fig. 2 shows the trajectory for a typical drive, in which the initial angle α of the flight path is very shallow and its final angle β, where it meets the ground is fairly steep.

Let x_0 be the total carry, v the ball velocity, and v_0 the initial velocity of ball.

Consider the trajectory AB for which the initial velocity is v_0 and the total carry x_0. Suppose now the ball is teed up at A' a very short distance $\delta_1 x_0$ behind A and slightly below it by an amount $\delta_1 x_0 \tan\alpha$. If, starting from A', the ball is given an added velocity δv_0 that sends it along precisely the same path AHB as before, it will reach a point B' on the same level as A' and beyond B by the distance BC', where

$$BC' = \delta_2 x_0 = B'C' \cot\beta = \delta_1 x_0 \tan\alpha \cot\beta. \tag{1}$$

The total carry on the level is thus

$$A'B' = (x_0 + \delta x_0) = (x_0 + \delta_1 x_0 + \delta_2 x_0) \tag{2}$$

and the increase in carry is

$$\delta x_0 = \delta_1 x_0 + \delta_2 x_0 = \delta_1 x_0 (1 + \tan\alpha \cot\beta). \tag{3}$$

Since, in order to follow the same trajectory, the velocity v_0 at A must be the same in both cases, the velocity $(v_0+\delta v_0)$ at A' must have dropped by the amount δv_0 in its passage from A' to A. We can therefore write

$$\frac{\delta v_0}{\delta_1 x_0} = -\frac{\delta v}{\delta x} \tag{4}$$

or, by (3), and introducing differentials,

$$(1+\tan\alpha\cot\beta)\frac{dv_0}{dx_0} = -\frac{dv}{dx}. \tag{5}$$

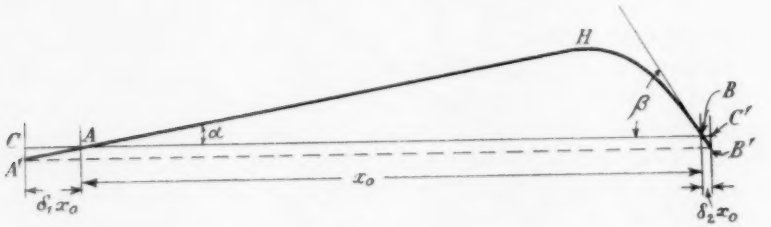

FIG. 2

Now α is normally about 6° and β about 45°, which makes

$$(1+\tan\alpha\cot\beta) = 1{\cdot}105, \tag{6}$$

and it is clear that small errors in α or β are of minor importance.

Reverting now to the experimental results of Fig. 1, we see that the constant slope as measured is

$$dx_0/dv_0 = 120\times 3/80 = 4{\cdot}5 \text{ sec}, \tag{7}$$

and therefore, by (5) and (6),

$$(dv/dx)_{v=v_0} = -(dv_0/dx_0)_{\text{measured}}\times 1{\cdot}105 = -\frac{1{\cdot}105}{4{\cdot}5} = -0{\cdot}246 \text{ sec}^{-1}. \tag{8}$$

The equation of motion of the ball in its line of travel as it leaves the tee (if we neglect gravity and the lift due to the spin, both negligible at this stage and also tending to cancel each other) takes the form

$$mv\frac{dv}{dx}\cos\alpha + Kv^2 = 0 \tag{9}$$

or, with sufficient accuracy, since $\cos\alpha \sim 1$

$$\frac{dv}{dx} + \frac{Kv}{m} = 0. \tag{10}$$

Here v = velocity of ball in ft/sec,

m = mass of ball of weight 1·62 oz = $(1{\cdot}62/16)/g$ slugs ($g = 32{\cdot}2$),

$K = \frac{1}{2}C_D\rho S = 17\times10^{-6}C_D$,

C_D = aerodynamic drag coefficient,

S = projected area of ball = $\frac{1}{4}\pi d^2 = 0{\cdot}0143$ ft^2,

d = diameter of ball = 1·62/12 ft,

ρ = mass of air per cu ft = 0·00237 slugs (at sea-level).

Inserting the appropriate numerical constants in (10) we obtain the relation

$$\frac{1}{v}\left(\frac{dv}{dx}\right) = -0{\cdot}00536C_D \tag{11}$$

or, from (8)

$$C_D = \frac{0{\cdot}246}{(0{\cdot}00536)v} = \frac{46{\cdot}0}{v}. \tag{12}$$

Thus, for ball velocities ranging from 150 ft/sec to 230 ft/sec, which represents the practical range, the drag coefficient varies inversely with the velocity. The total drag therefore increases only linearly with the velocity instead of as the velocity squared, as it would for a constant drag coefficient. The penalty suffered by the hard hitter is therefore substantially reduced.

Using the value of C_D given by (12) in the expression for K, we obtain the total drag on the ball as

$$(17\times10^{-6})C_D v^2 \text{ lb} = 0{\cdot}000783v \text{ lb}. \tag{13}$$

Thus at the initial velocity of 190 ft/sec, which gives a carry of 180 yd—a typical distance for the average player—the drag coefficient from formula (12) has the value 0·242. For a long drive of 232 yd carry the initial velocity is 225 ft/sec at which the drag coefficient is 0·204, a reduction of 16 per cent.

It is of interest to see how much of the difference in length between the long hitter and the average player is due to this drop in the drag coefficient. To determine this we use the numerical values just quoted and suppose that the drag coefficient for speeds between 190 ft/sec and 225 ft/sec remains constant at 0·242—the value appropriate to 190 ft/sec. From (11), on putting 0·242 for C_D, we have

$$\frac{1}{v}\frac{dv}{dx} = -0{\cdot}00536C_D = -0{\cdot}0013 \tag{11}$$

for which the solution is

$$\log_e v = -0{\cdot}0013x + \text{constant}.$$

Using the condition that $v = v_0$ when $x = 0$, we write

$$\log_e v/v_0 = -0{\cdot}0013x.$$

The distance travelled while the velocity drops from v_0 (= 225 ft/sec) to v_1 (= 190 ft/sec) is therefore

$$x = \left(\frac{1}{0{\cdot}0013}\right)\log_e \frac{225}{190} = 129 \text{ ft} = 43 \text{ yd}. \tag{14}$$

Comparing this with the actual distance of (232−180) = 52 yd, we see that the long hitter gains just over 9 yd. It can be said therefore that only some 17 per cent of the long hitter's advantage in distance can be attributed to the drop in drag coefficient. The rest apparently he gains by honest effort.

REFERENCE

1. J. M. Davies, 'The aerodynamics of golf balls', *J. Appl. Phys.* **20** (1949) 821–8.

Using the condition that $v = v_0$ when $x = 0$, we write

$$\log_e v/v_0 = -0{\cdot}0013x.$$

The distance travelled while the velocity drops from v_0 (= 225 ft sec) to v_1 (= 190 ft sec) is therefore

$$x = \left(\frac{1}{0{\cdot}0013}\right)\log_e \frac{225}{190} = 129 \text{ ft} = 43 \text{ yd}. \tag{14}$$

Comparing this with the actual distance of (232 − 180) = 52 yd, we see that the long hitter gains just over 9 yd. It can be said therefore that only some 17 per cent of the long hitter's advantage in distance can be attributed to the drop in drag coefficient. The rest apparently he gains by honest effort.

REFERENCE

1. J. M. Davies, 'The aerodynamics of golf balls', *J. Appl. Phys.* **20** (1949) 821–8.

THE QUARTERLY JOURNAL OF MECHANICS AND APPLIED MATHEMATICS

VOLUME XII PART 3 AUGUST 1959

CONTENTS

The Editorial Board gratefully acknowledge the support given by: Blackburn & General Aircraft Limited; Bristol Aeroplane Company; Courtaulds Scientific and Educational Trust Fund; English Electric Company; Hawker Siddeley Group Limited; Imperial Chemical Industries Limited; Metropolitan-Vickers Electrical Company Limited; The Shell Petroleum Co. Limited; Vickers-Armstrongs (Aircraft) Limited.